Ultracold Fermi gases and the BEC-BCS crossover

Sylvain Nascimbene

M2 ICFP, course *Ultracold atoms* - École Normale Supérieure

These lecture notes accompany the part of the Master 2 course *Ultracold atoms* (École Normale Supérieure, Paris) devoted to ultracold Fermi gases and the BEC-BCS crossover.

Contents

1 Introduction: attractive Fermi gases **3**
1.1 Attractive Fermi gases . . . 3
1.2 Weak attraction: Cooper pairing . . . 3
1.3 Strong attraction: molecular BEC . . . 4
1.4 The BEC-BCS crossover in atomic gases . . . 4
1.5 Motivations . . . 6
1.6 Outline of the notes . . . 6

2 Reaching the strongly-interacting regime **7**
2.1 Cold collisions, scattering length, pseudo-potential . . . 7
2.1.1 Two-body scattering: reminder . . . 7
2.1.2 Partial waves . . . 8
2.1.3 Restriction to s-wave scattering at low energy . . . 9
2.1.4 Cold collisions between identical particles . . . 10
2.1.5 Scattering length . . . 10
2.1.6 Scattering length in a toy model . . . 12
2.1.7 The pseudo-potential . . . 13
2.1.8 Scattering amplitude in momentum space . . . 14
2.1.9 Bound state of the pseudo-potential . . . 16
2.2 Feshbach resonances . . . 17
2.2.1 Principle of a Feshbach resonance . . . 18
2.2.2 A solvable two-channel model . . . 18
2.2.3 Magnetic-field dependence of the scattering length . . . 20
2.2.4 Examples of Feshbach resonances . . . 20
2.3 Collisional stability: bosons versus fermions . . . 21
2.3.1 Towards a strongly interacting regime . . . 22
2.3.2 Three-body recombination in Bose gases . . . 22
2.3.3 Three-body recombination in Fermi gases . . . 24

3 Theory of the BEC-BCS crossover **26**
3.1 The Cooper instability . . . 27
3.1.1 The attractive Fermi gas: possible scenarios . . . 27
3.1.2 The Cooper problem . . . 28
3.1.3 Binding energy of the Cooper pair . . . 29
3.2 Mean-field theory of the BEC-BCS crossover at zero temperature . . . 30
3.2.1 BCS variational ansatz . . . 30
3.2.2 The BCS mean-field Hamiltonian . . . 31
3.2.3 Ground state of the BCS Hamiltonian . . . 32
3.2.4 BCS equations . . . 33
3.2.5 The BCS limit . . . 34
3.2.6 The BEC limit . . . 35
3.2.7 Solution for all interaction strengths . . . 37
3.3 Superfluid critical temperature . . . 38
3.3.1 Finite-temperature BCS theory . . . 38
3.3.2 The BCS limit . . . 39
3.3.3 The BEC limit . . . 39
3.3.4 Critical temperature in the crossover . . . 40
3.4 Short-range correlations: Tan's contact . . . 41
3.4.1 Short-range correlations . . . 41
3.4.2 Tan relations . . . 41
3.4.3 Contact in the BEC-BCS crossover . . . 42
3.5 The unitary Fermi gas . . . 43
3.5.1 Scale invariance . . . 44
3.5.2 Universal thermodynamics . . . 44

4 Experimental characterization of the BEC-BCS crossover **45**
4.1 Thermodynamics of the unitary Fermi gas . . . 46
4.1.1 Testing the scale invariance . . . 46
4.1.2 Ground-state energy at unitarity: history . . . 46
4.1.3 Equation of state measurement . . . 48
4.1.4 Equation of state in the normal phase . . . 48
4.1.5 Superfluid λ transition . . . 49
4.2 Ground state in the BEC-BCS crossover . . . 51
4.2.1 Ground-state energy in the BEC-BCS crossover . . . 51
4.2.2 Collective mode measurements . . . 52
4.3 Measurement of the contact . . . 53
4.4 Excitations and superfluid gap . . . 54
4.5 Superfluidity . . . 55
4.5.1 Critical velocity . . . 55
4.5.2 Quantized vortices . . . 56
4.6 Spin-imbalanced Fermi gases . . . 57
4.7 Open questions . . . 60

1 Introduction: attractive Fermi gases

These lecture notes are devoted to the physics of ultracold gases of fermionic atoms with attractive interactions, and more specifically to the crossover between Bose-Einstein condensation (BEC) of tightly bound molecules and Bardeen-Cooper-Schrieffer (BCS) superfluidity of loosely bound Cooper pairs. They cover the part on ultracold Fermi gases of the course *Ultracold atoms* of the Master 2 ICFP (École Normale Supérieure, Paris), taught together with Fabrice Gerbier, Raphaël Lopes and Aurélien Perrin. In this introductory section, we formulate the central question addressed in the notes, namely the nature of the many-body ground state of an attractive Fermi gas, we describe the two limiting scenarios of weak and strong attraction, and we explain why ultracold atoms are an ideal platform to explore the intermediate regime. We end with an outline of the notes.

1.1 Attractive Fermi gases

We consider a gas of fermionic atoms of mass m, prepared in an equal mixture of two internal states, that we label as two spin components $\uparrow$ and $\downarrow$ (in practice, they are two hyperfine states of an alkali atom such as ^{6}Li or ^{40}K). We assume that the atoms interact via a short-range interaction, which is *attractive* between atoms of different spin components. As we will see in section 2, atoms in the same spin state do not interact at low temperature, as a consequence of the Pauli principle, so that the interaction only takes place between opposite spins.

In the absence of interactions, the ground state of the gas is the Fermi sea, in which each spin component fills all the plane-wave states of wave-vector $k < k_\mathrm{F}$. For a total density n (i.e. a density $n/2$ per spin component), the Fermi wave-vector and the Fermi energy read

$$n = \frac{k_\mathrm{F}^3}{3\pi^2}, \qquad E_\mathrm{F} = \frac{\hbar^2 k_\mathrm{F}^2}{2m} = k_\mathrm{B} T_\mathrm{F}, \tag{1.1}$$

where we also introduced the Fermi temperature T_F. The Fermi wave-vector sets the typical inter-particle distance, of the order of k_F^{-1}. In typical experiments, the total density is of the order of $n \sim 10^{13}\,\mathrm{cm}^{-3}$, which gives $k_\mathrm{F}^{-1} \simeq 150\,\mathrm{nm}$ and a Fermi temperature $T_\mathrm{F} \simeq 1.8\,\mu\mathrm{K}$ for ^{6}Li atoms ($T_\mathrm{F} \simeq 0.27\,\mu\mathrm{K}$ for ^{40}K). Quantum degeneracy, reached for temperatures $T \lesssim T_\mathrm{F}$, was first achieved with ^{40}K atoms in 1999 [1].

Let us now switch on an attractive interaction between the $\uparrow$ and $\downarrow$ atoms. The central question of these notes is:

What is the many-body ground state of an attractive Fermi gas?

In the following, we describe two limiting scenarios, for weak and strong attraction, which lead to two *a priori* very different superfluid states.

1.2 Weak attraction: Cooper pairing

We first consider a weak attraction. Fermions being unable to condense in a single-particle state, one may naively expect the attraction to give rise to small perturbative corrections to the properties of the Fermi sea. This is not the case: as shown by Cooper [2], the

Fermi sea is unstable for an arbitrarily weak attraction. Two fermions of opposite spins and opposite momenta close to the Fermi surface, $(\mathbf{k}\uparrow, -\mathbf{k}\downarrow)$ with $k \simeq k_{\rm F}$, form a bound state, called a Cooper pair, even when the attraction is too weak to bind two particles in vacuum. The Pauli blocking of the states $k < k_{\rm F}$ is essential for this pairing, which is a genuine many-body effect. We will study this Cooper instability in section 3.

The many-body ground state is then the BCS state [3], in which all particles close to the Fermi surface are paired. It is a superfluid, characterized by an energy gap Δ in its excitation spectrum. In the weak-coupling limit, the gap and the critical temperature are exponentially small in the inverse of the interaction strength. An essential feature of Cooper pairs is their large spatial extent, of the order of the coherence length $\xi \sim \hbar v_{\rm F}/\Delta$, with $v_{\rm F} = \hbar k_{\rm F}/m$ the Fermi velocity. Since $\Delta \ll E_{\rm F}$, we have $k_{\rm F}\xi \sim E_{\rm F}/\Delta \gg 1$: the pair size is much larger than the inter-particle distance, so that a given pair overlaps with a large number of other pairs (see Fig. 1, left). For instance, in conventional superconductors, the coherence length ranges from tens of nanometers to about a micrometer, while the distance between electrons is of the order of 0.1 nm. Cooper pairs can thus by no means be considered as pointlike bosons.

1.3 Strong attraction: molecular BEC

In the opposite limit of a strong attraction, two atoms of opposite spins can bind into a molecule, i.e. a two-body bound state, which exists even in vacuum. When the size of the molecule is much smaller than the inter-particle distance, the gas can be described as a gas of $N/2$ pointlike composite bosons of mass $2m$ and density $n/2$ (see Fig. 1, right). The many-body ground state is then a Bose-Einstein condensate of molecules, which is also a superfluid.

At finite temperature, the condensation of an ideal gas of molecules occurs below the critical temperature

$$k_{\rm B}T_{\rm c} = \frac{2\pi\hbar^2}{2m}\left(\frac{n/2}{\zeta(3/2)}\right)^{2/3} \simeq 0.218\, E_{\rm F}, \tag{1.2}$$

obtained from the standard result for an ideal Bose gas of particles of mass $2m$ and density $n/2$, with $\zeta(3/2) \simeq 2.612$, and expressed in terms of the Fermi energy (1.1). The critical temperature is thus a sizeable fraction of the Fermi temperature, in strong contrast with the exponentially small critical temperature of the weak-coupling BCS regime. Note that this critical temperature has nothing to do with the energy required to break a molecule, which can be much larger than $E_{\rm F}$.

1.4 The BEC-BCS crossover in atomic gases

The two scenarios described above appear very different: the BCS state results from a collective many-body instability of the Fermi sea, while the molecular BEC results from the condensation of preformed bosonic molecules. However, both states share the same broken symmetry (the $U(1)$ symmetry associated with particle number conservation) and both are superfluids. One can thus wonder whether they are continuously connected when the interaction strength is varied. This question was raised by Eagles [4] and Leggett [5], who showed that the BCS variational wave-function provides a description of the ground state that continuously interpolates between the two limits, without

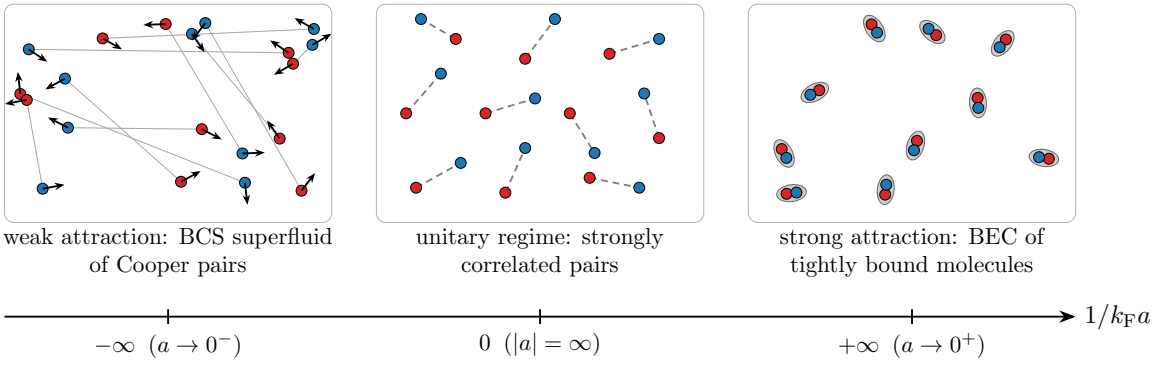


Figure 1: Schematic view of the BEC-BCS crossover in a two-component Fermi gas (red and blue disks represent the two spin states). Left: for a weak attraction ($1/k_{\mathrm{F}}a \to -\infty$), atoms of opposite spins and momenta (arrows) form Cooper pairs (gray lines), whose size is much larger than the inter-particle distance. Right: for a strong attraction ($1/k_{\mathrm{F}}a \to +\infty$), atoms bind into molecules much smaller than the inter-particle distance, which form a Bose-Einstein condensate. Middle: in the unitary regime ($1/k_{\mathrm{F}}a \simeq 0$), the pair size is comparable to the inter-particle distance and the gas is strongly correlated.

any phase transition, the extension to finite temperature being due to Nozières and Schmitt-Rink [6]. This continuous evolution is called the BEC-BCS crossover:

- On the BCS side, the pairs are loosely bound Cooper pairs, of size much larger than the inter-particle distance.
- On the BEC side, the pairs are tightly bound molecules, of size much smaller than the inter-particle distance.
- In the intermediate regime, the pair size is comparable to the inter-particle distance. No small parameter is available and the system exhibits complex many-body correlations.

Realization with ultracold atoms. Leggett's discussion was based on an idealized model of fermions interacting via a short-range attractive potential of tunable strength. While such a tunability is out of reach in solid-state systems, it has been realized with ultracold atomic gases. As we will see in section 2, in dilute ultracold gases the interactions are characterized by a single parameter, the s-wave scattering length a, which can be tuned over a wide range, from $-\infty$ to $+\infty$, using a magnetic Feshbach resonance. The relevant dimensionless interaction parameter is then

$$\frac{1}{k_{\mathrm{F}}a}, \tag{1.3}$$

which compares the scattering length with the inter-particle distance. The BCS regime corresponds to a small negative scattering length, $1/k_{\mathrm{F}}a \to -\infty$, and the BEC regime to a small positive scattering length, $1/k_{\mathrm{F}}a \to +\infty$, for which a weakly bound molecular state exists, of binding energy $E_b = \hbar^2/ma^2$. The intermediate regime $|1/k_{\mathrm{F}}a| \lesssim 1$ is

reached when the scattering length becomes larger than the inter-particle distance. Its center $1/k_{\mathrm{F}}a = 0$ defines the so-called unitary Fermi gas, whose properties are universal since no length scale related to interactions remains.

Strongly interacting degenerate Fermi gases were first produced in 2002 [7], Bose-Einstein condensates of Feshbach molecules in 2003 [8, 9, 10], and the condensation of fermion pairs across the whole crossover was demonstrated in 2004 [11, 12]. Superfluidity was unambiguously evidenced by the observation of quantized vortices throughout the crossover [13]. The physics of the crossover is reviewed in Refs. [14, 15, 16].

The quantitative description of the strongly interacting regime remains a challenge for many-body theories. Mean-field theory, which we will develop in section 3, captures the qualitative features of the crossover, but it is not quantitatively accurate in the unitary regime, which requires more advanced theoretical methods (e.g. quantum Monte Carlo simulations). In this context, precise measurements performed with ultracold gases provide benchmarks for many-body theories.

1.5 Motivations

Beyond the intrinsic interest of a continuous connection between two paradigmatic forms of superfluidity, the study of strongly interacting Fermi gases is motivated by several questions of broader interest.

- The basic understanding of superconductivity relies on the condensation of paired electrons. In conventional superconductors, the pairs are Cooper pairs much larger than the inter-particle distance, well described by BCS theory. The opposite limit of a condensate of tightly bound pairs is also well understood. The crossover provides a framework to discuss these two limits within a single theory.

- In unconventional superconductors, such as high-T_{c} cuprate superconductors, the pair size is only a few times larger than the inter-particle distance, so that these materials lie in a strongly-correlated regime that is not described by standard BCS theory. Ultracold Fermi gases in the crossover regime realize a simpler system sharing this feature, albeit with a different (short-range and s-wave) pairing mechanism.

- Nuclear matter also involves strongly interacting fermions. For instance, the neutron-neutron interaction has a scattering length $a \simeq -18.6\,\mathrm{fm}$, much larger in modulus than the range $\sim 2\,\mathrm{fm}$ of nuclear forces. Dilute neutron matter, present in the crust of neutron stars, thus lies close to the unitary regime, $k_{\mathrm{F}}|a| \gg 1$, and it shares universal properties with unitary atomic gases.

In all these situations, the pair size is comparable to the inter-particle distance, which defines a strongly correlated regime that challenges theories of quantum many-body systems. Ultracold Fermi gases, with their tunable interactions, provide a clean and controlled realization of this regime.

1.6 Outline of the notes

The notes are organized as follows.

- In section 2, we explain how the strongly interacting regime can be reached with ultracold atoms. We recall the physics of low-energy collisions, which are characterized by the scattering length a and can be modeled by a pseudo-potential. We then describe the Feshbach resonance mechanism, which allows one to tune the scattering length, and we explain why Fermi gases, contrary to Bose gases, remain collisionally stable in the strongly interacting regime.
- In section 3, we develop the theory of the BEC-BCS crossover. We first discuss the Cooper instability, and then develop the mean-field (BCS) theory of the crossover at zero temperature. We discuss the critical temperature, Tan's contact which characterizes the short-distance pair correlations, and the universal properties of the unitary Fermi gas.
- In section 4, we describe the experimental characterization of the crossover (pair condensation, superfluidity, thermodynamics, pairing gap and contact), and we conclude with a discussion of some open questions.

2 Reaching the strongly-interacting regime

In this section, we explain how ultracold atomic gases can be brought into the strongly interacting regime required to explore the BEC-BCS crossover. We first recall the physics of low-energy collisions between atoms: in the ultracold regime, the interactions are characterized by a single parameter, the s-wave scattering length a, and they can be modeled by a zero-range pseudo-potential. We then describe the Feshbach resonance mechanism, which allows one to tune the scattering length to arbitrary values with a magnetic field. We finally discuss the collisional stability of strongly interacting gases: while Bose gases suffer from fast three-body losses when the scattering length becomes large, two-component Fermi gases remain stable thanks to the Pauli principle. This stability is the key ingredient that made the experimental study of the BEC-BCS crossover possible.

The quantum theory of scattering is discussed in detail in the lecture notes of the course *Advanced quantum mechanics* (chapter on quantum scattering). We use the same conventions and notations, and we only recall here the main results, with an emphasis on their application to ultracold atoms.

2.1 Cold collisions, scattering length, pseudo-potential

In this subsection, we show that low-energy collisions between neutral atoms are dominated by the s-wave channel, and that they are entirely characterized by the scattering length a. We then introduce the pseudo-potential, a zero-range model interaction that reproduces the low-energy scattering properties, and that will be used throughout the notes. We finally determine the bound state of the pseudo-potential, which plays a central role on the BEC side of the crossover.

2.1.1 Two-body scattering: reminder

We consider two atoms of same mass m, interacting via a potential $V(\mathbf{r})$ that depends on their relative position $\mathbf{r}$. We assume that the potential is

- spherically symmetric, $V(\mathbf{r}) = V(r)$,
- decaying sufficiently fast at long distances (for neutral atoms, the potential decays as the van der Waals potential $-C_6/r^6$).

The center-of-mass motion being free, we focus on the relative motion, which is described by the Schrödinger equation of a fictitious particle of reduced mass $\mu = m/2$ evolving in the potential V. A stationary state of energy E is described by a wave-function $\psi(\mathbf{r})$ obeying

$$\left[-\frac{\hbar^2}{2\mu}\Delta + V(r)\right]\psi(\mathbf{r}) = E\,\psi(\mathbf{r}), \qquad \mu = \frac{m}{2}. \tag{2.1}$$

For a positive energy $E = \hbar^2k^2/2\mu = \hbar^2k^2/m$, a *scattering state* is the superposition of

- an incoming plane wave $\mathrm{e}^{\mathrm{i}kz}$, propagating along the z axis,
- a scattered wave, behaving at large distances as an outgoing spherical wave $f_k(\theta,\phi)\,\mathrm{e}^{\mathrm{i}kr}/r$,

i.e.

$$\psi(\mathbf{r}) \underset{r\to\infty}{\simeq} \mathrm{e}^{\mathrm{i}kz} + f_k(\theta,\phi)\frac{\mathrm{e}^{\mathrm{i}kr}}{r}, \tag{2.2}$$

where (θ,ϕ) are the polar angles of $\mathbf{r}$ with respect to the incident direction. The scattering amplitude $f_k(\theta,\phi)$ fully characterizes the collision. The flux scattered in a given direction gives the differential cross-section $\mathrm{d}\sigma/\mathrm{d}\Omega = |f_k(\theta,\phi)|^2$, and the total cross-section $\sigma = \int |f_k|^2\,\mathrm{d}^2\Omega$ for distinguishable particles.

2.1.2 Partial waves

The potential being spherically symmetric, the angular momentum of the relative motion is conserved. It is then convenient to decompose the scattering problem into partial waves of given angular momentum ℓ, which behave independently. For this, we expand the incoming plane wave on spherical harmonics, as

$$\mathrm{e}^{\mathrm{i}kz} = \sum_{\ell=0}^{\infty} \mathrm{i}^\ell \sqrt{4\pi(2\ell+1)}\, j_\ell(kr)\, Y_\ell^0(\theta) = \sum_{\ell=0}^{\infty} (2\ell+1)\,\mathrm{i}^\ell j_\ell(kr)\, P_\ell(\cos\theta), \tag{2.3}$$

where j_ℓ are the spherical Bessel functions and P_ℓ the Legendre polynomials. Only the spherical harmonics with zero projection $m_\ell = 0$ appear, since the incident direction is along z.

A partial wave of angular momentum ℓ is written as $\phi_\ell(\mathbf{r}) = u_\ell(r)\,Y_\ell^0(\theta)/r$, where the radial function u_ℓ (with $u_\ell(0) = 0$) obeys the one-dimensional Schrödinger equation

$$\left[-\frac{\hbar^2}{2\mu}\frac{\mathrm{d}^2}{\mathrm{d}r^2} + V_{\text{eff}}(r)\right] u_\ell(r) = E\,u_\ell(r), \qquad V_{\text{eff}}(r) = V(r) + \frac{\ell(\ell+1)\hbar^2}{2\mu r^2}. \tag{2.4}$$

The effective potential V_{eff} involves, for $\ell > 0$, a repulsive centrifugal term which creates a barrier at large distance, as shown in Fig. 2. At large distance, the radial function behaves as $u_\ell(r) \propto \sin(kr - \ell\pi/2 + \delta_\ell)$, which defines the scattering phase shift δ_ℓ of

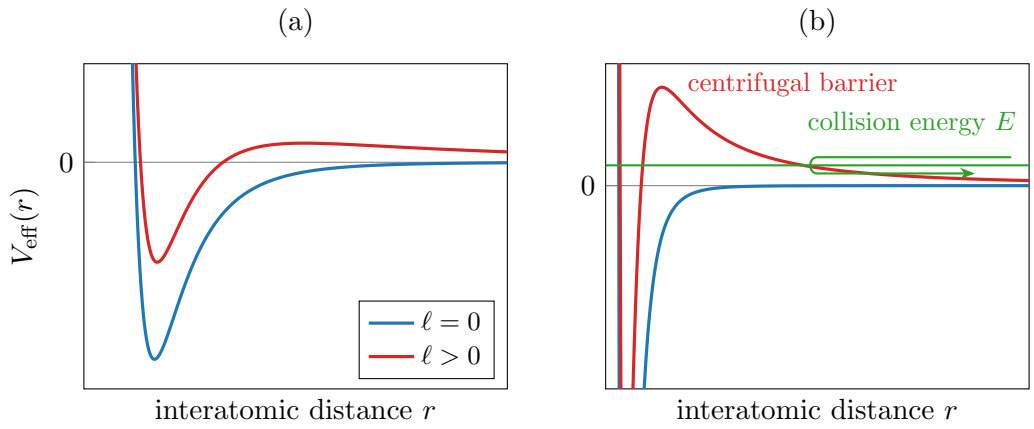


Figure 2: (a) Effective radial potential $V_{\text{eff}}(r)$ for the partial wave $\ell = 0$ (blue) and a partial wave $\ell > 0$ (red), for a schematic interatomic potential with a repulsive core and an attractive well. (b) Same potentials at large distance. For $\ell > 0$, the centrifugal term creates a barrier. At low collision energy E (green line), the atoms are reflected by the barrier at a distance much larger than the potential range, so that they do not feel the short-distance potential: only s-wave ($\ell = 0$) collisions remain.

the partial wave ℓ. The scattering amplitude, which only depends on θ, and the total cross-section are then given by

$$f_k(\theta) = \frac{1}{2\mathrm{i}k} \sum_{\ell=0}^{\infty} (2\ell+1) \left(\mathrm{e}^{2\mathrm{i}\delta_\ell} - 1\right) P_\ell(\cos\theta), \qquad \sigma = \sum_{\ell=0}^{\infty} \frac{4\pi}{k^2} (2\ell+1) \sin^2\delta_\ell. \tag{2.5}$$

Each partial wave thus contributes at most $4\pi(2\ell+1)/k^2$ to the cross-section, a value called the unitary limit, reached for $\delta_\ell = \pi/2 \pmod{\pi}$.

2.1.3 Restriction to s-wave scattering at low energy

At low collision energy, the centrifugal barrier prevents atoms with $\ell > 0$ from approaching each other. Classically, the atoms are reflected at the turning point r_E defined by $\ell(\ell+1)\hbar^2/(2\mu r_E^2) = E$, i.e. $r_E = \sqrt{\ell(\ell+1)}/k$. When the collision energy is small enough for r_E to be much larger than the range b of the potential, i.e. for $kb \ll 1$, the atoms only explore the region where the potential is negligible, and the partial wave ℓ is not affected by the interaction (see Fig. 2b). Quantum mechanically, the atoms can tunnel through the barrier, but with a probability that vanishes at low energy. The phase shifts follow the threshold laws

$$\tan\delta_\ell(k) \propto k^{2\ell+1} \quad \text{for} \quad k \to 0 \tag{2.6}$$

(valid for $\ell = 0$ and $\ell = 1$ for a van der Waals potential), so that the contribution $\sigma_\ell \propto \sin^2\delta_\ell/k^2 \propto k^{4\ell}$ of a partial wave $\ell > 0$ to the cross-section vanishes. Only the s-wave contribution remains finite at zero energy: this defines the regime of *cold collisions*, in which the scattering is isotropic.

2.1.4 Cold collisions between identical particles

For identical particles in the same internal state, the wave-function of the relative motion must be symmetrized according to quantum statistics. Exchanging the two particles amounts to changing $\mathbf{r}$ into $-\mathbf{r}$, under which a partial wave ℓ acquires a factor $(-1)^\ell$. Consequently,

- for identical bosons, the wave-function is symmetric and only even-ℓ partial waves contribute,
- for identical fermions, the wave-function is antisymmetric and only odd-ℓ partial waves contribute.

In the cold collision regime, where only the s-wave contributes, identical fermions do not interact. For identical bosons, the interference between the direct and exchange scattering amplitudes doubles the s-wave cross-section, which becomes $\sigma = 8\pi a^2$ at low energy (with a the scattering length introduced below), instead of $4\pi a^2$ for distinguishable particles.

This has a major consequence for Fermi gases: in a spin-polarized Fermi gas, collisions disappear at low temperature. This was observed with fermionic ^{40}K atoms by DeMarco *et al.* [17], who measured the elastic cross-section as a function of temperature from the rethermalization dynamics of the gas after a perturbation (see Fig. 3). For a spin-polarized gas, the cross-section strongly decreases at low temperature, according to the p-wave threshold law $\sigma_1 \propto k^4 \propto T^2$, while it remains of the order of $10^{-11}\,\mathrm{cm}^2$ for a mixture of two spin states, for which s-wave collisions are allowed. Indeed, two fermions in different internal states $\uparrow$ and $\downarrow$ behave as distinguishable particles: the antisymmetry of the total wave-function can be ensured by an antisymmetric combination of the internal states, associated with a symmetric relative wave-function, which allows for s-wave collisions. In order to obtain interactions in a Fermi gas, one thus needs to prepare a mixture of (at least) two spin states. Then, interactions only occur between atoms of different spin states, and they are characterized by the s-wave scattering length of the $\uparrow\downarrow$ collisions.

2.1.5 Scattering length

In the cold collision regime, the scattering state (2.2) reduces to its s-wave component, with an isotropic scattering amplitude f_k,

$$\psi(\mathbf{r}) \underset{r\to\infty}{\simeq} \mathrm{e}^{\mathrm{i}kz} + f_k \frac{\mathrm{e}^{\mathrm{i}kr}}{r}, \qquad f_k = \frac{\mathrm{e}^{2\mathrm{i}\delta_0} - 1}{2\mathrm{i}k} = \frac{1}{k\cot\delta_0 - \mathrm{i}k}. \tag{2.7}$$

The threshold law $\tan\delta_0 \propto k$ defines the scattering length

$$a = -\lim_{k\to 0} \frac{\tan\delta_0(k)}{k} = -\lim_{k\to 0} f_k. \tag{2.8}$$

Using $k\cot\delta_0 \simeq -1/a$ at low energy, we obtain the scattering amplitude

$$f_k = -\frac{a}{1 + \mathrm{i}ka}, \tag{2.9}$$

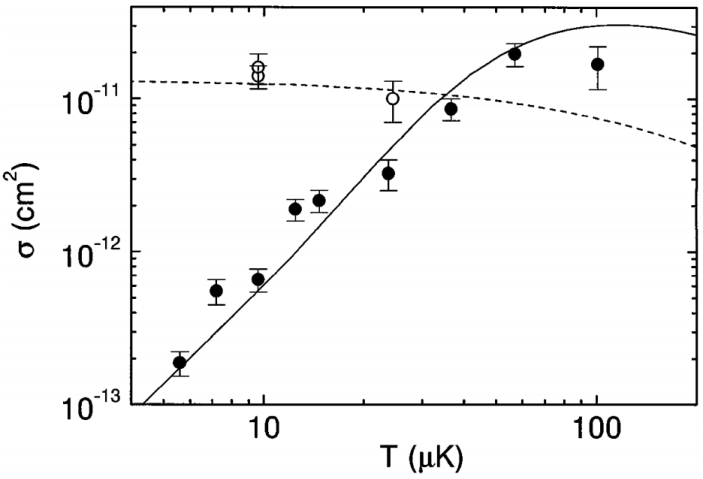


Figure 3: Elastic scattering cross-section of fermionic ^{40}K atoms as a function of temperature, for a spin-polarized gas (filled circles) and for a mixture of two spin states (open circles). For the polarized gas, only p-wave collisions are allowed, whose cross-section vanishes at low temperature. Figure from Ref. [17].

which is valid for $kb \ll 1$, the corrections being of order k^2ab in the denominator (effective range expansion). The corresponding cross-section for distinguishable particles is

$$\sigma = \frac{4\pi a^2}{1 + k^2 a^2}. \tag{2.10}$$

It reaches the value $4\pi a^2$ for $k|a| \ll 1$, and it saturates to the unitary limit $4\pi/k^2$ when $|a| \to \infty$.

In the zero-energy limit $k \to 0$, the scattering state takes the simple form, outside the range of the potential,

$$\psi(\mathbf{r}) = 1 - \frac{a}{r} \qquad (r \gg b). \tag{2.11}$$

The scattering length can thus be interpreted as the distance at which the extrapolation of the zero-energy radial wave-function $u_0(r) = r\psi(r) \propto r - a$ vanishes. For a hard-sphere potential of radius R, one finds $a = R$. More generally, $a > 0$ corresponds to an effective repulsion and $a < 0$ to an effective attraction, but we will see that the sign of a is not directly related to the sign of the potential.

Typical values. At long distance, the interaction between two neutral atoms in their electronic ground state is dominated by the van der Waals interaction

$$V(r) \simeq -\frac{C_6}{r^6}, \tag{2.12}$$

which results from the interaction between fluctuating electric dipoles. The only length and energy scales that can be constructed from C_6, $\hbar$ and the reduced mass are

$$R_{\rm vdW} = \frac{1}{2}\left(\frac{2\mu C_6}{\hbar^2}\right)^{1/4} \sim 100\, a_0 \simeq 5\,{\rm nm}, \tag{2.13}$$

$$E_{\rm vdW} = \frac{\hbar^2}{2\mu R_{\rm vdW}^2} \sim k_{\rm B} \times 1\,{\rm mK}, \tag{2.14}$$

where a_0 is the Bohr radius. More precisely, one finds $R_{\rm vdW} \simeq 31\, a_0$ and $E_{\rm vdW} \simeq k_{\rm B} \times 30\,{\rm mK}$ for ^{6}Li, $R_{\rm vdW} \simeq 65\, a_0$ and $E_{\rm vdW} \simeq k_{\rm B} \times 1\,{\rm mK}$ for ^{40}K, and $R_{\rm vdW} \simeq 83\, a_0$, $E_{\rm vdW} \simeq k_{\rm B} \times 0.3\,{\rm mK}$ for ^{87}Rb. The van der Waals length plays the role of the potential range b: it sets the typical value of the scattering length, $|a| \sim R_{\rm vdW}$, as we will see in the toy model below, while the van der Waals energy sets the energy scale below which collisions with $\ell > 0$ are suppressed. In ultracold gases, the temperature and the Fermi energy lie in the micro-kelvin range or below, so that the cold collision regime is very well satisfied. Moreover, the inter-particle distance, of the order of $k_{\rm F}^{-1} \sim 150\,{\rm nm}$, is much larger than $R_{\rm vdW}$: the gas is dilute, in the sense that the details of the interaction potential at short distance are not resolved.

2.1.6 Scattering length in a toy model

In order to understand the dependence of the scattering length on the short-distance potential, we consider a toy model defined by a van der Waals potential truncated at short distance by a hard core,

$$V(r) = +\infty, \quad r < r_c, \tag{2.15}$$

$$V(r) = -\frac{C_6}{r^6}, \quad r > r_c. \tag{2.16}$$

For real atoms, the repulsive core lies at a distance $r_c \ll R_{\rm vdW}$, so that the potential well is very deep compared to $E_{\rm vdW}$ and supports many bound states.

Zero-energy solution. We look for the zero-energy s-wave solution $u(r)$, obeying

$$u''(r) + \frac{2\mu C_6}{\hbar^2 r^6} u(r) = 0, \qquad u(r_c) = 0. \tag{2.17}$$

With the change of variables $x = 2R_{\rm vdW}^2/r^2$ and $u(r) = \sqrt{r}\, w(x)$, this equation takes the form of a Bessel equation of order $1/4$, whose solutions are $\sqrt{r}\, J_{\pm 1/4}(2R_{\rm vdW}^2/r^2)$. At large distance ($x \to 0$), the two solutions behave as $\sqrt{r}\, x^{\pm 1/4}$, i.e. as r^0 and r: they correspond to the two terms of the asymptotic form $u \propto r - a$. The scattering length is thus determined by the ratio of the weights of the two Bessel functions, which is fixed by the boundary condition $u(r_c) = 0$. Using the asymptotic expansion of the Bessel functions at large argument (since $r_c \ll R_{\rm vdW}$), one obtains [18]

$$a = \bar{a}\left[1 - \tan\left(\frac{2R_{\rm vdW}^2}{r_c^2} - \frac{3\pi}{8}\right)\right], \qquad \bar{a} = \frac{4\pi}{\Gamma(1/4)^2} R_{\rm vdW} \simeq 0.956\, R_{\rm vdW}. \tag{2.18}$$

We checked this formula against a numerical integration of the radial equation, with a relative accuracy better than 10^{-2} for $R_{\rm vdW}/r_c \simeq 10$.

Physical interpretation. The argument of the tangent is the semi-classical (WKB) phase accumulated by the zero-energy wave-function in the potential well,

$$\Phi = \int_{r_c}^{\infty} \sqrt{\frac{2\mu C_6}{\hbar^2 r^6}}\, {\rm d}r = \frac{2R_{\rm vdW}^2}{r_c^2}, \tag{2.19}$$

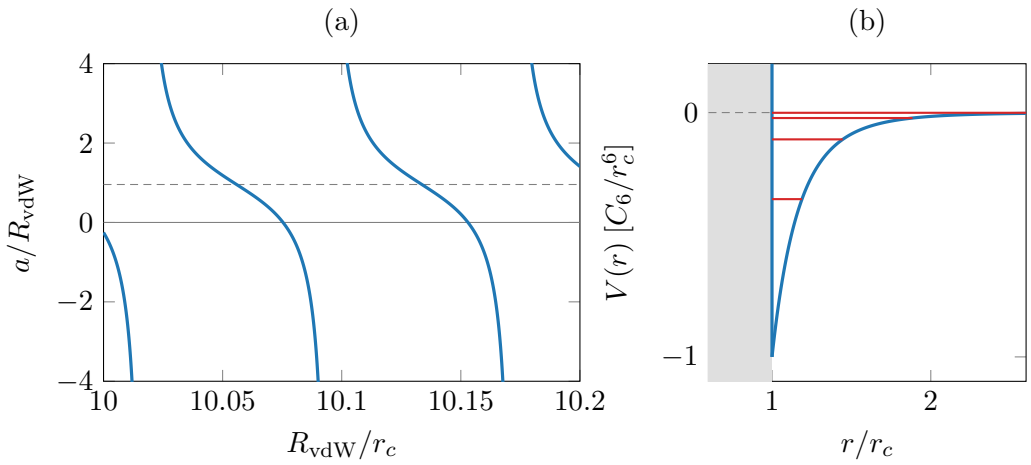


Figure 4: (a) Scattering length of the truncated van der Waals potential as a function of R_{vdW}/r_c, given by (2.18). The dashed line indicates the value $\bar{a} \simeq 0.956\, R_{\mathrm{vdW}}$. A tiny change of the potential leads to large variations of a, which diverges each time a new bound state appears. (b) Truncated van der Waals potential (blue) and its s-wave bound states (red lines, computed numerically for $R_{\mathrm{vdW}}/r_c = 2.6$; realistic potentials correspond to much larger values of R_{vdW}/r_c and host many more bound states). The shaded area is the hard core.

corrected by a constant phase. Since $\Phi \gg 1$ for a deep potential, the scattering length is extremely sensitive to the details of the short-distance potential: a tiny change of r_c changes Φ by a large amount, and the scattering length then varies over all values between $-\infty$ and $+\infty$ (see Fig. 4a). For real atoms, the short-distance potential is not known with sufficient accuracy to predict the scattering length, which must be measured. Nevertheless, for a random value of the phase $\Phi \pmod{\pi}$, the scattering length is of order $\bar{a} \sim R_{\mathrm{vdW}}$ in most cases: the typical value of $|a|$ is the van der Waals length.

The number of s-wave bound states of the potential is given by $N_b \simeq \Phi/\pi$ (up to rounding). The scattering length diverges each time $\Phi - 3\pi/8$ crosses $\pi/2 \pmod{\pi}$, i.e. each time the potential becomes deep enough to host a new bound state, which appears at the threshold $E = 0$. This phenomenon is a *shape resonance*: close to the appearance of a bound state, the scattering length is large and positive, while it is large and negative just before the bound state appears. This connection between the divergence of a and the threshold of a bound state is general, as we will see with the pseudo-potential.

2.1.7 The pseudo-potential

The zero-energy wave-function (2.11) shows that, outside the range of the potential, the low-energy scattering states only depend on the scattering length a. The scattering length thus contains all the relevant information on the interactions, and we expect to obtain the same low-energy physics with any potential leading to the same value of a. In a dilute gas, where the inter-particle distance is much larger than R_{vdW}, this allows one to replace the true interatomic potential, which is complicated and hosts many deep bound states, by a simple model potential. The simplest choice is a potential of zero range. A Dirac potential $g\,\delta(\mathbf{r})$ is not adequate in three dimensions, since the

wave-function (2.11) diverges at the origin. The appropriate zero-range potential is the pseudo-potential [19]

$$V_{\rm pp}[\psi(\mathbf{r})] = g\,\delta(\mathbf{r})\frac{\partial[r\psi(\mathbf{r})]}{\partial r}, \qquad g = \frac{4\pi\hbar^2 a}{m} = \frac{2\pi\hbar^2 a}{\mu}. \tag{2.20}$$

The operator $\partial_r(r\,\cdot)$ evaluated at the origin extracts the regular part of the wave-function: writing $\psi(\mathbf{r}) = c/r + \psi_{\rm reg}(\mathbf{r})$, with $\psi_{\rm reg}$ regular at the origin, we have $V_{\rm pp}[\psi] = g\,\psi_{\rm reg}(\mathbf{0})\,\delta(\mathbf{r})$. On a regular wave-function, the pseudo-potential acts as a simple Dirac potential $g\,\delta(\mathbf{r})$. The pseudo-potential is convenient since it has a simple expression, a single parameter, and an exactly zero range.

Zero-energy scattering state. Let us check that the wave-function (2.11) is an exact solution of the zero-energy Schrödinger equation with the pseudo-potential, for all $r > 0$ including the origin,

$$0 = -\frac{\hbar^2}{2\mu}\Delta\psi + V_{\rm pp}[\psi]. \tag{2.21}$$

We use the two properties

- $\Delta\psi = 4\pi a\,\delta(\mathbf{r})$, which follows from the identity $\Delta(1/r) = -4\pi\delta(\mathbf{r})$, valid in the sense of distributions;
- $\partial_r(r\psi) = \partial_r(r-a) = 1$, so that $V_{\rm pp}[\psi] = g\,\delta(\mathbf{r})$.

The Schrödinger equation then reads $-\frac{\hbar^2}{2\mu}4\pi a\,\delta(\mathbf{r}) + g\,\delta(\mathbf{r}) = 0$, which is satisfied for $g = 2\pi\hbar^2 a/\mu = 4\pi\hbar^2 a/m$. The singular term $-a/r$ of the wave-function is precisely the one that compensates the Dirac term produced by the pseudo-potential.

More generally, the pseudo-potential is equivalent to the free Schrödinger equation for $r > 0$ supplemented by the Bethe-Peierls boundary condition $\psi(\mathbf{r}) \propto 1 - a/r$ for $r \to 0$. One can check that the full scattering state $\psi(\mathbf{r}) = \mathrm{e}^{\mathrm{i}kz} + f_k \mathrm{e}^{\mathrm{i}kr}/r$, with f_k given by (2.9), is an exact eigenstate of the pseudo-potential at all energies: the pseudo-potential reproduces the low-energy scattering amplitude exactly. We now recover this result from the momentum-space representation.

2.1.8 Scattering amplitude in momentum space

Many-body calculations (in particular the BCS theory of section 3) are conveniently performed in momentum space. We decompose a wave-function on plane waves, with the conventions

$$\psi(\mathbf{r}) = \int \frac{\mathrm{d}^3k}{(2\pi)^3}\,\tilde\psi(\mathbf{k})\,\mathrm{e}^{\mathrm{i}\mathbf{k}\cdot\mathbf{r}}, \qquad \tilde\psi(\mathbf{k}) = \int \mathrm{d}^3r\,\psi(\mathbf{r})\,\mathrm{e}^{-\mathrm{i}\mathbf{k}\cdot\mathbf{r}}. \tag{2.22}$$

Since the pseudo-potential produces a term proportional to $\delta(\mathbf{r})$, whose Fourier transform is uniform, the Schrödinger equation (2.1) reads in momentum space

$$E\,\tilde\psi(\mathbf{k}) = \frac{\hbar^2k^2}{m}\tilde\psi(\mathbf{k}) + \frac{4\pi\hbar^2 a}{m}\int\frac{\mathrm{d}^3k'}{(2\pi)^3}\Lambda(k')\,\tilde\psi(\mathbf{k}'), \tag{2.23}$$

where we used $\hbar^2k^2/2\mu = \hbar^2k^2/m$, and where the function $\Lambda(k)$ encodes the action of the regularizing operator $\partial_r(r\,\cdot)$ on a plane wave,

$$\delta(\mathbf{r})\frac{\partial}{\partial r}\left(r\,\mathrm{e}^{\mathrm{i}\mathbf{k}\cdot\mathbf{r}}\right) = \Lambda(k)\,\delta(\mathbf{r}). \tag{2.24}$$

The function $\Lambda(k)$ is a generalized distribution characterized by the two properties

$$\Lambda(k) = 1 \quad \text{for} \quad k < \infty, \tag{2.25}$$

$$\int \mathrm{d}^3k\,\frac{\Lambda(k)}{k^2} = 4\pi\int_0^\infty \Lambda(k)\,\mathrm{d}k = 0. \tag{2.26}$$

The first property expresses that the pseudo-potential acts as a Dirac potential on regular functions such as plane waves. The second one results from the action of the pseudo-potential on the singular function $\psi(\mathbf{r}) = 1/r$, for which $\partial_r(r\psi) = 0$: since the Fourier transform of $1/r$ is $4\pi/k^2$, the integral in (2.23) must vanish for $\tilde\psi(\mathbf{k}) = 4\pi/k^2$. These two properties are incompatible for an ordinary function: $\Lambda(k)$ includes a singular contribution at $k = \infty$, which can be represented as the limit $k_c \to \infty$ of $\theta(k_c - k) - k_c\,\delta(k - k_c)$. In practice, one never needs this explicit form: one uses (2.26) to subtract a term that makes the integrals convergent, and then sets $\Lambda = 1$.

A useful identity. For $\alpha > 0$, we have

$$\int \frac{\mathrm{d}^3k}{(2\pi)^3}\frac{\Lambda(k)}{k^2+\alpha} = -\frac{\sqrt{\alpha}}{4\pi}. \tag{2.27}$$

Indeed, subtracting the vanishing integral (2.26), we obtain a convergent integral in which we can set $\Lambda = 1$,

$$\int \frac{\mathrm{d}^3k}{(2\pi)^3}\Lambda(k)\left[\frac{1}{k^2+\alpha} - \frac{1}{k^2}\right] = -\frac{\alpha}{2\pi^2}\int_0^\infty \frac{\mathrm{d}k}{k^2+\alpha} = -\frac{\alpha}{2\pi^2}\frac{\pi}{2\sqrt{\alpha}} = -\frac{\sqrt{\alpha}}{4\pi}. \tag{2.28}$$

The identity extends by analytic continuation to complex values of α, with the determination of $\sqrt{\alpha}$ of positive real part. In particular, for $\alpha = -k^2 - \mathrm{i}\eta$ (with $\eta \to 0^+$), we have $\sqrt{\alpha} = -\mathrm{i}k$.

Scattering amplitude. We look for a scattering state of energy $E = \hbar^2k^2/m$, with an incoming plane wave $\mathbf{k} = k\mathbf{e}_z$. We write the integral in (2.23) as $\mathcal{I} = \int \Lambda(k')\tilde\psi(\mathbf{k}')\,\mathrm{d}^3k'/(2\pi)^3$. The solution of (2.23) containing the incoming plane wave and an outgoing scattered wave reads

$$\tilde\psi(\mathbf{k}') = (2\pi)^3\delta(\mathbf{k}' - \mathbf{k}) + \frac{g\,\mathcal{I}}{E - \hbar^2k'^2/m + \mathrm{i}\eta}. \tag{2.29}$$

Inserting this expression in the definition of $\mathcal{I}$ and using (2.27) with $\alpha = -k^2 - \mathrm{i}\eta$, we get

$$\mathcal{I} = \Lambda(k) - g\,\mathcal{I}\,\frac{m}{\hbar^2}\int \frac{\mathrm{d}^3k'}{(2\pi)^3}\frac{\Lambda(k')}{k'^2 - k^2 - \mathrm{i}\eta} = 1 - \mathrm{i}ka\,\mathcal{I}, \qquad \text{i.e.} \qquad \mathcal{I} = \frac{1}{1+\mathrm{i}ka}. \tag{2.30}$$

The scattered wave is then $g\mathcal{I}$ times the Fourier transform of $1/(E - \hbar^2k'^2/m + \mathrm{i}\eta)$, which is the outgoing Green function $-(m/4\pi\hbar^2)\mathrm{e}^{\mathrm{i}kr}/r$. We thus obtain

$$\psi(\mathbf{r}) = \mathrm{e}^{\mathrm{i}kz} - \frac{a}{1+\mathrm{i}ka}\frac{\mathrm{e}^{\mathrm{i}kr}}{r}, \tag{2.31}$$

which is the expected scattering state, with the scattering amplitude (2.9), valid here at all energies and for all $r > 0$.

Renormalized coupling constant. The pseudo-potential is equivalent to a contact interaction with a bare coupling constant g_0 and a momentum cutoff k_c, provided that g_0 is adjusted so as to reproduce the scattering length,

$$\frac{1}{g_0} = \frac{m}{4\pi\hbar^2 a} - \int_{k<k_c} \frac{\mathrm{d}^3k}{(2\pi)^3}\frac{m}{\hbar^2k^2} = \frac{m}{4\pi\hbar^2 a} - \frac{mk_c}{2\pi^2\hbar^2}. \tag{2.32}$$

The subtracted counterterm plays the same role as the property (2.26). Physical results only depend on a when $k_c \to \infty$. This form is commonly used in the BCS theory of the crossover.

2.1.9 Bound state of the pseudo-potential

We now look for a bound state of the pseudo-potential, i.e. a molecular state of negative energy $E_\mathrm{m} < 0$. Its wave-function obeys the momentum-space Schrödinger equation (2.23),

$$E_\mathrm{m}\tilde{\psi}_\mathrm{m}(\mathbf{k}) = \frac{\hbar^2k^2}{m}\tilde{\psi}_\mathrm{m}(\mathbf{k}) + A, \qquad A = \frac{4\pi\hbar^2 a}{m}\int\frac{\mathrm{d}^3k'}{(2\pi)^3}\Lambda(k')\tilde{\psi}_\mathrm{m}(\mathbf{k}'), \tag{2.33}$$

where the constant A does not depend on $\mathbf{k}$. This gives the momentum-space wave-function

$$\tilde{\psi}_\mathrm{m}(\mathbf{k}) = -\frac{A}{\hbar^2k^2/m - E_\mathrm{m}} = -\frac{mA}{\hbar^2}\frac{1}{k^2+\alpha}, \qquad \alpha = -\frac{mE_\mathrm{m}}{\hbar^2} > 0. \tag{2.34}$$

Inserting this expression in the definition of A and using the identity (2.27), we obtain the self-consistency relation

$$A = -\frac{4\pi\hbar^2 a}{m}\frac{mA}{\hbar^2}\left(-\frac{\sqrt{\alpha}}{4\pi}\right) = A\,a\sqrt{\frac{-mE_\mathrm{m}}{\hbar^2}}. \tag{2.35}$$

A non-trivial solution ($A \neq 0$) requires $a\sqrt{-mE_\mathrm{m}}/\hbar = 1$, which is only possible for $a > 0$. We thus obtain:

- for $a < 0$, the pseudo-potential has no bound state;
- for $a > 0$, it has a single bound state, of energy and wave-function

$$E_\mathrm{m} = -E_b = -\frac{\hbar^2}{ma^2}, \qquad \tilde{\psi}_\mathrm{m}(\mathbf{k}) \propto \frac{1}{1+(ka)^2}, \qquad \psi_\mathrm{m}(\mathbf{r}) = \frac{1}{\sqrt{2\pi a}}\frac{\mathrm{e}^{-r/a}}{r}. \tag{2.36}$$

The real-space wave-function is obtained as the Fourier transform of the Lorentzian (2.34), and it is normalized, since $\int 4\pi r^2|\psi_\mathrm{m}|^2\mathrm{d}r = (2/a)\int_0^\infty \mathrm{e}^{-2r/a}\mathrm{d}r = 1$. The size of the molecule is set by the scattering length, with a mean inter-atomic distance $\langle r\rangle = a/2$. The binding energy $E_b = \hbar^2/ma^2$ coincides with the pole of the scattering amplitude (2.9) at $k = \mathrm{i}/a$.

This bound state is the zero-range limit of the most weakly bound state of a real potential, when the scattering length is much larger than the potential range, $a \gg R_\mathrm{vdW}$. It is then called a *halo* or universal dimer, since its properties only depend on a: the

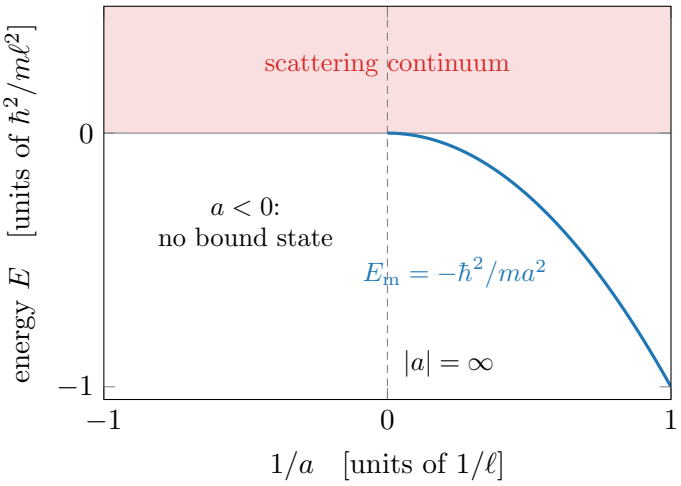


Figure 5: Two-body spectrum of the pseudo-potential as a function of the inverse scattering length, in units of an arbitrary length ℓ. Above the threshold $E = 0$ lies the continuum of scattering states. For $a > 0$, a bound state exists, of energy $E_m = -\hbar^2/ma^2$ (blue line), which merges into the continuum when $a \to +\infty$.

wave-function mostly lies outside the potential range, in the classically forbidden region. The deeper bound states of the real potential, of size $\sim R_{vdW}$ or smaller, are not described by the pseudo-potential; they will play a role in the inelastic losses discussed in section 2.3.

The variation of the bound-state energy with $1/a$ is shown in Fig. 5. The binding energy vanishes when $a \to +\infty$: as for the toy model, the divergence of the scattering length coincides with the appearance of a bound state at threshold. When $1/a$ is varied continuously from negative to positive values, through $1/a = 0$, the two-body physics evolves smoothly from a weak attraction without bound state to the existence of a deeper and deeper molecular state. This is the two-body counterpart of the BEC-BCS crossover: in a many-body system, the BCS regime corresponds to $1/k_F a \to -\infty$, the BEC regime of molecules to $1/k_F a \to +\infty$, and the strongly interacting regime to $|1/k_F a| \lesssim 1$, for which the binding energy E_b, when it exists, is comparable to or smaller than the Fermi energy (since $E_b/E_F = 2/(k_F a)^2$).

2.2 Feshbach resonances

The toy model shows that the scattering length diverges when a bound state crosses the collision threshold. In order to explore the BEC-BCS crossover, we need a way to tune the scattering length in a controlled manner. Since the interatomic potential cannot be modified directly, one uses the internal structure of the atoms: a scattering resonance occurs when the energy of the colliding atoms is tuned close to a bound state of a different internal state, called a Feshbach resonance. In this subsection, we describe its principle, solve a simple two-channel model, and discuss experimental examples.

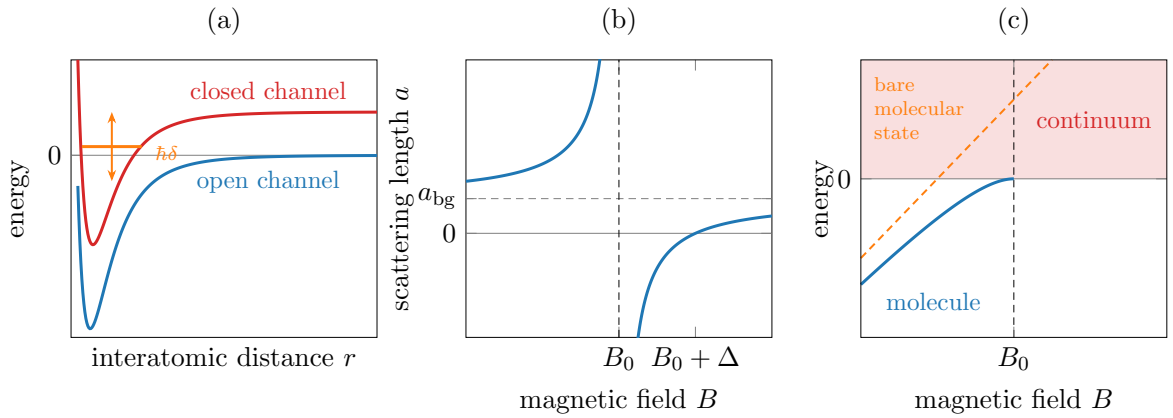


Figure 6: (a) Principle of a Feshbach resonance: two atoms collide in the open channel (blue) and are coupled to a molecular state (orange) of the closed channel (red), whose energy $\hbar\delta$ relative to the open-channel threshold is tuned with the magnetic field. (b) Scattering length close to a Feshbach resonance, given by (2.45) (here for $a_{\rm bg} > 0$, $\Delta > 0$). (c) Two-body spectrum (schematic): a weakly bound molecular state exists on the side of the resonance where $a > 0$, with the universal energy $-\hbar^2/ma^2$ close to resonance. Far from resonance, it continuously connects to the bare closed-channel state (dashed line).

2.2.1 Principle of a Feshbach resonance

Alkali atoms have a hyperfine structure, and two colliding atoms can be in different internal (spin) configurations, called collision *channels*, each of them associated with an interatomic potential. We consider two atoms colliding at low energy in a given channel, the *open channel*, whose asymptotic energy defines the threshold $E = 0$. We assume that the atoms are coupled, at short distance, to another channel, the *closed channel*, whose asymptotic energy lies above the collision energy, so that two atoms cannot exit the collision in this channel. The closed-channel potential nevertheless hosts molecular bound states, and one of them may lie close to the open-channel threshold (see Fig. 6a).

The coupling between the two channels results from the part of the interaction that depends on the electron spins (exchange interaction, combined with the hyperfine coupling). During the collision, the atoms are virtually transferred into the closed-channel molecular state. This virtual population modifies the scattering phase shift in the open channel, in a resonant manner when the energy of the molecular state approaches the threshold. Since the two channels correspond to different spin configurations, they usually have different magnetic moments, so that the energy difference between the closed and open channels can be tuned with an external magnetic field B, via the Zeeman effect. This allows one to tune the scattering length. Feshbach resonances were first observed with ultracold atoms in a Bose-Einstein condensate of sodium atoms [20]; they are reviewed in Ref. [21].

2.2.2 A solvable two-channel model

We consider a simplified model, which captures the essential physics and can be solved exactly. The relative motion of the two atoms is described by a wave-function with two components, in the open channel $|\mathrm{o}\rangle$ and in the closed channel $|\mathrm{c}\rangle$. We assume that:

- there are no interactions in the open channel, whose Hamiltonian is $\hat{H}_{\rm o} = -\frac{\hbar^2}{2\mu}\Delta$;
- the closed channel only contributes via a single molecular state, of normalized real wave-function $\phi_{\rm m}(\mathbf{r})$ (of size $r_{\rm m}$, spherically symmetric), and of energy $\hbar\delta$ relative to the open-channel threshold, i.e. $\hat{H}_{\rm c} = \hbar\delta|\phi_{\rm m}\rangle\langle\phi_{\rm m}|$;
- the two channels are coupled by a position-independent coupling $\hbar\Omega$, i.e. $\hat{W} = \hbar\Omega(|{\rm c}\rangle\langle{\rm o}| + |{\rm o}\rangle\langle{\rm c}|)$.

We look for a scattering state of the form

$$|\psi\rangle = [{\rm e}^{{\rm i}kz} + \psi_{\rm sc}(\mathbf{r})]|{\rm o}\rangle + \alpha\,\phi_{\rm m}(\mathbf{r})|{\rm c}\rangle, \tag{2.37}$$

of energy $E = \hbar^2k^2/m$, where α is the amplitude in the closed channel. Projecting the Schrödinger equation on the two channels, we obtain

$$\left(E + \frac{\hbar^2}{2\mu}\Delta\right)\psi_{\rm sc}(\mathbf{r}) = \hbar\Omega\,\alpha\,\phi_{\rm m}(\mathbf{r}), \tag{2.38}$$

$$(E - \hbar\delta)\,\alpha = \hbar\Omega\int {\rm d}^3r\,\phi_{\rm m}(\mathbf{r})\left[{\rm e}^{{\rm i}kz} + \psi_{\rm sc}(\mathbf{r})\right]. \tag{2.39}$$

The first equation shows that the open channel is fed by a source term proportional to the molecular wave-function. Its outgoing solution reads, in terms of the Fourier transform $\tilde{\phi}_{\rm m}(q) = \int {\rm d}^3r\,\phi_{\rm m}(\mathbf{r}){\rm e}^{-{\rm i}\mathbf{q}\cdot\mathbf{r}}$,

$$\psi_{\rm sc}(\mathbf{r}) = \hbar\Omega\,\alpha\int\frac{{\rm d}^3q}{(2\pi)^3}\frac{\tilde{\phi}_{\rm m}(q)\,{\rm e}^{{\rm i}\mathbf{q}\cdot\mathbf{r}}}{E - \hbar^2q^2/m + {\rm i}\eta} \underset{r\to\infty}{\simeq} -\frac{m\,\Omega\,\alpha\,\tilde{\phi}_{\rm m}(k)}{4\pi\hbar}\frac{{\rm e}^{{\rm i}kr}}{r}, \tag{2.40}$$

where the asymptotic form is obtained, as in the standard derivation of the Lippmann-Schwinger equation, from the outgoing Green function $-(m/4\pi\hbar^2){\rm e}^{{\rm i}k|\mathbf{r}-\mathbf{r}'|}/|\mathbf{r}-\mathbf{r}'|$. Inserting the expression of $\psi_{\rm sc}$ in (2.39), we obtain a closed equation for α,

$$(E - \hbar\delta)\,\alpha = \hbar\Omega\,\tilde{\phi}_{\rm m}(k) + \hbar^2\Omega^2\alpha\int\frac{{\rm d}^3q}{(2\pi)^3}\frac{\tilde{\phi}_{\rm m}(q)^2}{E - \hbar^2q^2/m + {\rm i}\eta}. \tag{2.41}$$

In the low-energy limit $E \to 0$, the integral reduces to $-(m/2\pi^2\hbar^2)\int_0^\infty \tilde{\phi}_{\rm m}(q)^2{\rm d}q$, and we obtain

$$\alpha = \frac{\Omega\,\tilde{\phi}_{\rm m}(0)}{\delta_0 - \delta}, \qquad \delta_0 = \frac{m\Omega^2}{2\pi^2\hbar}\int_0^\infty \tilde{\phi}_{\rm m}(q)^2\,{\rm d}q. \tag{2.42}$$

The closed channel is populated resonantly, with a pole at $\delta = \delta_0$. The resonance does not occur when the bare molecular state crosses the threshold ($\delta = 0$), but for a detuning $\delta_0 > 0$: the coupling to the continuum of open-channel states, which lie above the molecular state, shifts it downwards, by an amount which is the second-order energy shift $-\hbar\delta_0$ due to the coupling to all open-channel states. Note that this shift scales as $\int\tilde{\phi}_{\rm m}^2{\rm d}q \sim \tilde{\phi}_{\rm m}(0)^2/r_{\rm m}$ and it would diverge for a pointlike molecule.

The scattered wave gives the scattering amplitude $f = -m\Omega\alpha\tilde{\phi}_{\rm m}(0)/(4\pi\hbar)$, hence the scattering length

$$a = -\frac{m\,\Omega^2\,\tilde{\phi}_{\rm m}(0)^2}{4\pi\hbar\,(\delta - \delta_0)}. \tag{2.43}$$

The scattering length diverges at the resonance $\delta = \delta_0$. It is positive for $\delta < \delta_0$ and negative for $\delta > \delta_0$, and it can thus be tuned to arbitrary values by varying the detuning δ. Far from resonance, a vanishes in this model, since we neglected interactions in the open channel.

Bound state. The same equations, written for a negative energy $E = -\hbar^2\kappa^2/m$ and without incoming wave, give the bound states of the model. The closed-channel amplitude obeys $(E - \hbar\delta)\alpha = \hbar^2\Omega^2\alpha \int \mathrm{d}^3q/(2\pi)^3\, \tilde{\phi}_{\mathrm{m}}(q)^2/(E - \hbar^2q^2/m)$. Close to resonance, we expect a small binding energy, and we split the integral into its value at $E = 0$ (giving $-\hbar\delta_0$) and a remainder dominated by small momenta $q \sim \kappa \ll 1/r_{\mathrm{m}}$, for which $\tilde{\phi}_{\mathrm{m}}(q) \simeq \tilde{\phi}_{\mathrm{m}}(0)$. Using the identity (2.27), we get

$$E - \hbar(\delta - \delta_0) = \frac{m\Omega^2\tilde{\phi}_{\mathrm{m}}(0)^2}{4\pi}\,\kappa = \hbar(\delta_0 - \delta)\,a\,\kappa, \tag{2.44}$$

where we used (2.43). Close enough to resonance, when the binding energy $|E|$ is small compared to $\hbar|\delta - \delta_0|$, this gives $\kappa = 1/a$, i.e. the universal bound state $E = -\hbar^2/ma^2$ of the pseudo-potential, which exists for $a > 0$ only. This condition reads $a \gg R^*$, with $R^* = 4\pi\hbar^2/[m^2\Omega^2\tilde{\phi}_{\mathrm{m}}(0)^2]$ a length characterizing the strength of the resonance. In this universal regime, the molecular state mostly lies in the open channel, as a halo dimer of size $\sim a$. Far from resonance, the bound state energy instead follows the (shifted) energy of the closed-channel molecular state, varying linearly with δ, and the molecule mostly lies in the closed channel (see Fig. 6c). Resonances for which R^* is much smaller than the inter-particle distance (called broad, or open-channel dominated, resonances) are well described by the pseudo-potential over the whole strongly interacting regime.

2.2.3 Magnetic-field dependence of the scattering length

When the open and closed channels have different magnetic moments, with a difference $\delta\mu$, the detuning varies linearly with the magnetic field, $\hbar\delta = \delta\mu\,(B - B_c)$, where B_c is the field at which the bare molecular state crosses the threshold. The resonance occurs at the field $B_0 = B_c + \hbar\delta_0/\delta\mu$, and the scattering length (2.43) takes the form $a \propto -1/(B - B_0)$. Including a background scattering length a_{bg} due to the interactions in the open channel, one obtains the generic form of the scattering length close to a Feshbach resonance [21],

$$a(B) = a_{\mathrm{bg}}\left(1 - \frac{\Delta}{B - B_0}\right), \tag{2.45}$$

where Δ is the width of the resonance, which corresponds to the distance between the resonance position B_0 and the zero crossing of the scattering length at $B = B_0 + \Delta$ (see Fig. 6b). Comparing with (2.43), the resonance strength is related to the parameters of the model as $a_{\mathrm{bg}}\Delta\,\delta\mu = m\Omega^2\tilde{\phi}_{\mathrm{m}}(0)^2/4\pi$, and the length R^* introduced above reads $R^* = \hbar^2/(ma_{\mathrm{bg}}\Delta\,\delta\mu)$.

On the side of the resonance where $a > 0$, a weakly bound molecular state exists, of energy $-\hbar^2/ma^2$ close to resonance, which disappears into the continuum at $B = B_0$ (see Fig. 6c). Scanning the magnetic field across the resonance thus allows one to continuously connect a gas of atoms with attractive interactions ($a < 0$) to a gas of weakly bound molecules ($a > 0$): this is the experimental knob used to explore the BEC-BCS crossover.

2.2.4 Examples of Feshbach resonances

Two fermionic alkali atoms have been mostly used to study the BEC-BCS crossover, ^{40}K and ^{6}Li, whose resonances are shown in Fig. 7.

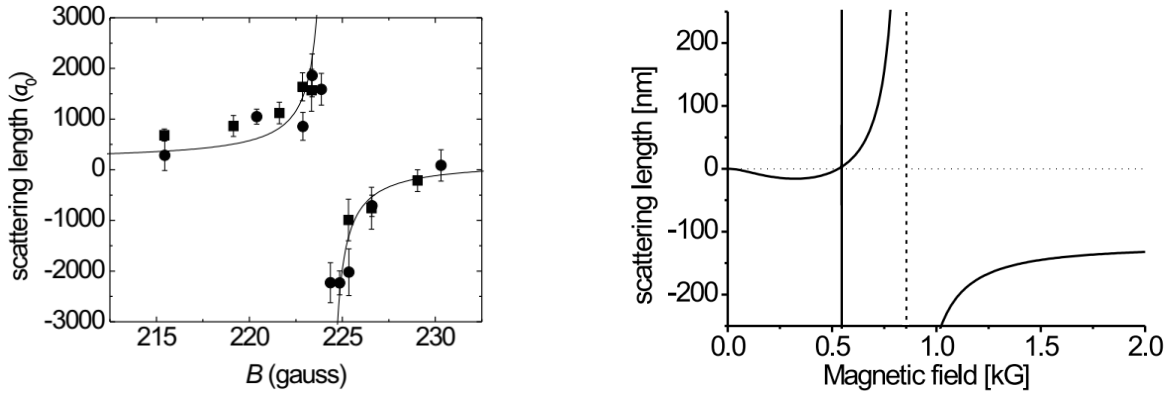


Figure 7: Left: scattering length of ^{40}K atoms in the states $|9/2, -9/2\rangle$ and $|9/2, -7/2\rangle$ close to the Feshbach resonance at 224 G, measured from the mean-field interaction energy, figure from Ref. [22]. The line is a fit with the form (2.45). Right: scattering length of ^{6}Li atoms in the two lowest hyperfine states, from coupled-channel calculations, showing the broad resonance at 832 G (dashed line) and the zero crossing at 527 G (solid line), adapted from the work of Ref. [23].

- For ^{40}K atoms prepared in the two lowest Zeeman states $|F = 9/2, m_F = -9/2\rangle$ and $|F = 9/2, m_F = -7/2\rangle$, a resonance occurs at $B_0 \simeq 224\,\mathrm{G}$, with a width $\Delta \simeq 10\,\mathrm{G}$ and a background scattering length $a_{\mathrm{bg}} \simeq 174\,a_0$ [22]. The scattering length was measured from the mean-field interaction energy, which shifts the frequency of a radio-frequency transition towards a third, non-interacting spin state. The measurements reproduce the dispersive shape (2.45), with values of $|a|$ up to a few thousand Bohr radii.

- For ^{6}Li atoms in the two lowest hyperfine states, a very broad resonance occurs at $B_0 \simeq 832\,\mathrm{G}$. The background scattering length is large and negative (of the order of $-2000\,a_0$ at high field), and the scattering length crosses zero at $B \simeq 527\,\mathrm{G}$. The extremely large width of this resonance (several hundreds of gauss) makes it particularly convenient to explore the whole crossover, since the scattering length can be controlled with a very good relative accuracy. It is the resonance used in most experiments on the BEC-BCS crossover.

Atoms with a richer electronic structure, such as the magnetic lanthanides erbium and dysprosium, exhibit much denser spectra of Feshbach resonances, with several resonances per gauss, as a consequence of their anisotropic interactions.

2.3 Collisional stability: bosons versus fermions

Feshbach resonances allow one to reach very large scattering lengths. However, the pseudo-potential only describes elastic two-body collisions, and it ignores the deep molecular states of the true interaction potential. In this subsection, we show that inelastic processes towards these deep states, which involve three atoms, prevent the study of strongly interacting Bose gases, while two-component Fermi gases are protected by the Pauli principle. We first discuss what is meant by a strongly interacting regime.

2.3.1 Towards a strongly interacting regime

In most experiments, a Bose-Einstein condensate is well described by mean-field theory, i.e. by a classical field obeying the Gross-Pitaevskii equation, with an interaction energy density $gn^2/2$ (with $g = 4\pi\hbar^2 a/m$ and n the density). The first quantum corrections to mean-field theory are given by the Bogoliubov theory of the weakly interacting Bose gas, which predicts:

- the Lee-Huang-Yang correction to the ground-state energy [24],

$$\frac{E}{V} = \frac{1}{2}\frac{4\pi\hbar^2 a}{m} n^2 \left(1 + \frac{128}{15\sqrt{\pi}}\sqrt{na^3}\right), \tag{2.46}$$

  where V is the volume;

- the quantum depletion of the condensate at zero temperature, i.e. the fraction of atoms that do not occupy the condensate mode,

$$\frac{n_0}{n} = 1 - \frac{8}{3\sqrt{\pi}}\sqrt{na^3}, \tag{2.47}$$

  where n_0 is the condensate density.

Both corrections involve the gas parameter na^3, which compares the scattering length to the inter-particle distance $n^{-1/3}$. In standard conditions, with $n = 10^{14}\,\mathrm{cm}^{-3}$ and $a = 100\,a_0$, we have $na^3 \simeq 10^{-5}$, so that the corrections are of the order of $\sqrt{na^3} \sim 3 \times 10^{-3}$ and the gas is weakly interacting. The strongly interacting regime corresponds to $na^3 \sim 1$, where the Bogoliubov expansion breaks down. Using a Feshbach resonance to increase the scattering length, the beyond-mean-field corrections could be observed, as shown in Fig. 8: the equation of state of a strongly interacting ^{7}Li Bose gas revealed the Lee-Huang-Yang correction [25], and the quantum depletion was measured in a homogeneous ^{39}K condensate [26]. However, these experiments remained limited to moderate values of the gas parameter ($\sqrt{na^3} \lesssim 0.04$ in Fig. 8), because of the inelastic losses discussed below.

2.3.2 Three-body recombination in Bose gases

The atoms of an ultracold gas are not in the absolute ground state of the system: the interatomic potential supports many deeply bound molecular states, of binding energies of the order of E_{vdW} or larger, i.e. much larger than the temperature and the trap depth. The gas is thus a metastable state, which survives only because the formation of molecules is slow. Indeed, the formation of a molecule in a two-body collision is forbidden by energy and momentum conservation, and it requires a third body that carries away the binding energy. In a three-body recombination event (see Fig. 9), two atoms form a deeply bound molecule, and the released binding energy is converted into kinetic energy of the molecule and of the third atom, which both escape from the trap. The resulting losses are described by the rate equation

$$\dot{N} \simeq -L_3\, n^2 N, \tag{2.48}$$

where L_3 is the three-body loss coefficient, expressed in $\mathrm{cm}^6\,\mathrm{s}^{-1}$ (for an inhomogeneous gas, n^2 is replaced by the average $\langle n^2 \rangle$).

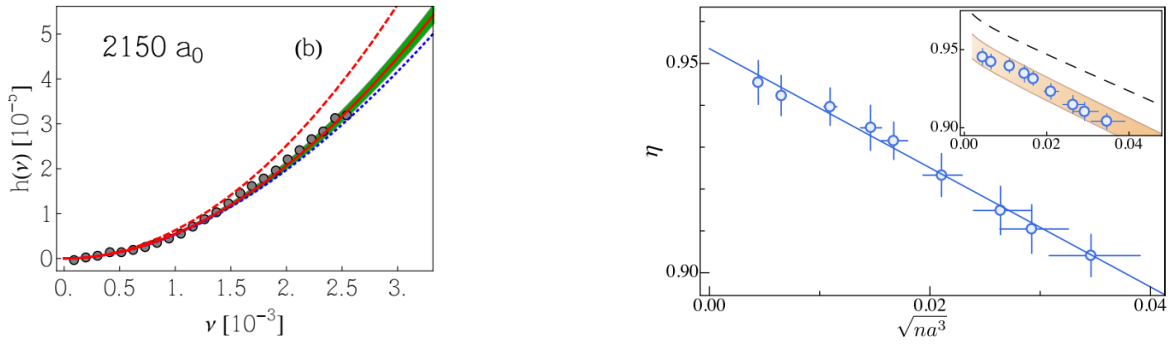


Figure 8: Beyond-mean-field effects in Bose-Einstein condensates with large scattering lengths. Left: dimensionless equation of state of a ^{7}Li Bose gas with a scattering length $a = 2150\, a_0$, measured from in situ density profiles and compared with theoretical predictions with and without the Lee-Huang-Yang correction, figure from Ref. [25] (see this reference for the definition of the dimensionless variables). Right: condensed fraction η of a homogeneous ^{39}K condensate as a function of $\sqrt{na^3}$. Its linear decrease reveals the quantum depletion (2.47), figure from Ref. [26].

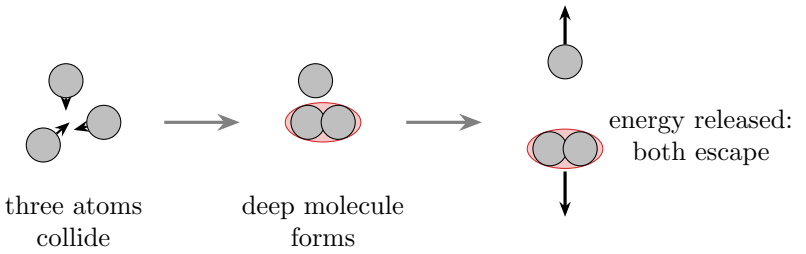


Figure 9: Three-body recombination: when three atoms come close to each other, two of them can form a deeply bound molecule (red). The binding energy is released as kinetic energy, and both the molecule and the third atom are lost from the trap.

Scaling with the scattering length. For a large scattering length, $a \gg R_{\rm vdW}$, the three-body problem at low energy becomes universal, and the scattering length is the only relevant length scale. The loss coefficient L_3, which has the dimension of a length to the power six divided by a time, can only be constructed from a and $\hbar/m$ (which has the dimension of a length squared divided by a time), leading to

$$L_3 = C\,\frac{\hbar a^4}{m}, \tag{2.49}$$

where C is a dimensionless coefficient. In fact, C is not strictly constant, but it exhibits log-periodic oscillations in a, associated with the Efimov effect, i.e. the existence of an infinite series of three-body bound states for $|a| \to \infty$ [27]. The a^4 scaling was observed with cesium atoms [28] (see Fig. 10). For instance, for $a = 1500\,a_0$, we have $\hbar a^4/m \simeq 2 \times 10^{-26}\,\mathrm{cm^6\,s^{-1}}$, while the measured value is of the order of $L_3 \sim 4 \times 10^{-24}\,\mathrm{cm^6\,s^{-1}}$, corresponding to $C \sim 200$. For a density $n = 10^{13}\,\mathrm{cm^{-3}}$, this gives a loss rate $L_3 n^2 \sim 400\,\mathrm{s^{-1}}$, i.e. a lifetime of a few milliseconds.

Consequence for strongly interacting Bose gases. The losses become a severe limitation for scattering lengths $a \gtrsim 1000\,a_0$. The loss rate can be written as

$$L_3 n^2 = C\,(na^3)^2\,\frac{\hbar}{ma^2}. \tag{2.50}$$

In the strongly interacting regime $na^3 \sim 1$, the lifetime of the gas becomes comparable to $ma^2/\hbar \sim mn^{-2/3}/\hbar$, which is also the time scale associated with the interaction and kinetic energies. The gas thus decays before reaching thermal equilibrium, and strongly interacting Bose gases cannot be studied at equilibrium (they can only be probed with dynamical protocols, faster than the losses).

2.3.3 Three-body recombination in Fermi gases

The situation is very different for a two-component Fermi gas. We recall that two-body collisions between identical fermions are suppressed at low energy (see section 2.1.4). A three-body recombination event in a mixture of $\uparrow$ and $\downarrow$ atoms necessarily involves two identical fermions, e.g. $\uparrow\uparrow\downarrow$. Since the deep molecular states have a size $\sim R_{\rm vdW}$, the recombination requires the three atoms to approach each other within a distance $\sim R_{\rm vdW}$, and thus two identical fermions to be at a distance $\lesssim R_{\rm vdW}$ from each other. This is suppressed by the Pauli principle.

Pauli suppression argument. The argument was made quantitative by Petrov, Salomon and Shlyapnikov [29], who considered a gas of weakly bound dimers on the $a > 0$ side of a resonance, with $a \gg R_{\rm vdW}$. Since the atoms of a dimer are at a typical distance a, the relative motion of the atoms involved in a collision between two dimers (or between a dimer and an atom) is characterized by momenta of order $1/a$. The relaxation of a weakly bound dimer into a deep molecular state requires three atoms within a distance $R_{\rm vdW}$, among which two identical fermions. The relative wave-function of two identical fermions being antisymmetric, its amplitude at a short distance r vanishes as $kr \sim r/a$ (it involves odd partial waves only), so that the probability to find them within $R_{\rm vdW}$ is suppressed by a factor of order $(R_{\rm vdW}/a)^2$. A complete solution of the

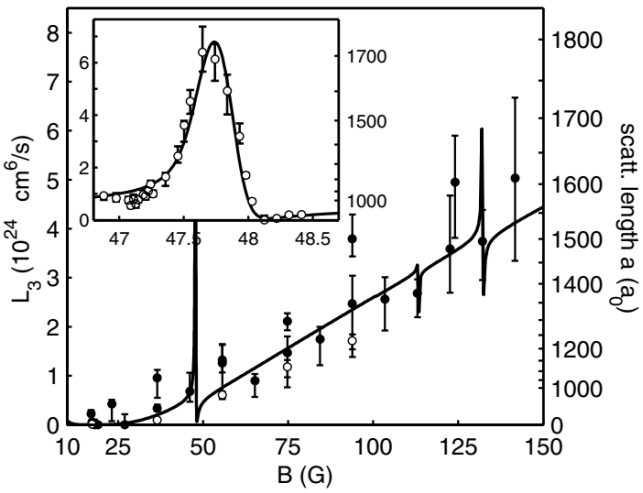


Figure 10: Three-body loss coefficient L_3 of a cesium Bose gas as a function of the magnetic field (data points, left axis). The solid line shows the scattering length (right axis), which increases with the magnetic field (up to narrow resonances). The losses strongly increase with the scattering length, consistently with the scaling $L_3 \propto a^4$. Figure from Ref. [28].

three-body (atom-dimer) and four-body (dimer-dimer) problems gives the scaling laws of the relaxation rate constants

$$\alpha_{\rm ad} \propto \frac{\hbar R_{\rm vdW}}{m}\left(\frac{R_{\rm vdW}}{a}\right)^{3.33}, \qquad \alpha_{\rm dd} \propto \frac{\hbar R_{\rm vdW}}{m}\left(\frac{R_{\rm vdW}}{a}\right)^{2.55}, \tag{2.51}$$

for atom-dimer and dimer-dimer collisions respectively. Contrary to the case of bosons, the inelastic losses thus *decrease* when the scattering length increases. In the same work, the dimer-dimer elastic scattering length was found to be $a_{\rm dd} \simeq 0.6\,a$: weakly bound dimers interact repulsively, which ensures the stability of a Bose-Einstein condensate of such molecules. The ratio between elastic and inelastic collision rates is thus very large close to resonance, which allows the gas to reach thermal equilibrium in the strongly interacting regime. A similar Pauli suppression of three-body recombination holds on the $a < 0$ side of the resonance.

Experimental observation. The suppression of inelastic losses was observed in several experiments with ^{6}Li and ^{40}K, which demonstrated the long lifetime of weakly bound Feshbach molecules close to resonance [30, 31, 32], in agreement with the predictions of Ref. [29]. As an example, Fig. 11 shows the creation of molecules by sweeping the magnetic field across the ^{40}K resonance [33]: about half of the atoms are converted into weakly bound molecules (which are not detected by the atom imaging), and these molecules can then be dissociated back into atoms. This reversible conversion illustrates the stability of Fermi gases close to a Feshbach resonance, which made the exploration of the whole BEC-BCS crossover possible.

Summary. Two-component Fermi gases combine two essential features: the scattering length between $\uparrow$ and $\downarrow$ atoms can be tuned to arbitrary values with a Feshbach resonance,

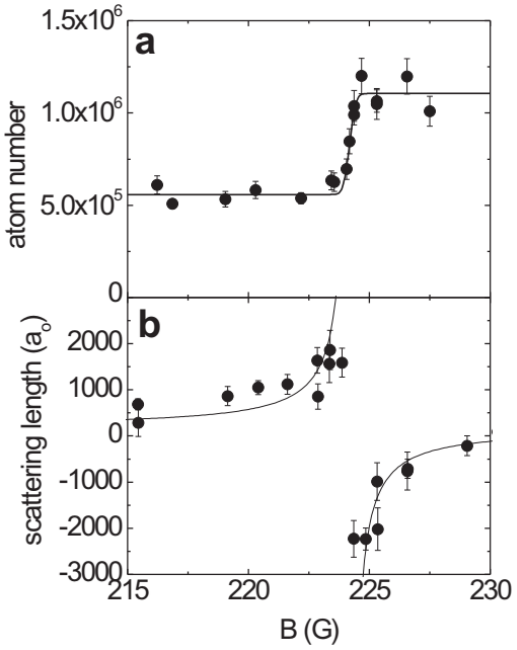


Figure 11: Association of ^{40}K atoms into weakly bound molecules close to the Feshbach resonance at 224 G. (a) Number of atoms detected after a magnetic field sweep across the resonance, ending at the field B: about half of the atoms are converted into molecules when the final field lies on the $a > 0$ side of the resonance. (b) Scattering length across the resonance (same data as Fig. 7). Figure from Ref. [33].

and the gas remains collisionally stable for large scattering lengths. The strongly interacting regime $k_{\rm F}|a| \gtrsim 1$ is thus accessible at thermal equilibrium, with all the properties of the gas determined by the single parameter $1/k_{\rm F}a$ (and the temperature), since the range of the potential is negligible compared to the inter-particle distance. In the following section, we develop the theory of this crossover.

3 Theory of the BEC-BCS crossover

In this section, we develop the theoretical description of a two-component Fermi gas with attractive contact interactions, characterized by the scattering length a (see section 2). We first show, by solving the Cooper problem, that the Fermi sea is unstable towards pairing for an arbitrarily weak attraction. This instability motivates the BCS variational ansatz, which we use to build a mean-field theory of the whole BEC-BCS crossover at zero temperature, in the spirit of Eagles and Leggett [4, 5]. We then extend the theory to finite temperature and discuss the superfluid critical temperature, for which mean-field theory fails on the BEC side. We introduce Tan's contact, which quantifies the short-distance pair correlations, and we end with the universal properties of the unitary Fermi gas, obtained when the scattering length diverges.

Throughout this section, we consider a homogeneous gas of total density n (density $n/2$ per spin component), with the Fermi wave-vector $k_{\rm F} = (3\pi^2 n)^{1/3}$, Fermi energy $E_{\rm F} = \hbar^2 k_{\rm F}^2/2m$ and Fermi temperature $T_{\rm F} = E_{\rm F}/k_{\rm B}$. The interaction strength is

characterized by the dimensionless parameter $1/k_{\mathrm{F}}a$. We use the notations of the AQM lecture notes (chapter on BCS theory): $\epsilon_k = \hbar^2 k^2/2m$ is the free-particle kinetic energy, $\xi_k = \epsilon_k - \mu$ the kinetic energy measured from the chemical potential, Δ the gap parameter and $E_k = \sqrt{\xi_k^2 + \Delta^2}$ the energy of Bogoliubov quasiparticles.

3.1 The Cooper instability

Before developing a full many-body theory, we discuss the possible fates of a Fermi sea subjected to a weak attraction. We show, following Cooper [2], that a pair of fermions above a frozen Fermi sea forms a bound state for an arbitrarily weak attraction, even though no bound state exists in vacuum for $a < 0$. This instability of the Fermi sea is the key to understanding superconductivity and fermionic superfluidity.

3.1.1 The attractive Fermi gas: possible scenarios

In the absence of interactions, the ground state is the Fermi sea, in which each spin component occupies all plane-wave states of wave-vector $k < k_{\mathrm{F}}$. The momentum distribution $n_{\mathbf{k}\sigma} = \langle \hat{a}^\dagger_{\mathbf{k}\sigma} \hat{a}_{\mathbf{k}\sigma} \rangle$ is a step function, equal to 1 for $k < k_{\mathrm{F}}$ and 0 for $k > k_{\mathrm{F}}$ (see Fig. 12a). When a weak interaction is switched on, two scenarios can be considered.

Scenario 1: Fermi liquid. A natural guess is that the interactions only weakly perturb the Fermi sea. According to Landau's theory of Fermi liquids, the low-energy excitations of the interacting system are then quasiparticles, which are in one-to-one correspondence with the excitations of the ideal Fermi gas, but carry renormalized properties (effective mass, interactions between quasiparticles). The momentum distribution is smoothened by interactions, but it keeps a discontinuity at $k = k_{\mathrm{F}}$, of amplitude $Z < 1$, called the quasiparticle residue (see Fig. 12a). In this scenario, the ground-state energy can be computed perturbatively in powers of $k_{\mathrm{F}}a$. To second order, one obtains for a dilute two-component Fermi gas [19, 34]

$$\frac{E}{N} = \frac{3}{5} E_{\mathrm{F}} \left[1 + \frac{10}{9\pi} k_{\mathrm{F}} a + \frac{4(11 - 2\ln 2)}{21\pi^2} (k_{\mathrm{F}} a)^2 + \dots \right]. \tag{3.1}$$

The first-order term is the mean-field (Hartree) energy $g\, n_\uparrow n_\downarrow / n = gn/4$ per particle, with $g = 4\pi\hbar^2 a/m$, which can be checked using $n = k_{\mathrm{F}}^3/3\pi^2$.

Scenario 2: Cooper pairing and superfluidity. For an attractive interaction ($a < 0$), the Fermi liquid is unstable: particles of opposite spins and momenta pair up into Cooper pairs, and the ground state is a superfluid. We will show that this scenario always wins at zero temperature, whatever the strength of the attraction. However, the pairing energy scales and the superfluid critical temperature are non-analytic in the interaction strength and exponentially small in the weak-coupling limit,

$$T_{\mathrm{c}} \sim T_{\mathrm{F}}\, \mathrm{e}^{-\pi/(2k_{\mathrm{F}}|a|)}. \tag{3.2}$$

This expression cannot be expanded in powers of $k_{\mathrm{F}}a$, which explains why superfluidity cannot be obtained at any finite order of the perturbative expansion (3.1). In practice, for weak attractions, superfluidity only occurs at extremely low temperatures, and the Fermi-liquid description remains relevant above T_{c}.

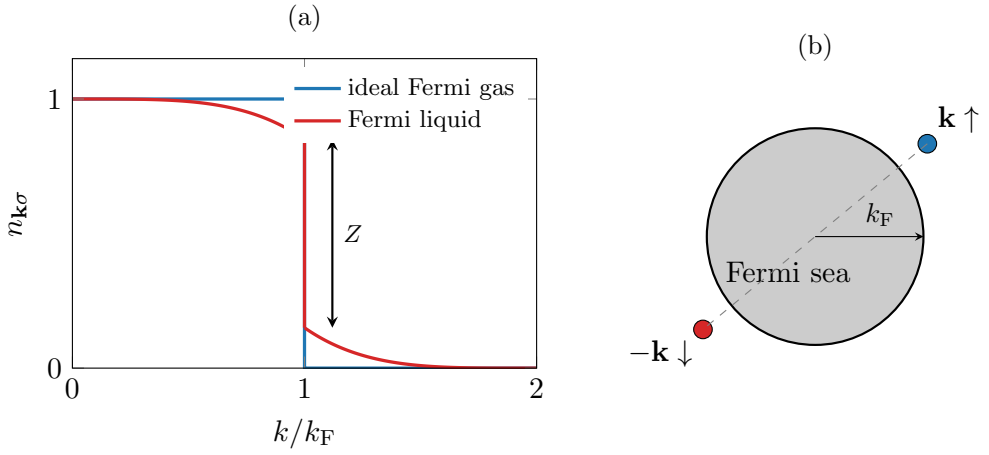


Figure 12: (a) Momentum distribution of an ideal Fermi gas at zero temperature (blue) and schematic momentum distribution of a Fermi liquid (red), which exhibits a discontinuity of amplitude $Z < 1$ at the Fermi momentum. (b) Cooper problem: two particles of opposite spins and momenta $\mathbf{k}\uparrow$ and $-\mathbf{k}\downarrow$ interact above a frozen Fermi sea, which blocks all momentum states $k < k_\mathrm{F}$.

3.1.2 The Cooper problem

In order to understand the pairing instability, Cooper considered a simplified problem: two particles of opposite spins interact via an attractive potential, in the presence of a Fermi sea of other particles that are assumed to be frozen [2]. The only role of the Fermi sea is to block, via the Pauli principle, all momentum states $k < k_\mathrm{F}$ (see Fig. 12b). We consider a pair of zero total momentum, with a relative wave-function $\tilde{\psi}(\mathbf{k})$ in momentum space, the particle $\uparrow$ having momentum $\hbar\mathbf{k}$ and the particle $\downarrow$ momentum $-\hbar\mathbf{k}$. The two-body kinetic energy is $2\epsilon_k = \hbar^2k^2/m$. We look for a bound state of energy

$$E = 2E_\mathrm{F} + \epsilon, \qquad \epsilon < 0, \tag{3.3}$$

i.e. a state of energy lower than the minimal energy $2E_\mathrm{F}$ of two non-interacting particles above the Fermi sea.

We model the interaction by the pseudo-potential of section 2, whose matrix elements between plane waves read $(g/V)\Lambda(k)$, where V is the volume, $g = 4\pi\hbar^2a/m$, and $\Lambda(k)$ is the regularizing distribution, such that $\Lambda(k) = 1$ for finite k and $\int_0^\infty \Lambda(k)\,\mathrm{d}k = 0$. In the thermodynamic limit, the Schrödinger equation reads

$$(2E_\mathrm{F} + \epsilon)\tilde{\psi}(\mathbf{k}) = \frac{\hbar^2k^2}{m}\tilde{\psi}(\mathbf{k}) + A, \qquad A = \frac{4\pi\hbar^2a}{m}\int_{k'>k_\mathrm{F}} \Lambda(k')\tilde{\psi}(\mathbf{k}')\frac{\mathrm{d}^3k'}{(2\pi)^3}, \tag{3.4}$$

with the restriction $k, k' > k_\mathrm{F}$ imposed by Pauli blocking. This is the same equation as for the two-body bound state in vacuum (see section 2), except for this restriction.

3.1.3 Binding energy of the Cooper pair

Since A does not depend on $\mathbf{k}$, the Schrödinger equation (3.4) can be solved for the wave-function, using $2mE_\mathrm{F}/\hbar^2 = k_\mathrm{F}^2$:

$$\tilde{\psi}(\mathbf{k}) = -\frac{mA}{\hbar^2}\,\frac{1}{k^2 - k_\mathrm{F}^2 + \kappa^2}, \qquad \kappa^2 = \frac{m|\epsilon|}{\hbar^2}. \tag{3.5}$$

Inserting this expression in the definition of A, we obtain the self-consistency relation

$$A = -4\pi a A \int_{k>k_\mathrm{F}} \frac{\Lambda(k)}{k^2 - k_\mathrm{F}^2 + \kappa^2}\frac{\mathrm{d}^3k}{(2\pi)^3}. \tag{3.6}$$

The integral is ultraviolet divergent if one sets $\Lambda(k) = 1$. As explained in section 2, the divergence is removed by adding the vanishing term

$$0 = \int_0^\infty \frac{\Lambda(k)}{k^2}\frac{\mathrm{d}^3k}{(2\pi)^3} = \frac{1}{2\pi^2}\int_0^\infty \Lambda(k)\,\mathrm{d}k. \tag{3.7}$$

For a non-trivial solution ($A \neq 0$), we divide by $-4\pi aA$ and subtract this term, which gives a convergent expression in which we can safely set $\Lambda(k) = 1$:

$$\frac{1}{4\pi a} = \int_0^{k_\mathrm{F}} \frac{1}{k^2}\frac{\mathrm{d}^3k}{(2\pi)^3} + \int_{k_\mathrm{F}}^\infty \left(\frac{1}{k^2} - \frac{1}{k^2 - k_\mathrm{F}^2 + \kappa^2}\right)\frac{\mathrm{d}^3k}{(2\pi)^3}. \tag{3.8}$$

The first integral equals $k_\mathrm{F}/2\pi^2$. The second integral is computed by introducing $b^2 = k_\mathrm{F}^2 - \kappa^2$ (we anticipate a weak binding $\kappa \ll k_\mathrm{F}$):

$$\begin{aligned}\frac{1}{2\pi^2}\int_{k_\mathrm{F}}^\infty \left(1 - \frac{k^2}{k^2 - b^2}\right)\mathrm{d}k &= -\frac{b^2}{2\pi^2}\int_{k_\mathrm{F}}^\infty \frac{\mathrm{d}k}{k^2 - b^2} = -\frac{b}{4\pi^2}\ln\frac{k_\mathrm{F} + b}{k_\mathrm{F} - b} \\ &\simeq \frac{k_\mathrm{F}}{4\pi^2}\ln\frac{\kappa^2}{4k_\mathrm{F}^2} = \frac{k_\mathrm{F}}{4\pi^2}\ln\frac{|\epsilon|}{8E_\mathrm{F}},\end{aligned} \tag{3.9}$$

where we used $k_\mathrm{F} - b \simeq \kappa^2/2k_\mathrm{F}$, $k_\mathrm{F} + b \simeq 2k_\mathrm{F}$ and $\kappa^2/k_\mathrm{F}^2 = |\epsilon|/2E_\mathrm{F}$. Multiplying by $4\pi^2/k_\mathrm{F}$, we obtain

$$\frac{\pi}{k_\mathrm{F}a} = 2 + \ln\frac{|\epsilon|}{8E_\mathrm{F}}, \tag{3.10}$$

leading to the binding energy of the Cooper pair

$$\epsilon = -\frac{8}{\mathrm{e}^2}\,E_\mathrm{F}\,\mathrm{e}^{\pi/(k_\mathrm{F}a)} = -\frac{8}{\mathrm{e}^2}\,E_\mathrm{F}\,\mathrm{e}^{-\pi/(k_\mathrm{F}|a|)}. \tag{3.11}$$

This result calls for several comments.

- A bound state exists for any negative scattering length, however small, while no two-body bound state exists in vacuum for $a < 0$. The origin of this difference lies in the density of states: in vacuum, the density of pair states vanishes at zero energy in three dimensions, while the pair states available above the Fermi sea have a finite density of states at the Fermi surface. The problem is then similar to a two-dimensional bound-state problem, for which an arbitrarily weak attraction binds, and the logarithmic divergence at small $|\epsilon|$ of the integral above is the signature of this effective dimensional reduction.

- The binding energy is a non-analytic function of a, which cannot be obtained at any order of perturbation theory.
- The pair is weakly bound, $|\epsilon| \ll E_{\rm F}$, and it is made of momentum states within a shell of thickness $\delta k \sim \kappa^2/k_{\rm F}$ above the Fermi surface. Its spatial extent is thus of the order of $1/\delta k \sim \hbar v_{\rm F}/|\epsilon|$, much larger than the inter-particle distance $\sim 1/k_{\rm F}$.
- The Cooper problem is not a consistent many-body calculation: the Fermi sea is assumed to be frozen, while all particles close to the Fermi surface should be allowed to pair. Since pairing lowers the energy of any pair close to the Fermi surface, the Fermi sea itself is unstable, and a self-consistent treatment is required. This is achieved by BCS theory, discussed in the next subsection. We will see that the energy scale of pairing in the BCS state is the gap $\Delta \propto {\rm e}^{-\pi/(2k_{\rm F}|a|)}$, which involves half the exponent of the Cooper problem: in the self-consistent theory, both particle states above the Fermi surface and hole states below it contribute to pairing.

3.2 Mean-field theory of the BEC-BCS crossover at zero temperature

We now develop the mean-field theory of the many-body problem, based on the variational ansatz introduced by Bardeen, Cooper and Schrieffer [3]. Remarkably, this ansatz describes not only the weak-coupling BCS regime, but also the opposite limit of a Bose-Einstein condensate of tightly bound molecules, as first noticed by Eagles and Leggett [4, 5]. It thus provides a qualitative description of the whole BEC-BCS crossover, with a smooth evolution between the two limits. This derivation follows the BCS chapter of the AQM notes, to which we refer for some technical details, with an emphasis on the crossover physics.

3.2.1 BCS variational ansatz

We describe the gas in the grand-canonical ensemble, with a chemical potential μ common to both spin components. The many-body Hamiltonian reads

$$\hat{H} = \sum_{\mathbf{k},\sigma=\uparrow,\downarrow} \xi_k \, \hat{a}^\dagger_{\mathbf{k}\sigma}\hat{a}_{\mathbf{k}\sigma} + \frac{g}{V}\sum_{\mathbf{k},\mathbf{k}',\mathbf{K}} \Lambda(k)\, \hat{a}^\dagger_{\mathbf{K}+\mathbf{k}'\uparrow}\hat{a}^\dagger_{\mathbf{K}-\mathbf{k}'\downarrow}\hat{a}_{\mathbf{K}-\mathbf{k}\downarrow}\hat{a}_{\mathbf{K}+\mathbf{k}\uparrow}, \tag{3.12}$$

where $\xi_k = \epsilon_k - \mu$, $\hat{a}_{\mathbf{k}\sigma}$ annihilates a fermion of spin σ in the plane wave of wave-vector $\mathbf{k}$ (normalized in the volume V), $2\mathbf{K}$ is the total wave-vector of the colliding pair and $\mathbf{k}$, $\mathbf{k}'$ are the incoming and outgoing relative wave-vectors.

The Cooper problem suggests to look for a ground state in which all particles are paired, with pairs of zero total momentum. The BCS variational ansatz is a 'Glauber coherent state' of such pairs:

$$|\psi_{\rm BCS}\rangle \propto \exp(\hat{C}^\dagger)|\varnothing\rangle, \qquad \hat{C}^\dagger = \sum_{\mathbf{k}} \Gamma_{\mathbf{k}}\, \hat{a}^\dagger_{\mathbf{k}\uparrow}\hat{a}^\dagger_{-\mathbf{k}\downarrow}, \tag{3.13}$$

where $|\varnothing\rangle$ is the vacuum and the operator $\hat{C}^\dagger$ creates a pair of particles of opposite spins and zero total momentum, with a relative wave-function of Fourier components $\Gamma_{\mathbf{k}}$ (to be

determined variationally, with $\Gamma_{-\mathbf{k}} = \Gamma_{\mathbf{k}}$). The amplitude of the coherent state, which fixes the mean number of pairs, has been absorbed in the $\Gamma_{\mathbf{k}}$. The pair operators do not satisfy bosonic commutation relations: one finds

$$[\hat{a}_{-\mathbf{k}\downarrow}\hat{a}_{\mathbf{k}\uparrow}, \hat{a}^\dagger_{\mathbf{k}\uparrow}\hat{a}^\dagger_{-\mathbf{k}\downarrow}] = 1 - \hat{n}_{\mathbf{k}\uparrow} - \hat{n}_{-\mathbf{k}\downarrow}, \tag{3.14}$$

so that $\hat{C}^\dagger$ is not a bosonic creation operator, except when the occupation numbers of all relevant momentum states are small. This is the case in the BEC regime, where the pair wave-function is spread over a large momentum range $\sim 1/a \gg k_{\mathrm{F}}$, and the state (3.13) then describes a genuine Bose-Einstein condensate of molecules.

The pair operators $\hat{a}^\dagger_{\mathbf{k}\uparrow}\hat{a}^\dagger_{-\mathbf{k}\downarrow}$ of different momenta commute, and their square vanishes because of the Pauli principle. The exponential thus factorizes into a product over pairs of modes $(\mathbf{k}\uparrow, -\mathbf{k}\downarrow)$, each factor reducing to $1 + \Gamma_{\mathbf{k}}\hat{a}^\dagger_{\mathbf{k}\uparrow}\hat{a}^\dagger_{-\mathbf{k}\downarrow}$. After normalization, we obtain the canonical form

$$|\psi_{\mathrm{BCS}}\rangle = \prod_{\mathbf{k}} \left(u_{\mathbf{k}} - v_{\mathbf{k}}\, \hat{a}^\dagger_{\mathbf{k}\uparrow}\hat{a}^\dagger_{-\mathbf{k}\downarrow}\right)|\emptyset\rangle, \qquad u_{\mathbf{k}} = \frac{1}{\sqrt{1+\Gamma^2_{\mathbf{k}}}}, \quad v_{\mathbf{k}} = \frac{-\Gamma_{\mathbf{k}}}{\sqrt{1+\Gamma^2_{\mathbf{k}}}}, \tag{3.15}$$

where we took $\Gamma_{\mathbf{k}}$ real, such that $u^2_{\mathbf{k}} + v^2_{\mathbf{k}} = 1$. Each pair of modes $(\mathbf{k}\uparrow, -\mathbf{k}\downarrow)$ is empty with probability $u^2_{\mathbf{k}}$ and doubly occupied with probability $v^2_{\mathbf{k}}$. The sign convention $-v_{\mathbf{k}}$ is the one of the AQM notes.

The BCS state does not have a fixed number of particles. The relative fluctuations of the particle number scale as $1/\sqrt{N}$, as for a Glauber coherent state, and they are irrelevant in the thermodynamic limit. This is why we work in the grand-canonical ensemble, the mean particle number being fixed by the chemical potential μ.

3.2.2 The BCS mean-field Hamiltonian

The BCS state is a Gaussian state (it is the vacuum of quasiparticle operators, see below), so that all expectation values can be computed using Wick's theorem. The only non-zero two-point averages are

$$\langle \hat{a}^\dagger_{\mathbf{k}\sigma}\hat{a}_{\mathbf{k}\sigma}\rangle = v^2_{\mathbf{k}}, \tag{3.16}$$

$$\langle \hat{a}_{-\mathbf{k}\downarrow}\hat{a}_{\mathbf{k}\uparrow}\rangle = -u_{\mathbf{k}}v_{\mathbf{k}}, \tag{3.17}$$

the second one being the 'anomalous average' that characterizes the pair condensate. The expectation value of the quartic interaction term can then be decomposed into products of these averages. Equivalently, one can replace the Hamiltonian by a quadratic mean-field Hamiltonian, whose expectation value coincides with the one of $\hat{H}$ for all BCS states. For the zero-momentum pairs $\hat{a}^\dagger_{\mathbf{k}\uparrow}\hat{a}^\dagger_{-\mathbf{k}\downarrow}\hat{a}_{-\mathbf{k}'\downarrow}\hat{a}_{\mathbf{k}'\uparrow}$, this decoupling contains

- Hartree terms, of the form $\langle \hat{a}^\dagger_{\mathbf{k}\uparrow}\hat{a}_{\mathbf{k}\uparrow}\rangle \hat{a}^\dagger_{-\mathbf{k}\downarrow}\hat{a}_{-\mathbf{k}\downarrow}$, which describe the mean-field energy shift $gn_{-\sigma} = gn/2$ felt by an atom of spin σ in the presence of the atoms of opposite spin;

- pairing terms, of the form $\langle \hat{a}^\dagger_{\mathbf{k}\uparrow}\hat{a}^\dagger_{-\mathbf{k}\downarrow}\rangle \hat{a}_{-\mathbf{k}'\downarrow}\hat{a}_{\mathbf{k}'\uparrow} + \langle \hat{a}_{-\mathbf{k}'\downarrow}\hat{a}_{\mathbf{k}'\uparrow}\rangle \hat{a}^\dagger_{\mathbf{k}\uparrow}\hat{a}^\dagger_{-\mathbf{k}\downarrow}$, which describe the coherent conversion of pairs of particles into the condensate and vice versa.

Exchange (Fock) terms vanish since the interaction only couples opposite spins.

Regularization and the fate of the Hartree term. The treatment of the ultraviolet divergences is more transparent if we describe the interaction by a bare contact coupling constant g_0 restricted to momenta $k < k_c$, which is equivalent to the pseudo-potential $g\Lambda(k)$ (see section 2). The bare coupling is related to the scattering length by

$$\frac{1}{g_0} = \frac{1}{g} - \frac{1}{V}\sum_{k<k_c}\frac{1}{2\epsilon_k} = \frac{m}{4\pi\hbar^2 a} - \frac{mk_c}{2\pi^2\hbar^2}, \tag{3.18}$$

and it tends to zero when $k_c \to \infty$. In this limit, the Hartree term $g_0 n/2$ vanishes. On the contrary, the pairing term survives, since the anomalous average (3.17) decays only as $1/k^2$ at large momentum (see below), so that the sum $\sum_{\mathbf{k}}\langle \hat{a}_{-\mathbf{k}\downarrow}\hat{a}_{\mathbf{k}\uparrow}\rangle$ diverges linearly with k_c, and compensates the vanishing of g_0. The standard mean-field theory of the crossover, due to Eagles and Leggett, thus only retains the pairing term. We note that the Hartree energy $gn/2$ is physical in the weak-coupling limit: it corresponds to the first-order term of the expansion (3.1), which is not captured by the mean-field theory with a renormalized interaction. It cannot be consistently included in the crossover, since it diverges at unitarity.

The BCS Hamiltonian. Keeping only the pairing terms, we obtain the BCS mean-field Hamiltonian

$$\hat{H}_{\rm BCS} = \sum_{\mathbf{k}}\left[\xi_k\left(\hat{a}^\dagger_{\mathbf{k}\uparrow}\hat{a}_{\mathbf{k}\uparrow} + \hat{a}^\dagger_{-\mathbf{k}\downarrow}\hat{a}_{-\mathbf{k}\downarrow}\right) + \Delta\,\hat{a}^\dagger_{\mathbf{k}\uparrow}\hat{a}^\dagger_{-\mathbf{k}\downarrow} + \Delta^*\hat{a}_{-\mathbf{k}\downarrow}\hat{a}_{\mathbf{k}\uparrow}\right] - \frac{V|\Delta|^2}{g_0}, \tag{3.19}$$

where the sum now runs over all wave-vectors, and where we introduced the gap parameter

$$\Delta = \frac{g_0}{V}\sum_{\mathbf{k}}\langle \hat{a}_{-\mathbf{k}\downarrow}\hat{a}_{\mathbf{k}\uparrow}\rangle = -\frac{g_0}{V}\sum_{\mathbf{k}} u_{\mathbf{k}} v_{\mathbf{k}}. \tag{3.20}$$

The constant term avoids the double counting of the interaction energy in the mean-field decoupling $\hat{A}^\dagger\hat{A} \simeq \langle\hat{A}^\dagger\rangle\hat{A} + \hat{A}^\dagger\langle\hat{A}\rangle - \langle\hat{A}^\dagger\rangle\langle\hat{A}\rangle$, with $\hat{A} = \sum_{\mathbf{k}}\hat{a}_{-\mathbf{k}\downarrow}\hat{a}_{\mathbf{k}\uparrow}$. In the pseudo-potential language, the gap reads $\Delta = g\int\Lambda(k)\langle\hat{a}_{-\mathbf{k}\downarrow}\hat{a}_{\mathbf{k}\uparrow}\rangle\,\mathrm{d}^3k/(2\pi)^3$, as in the AQM notes. The phase of Δ can be chosen arbitrarily, by redefining the phase of the operators $\hat{a}_{\mathbf{k}\uparrow}$. This freedom reflects the $U(1)$ symmetry associated with particle number conservation, which is spontaneously broken by the choice of a given phase for the pair condensate. In the following, we take Δ real and positive.

3.2.3 Ground state of the BCS Hamiltonian

The BCS Hamiltonian (3.19) is quadratic and couples the modes $\mathbf{k}\uparrow$ and $-\mathbf{k}\downarrow$ only. Introducing the Nambu spinor $(\hat{a}_{\mathbf{k}\uparrow}, \hat{a}^\dagger_{-\mathbf{k}\downarrow})$ and using $\hat{a}^\dagger_{-\mathbf{k}\downarrow}\hat{a}_{-\mathbf{k}\downarrow} = 1 - \hat{a}_{-\mathbf{k}\downarrow}\hat{a}^\dagger_{-\mathbf{k}\downarrow}$, we write it as

$$\hat{H}_{\rm BCS} = \sum_{\mathbf{k}}\left[\begin{pmatrix}\hat{a}^\dagger_{\mathbf{k}\uparrow} & \hat{a}_{-\mathbf{k}\downarrow}\end{pmatrix}\begin{pmatrix}\xi_k & \Delta\\ \Delta & -\xi_k\end{pmatrix}\begin{pmatrix}\hat{a}_{\mathbf{k}\uparrow}\\ \hat{a}^\dagger_{-\mathbf{k}\downarrow}\end{pmatrix} + \xi_k\right] - \frac{V\Delta^2}{g_0}. \tag{3.21}$$

Each 2×2 matrix has eigenvalues $\pm E_k$, with

$$E_k = \sqrt{\xi_k^2 + \Delta^2}. \tag{3.22}$$

It is diagonalized by the Bogoliubov transformation (see the AQM notes, section on the diagonalization of quadratic Hamiltonians)

$$\hat{b}_{\mathbf{k}\uparrow} = u_{\mathbf{k}}\, \hat{a}_{\mathbf{k}\uparrow} + v_{\mathbf{k}}\, \hat{a}^\dagger_{-\mathbf{k}\downarrow}, \tag{3.23}$$

$$\hat{b}_{-\mathbf{k}\downarrow} = u_{\mathbf{k}}\, \hat{a}_{-\mathbf{k}\downarrow} - v_{\mathbf{k}}\, \hat{a}^\dagger_{\mathbf{k}\uparrow}, \tag{3.24}$$

which preserves the fermionic anticommutation relations for $u_{\mathbf{k}}^2 + v_{\mathbf{k}}^2 = 1$, with the coefficients

$$u_{\mathbf{k}}^2 = \frac{1}{2}\left(1 + \frac{\xi_k}{E_k}\right), \qquad v_{\mathbf{k}}^2 = \frac{1}{2}\left(1 - \frac{\xi_k}{E_k}\right), \qquad u_{\mathbf{k}} v_{\mathbf{k}} = \frac{\Delta}{2E_k}. \tag{3.25}$$

The BCS Hamiltonian then takes the diagonal form

$$\hat{H}_{\mathrm{BCS}} = E_0 + \sum_{\mathbf{k}} E_k \left(\hat{b}^\dagger_{\mathbf{k}\uparrow}\hat{b}_{\mathbf{k}\uparrow} + \hat{b}^\dagger_{-\mathbf{k}\downarrow}\hat{b}_{-\mathbf{k}\downarrow}\right), \qquad E_0 = \sum_{\mathbf{k}} (\xi_k - E_k) - \frac{V\Delta^2}{g_0}. \tag{3.26}$$

The ground state is the vacuum of all quasiparticle operators $\hat{b}_{\mathbf{k}\sigma}$. One checks that $\hat{b}_{\mathbf{k}\uparrow}$ and $\hat{b}_{-\mathbf{k}\downarrow}$ annihilate the state $(u_{\mathbf{k}} - v_{\mathbf{k}}\hat{a}^\dagger_{\mathbf{k}\uparrow}\hat{a}^\dagger_{-\mathbf{k}\downarrow})|\emptyset\rangle$, so that the ground state is precisely the BCS state (3.15), with the coefficients (3.25). Using the inverse transformation $\hat{a}_{\mathbf{k}\uparrow} = u_{\mathbf{k}}\hat{b}_{\mathbf{k}\uparrow} - v_{\mathbf{k}}\hat{b}^\dagger_{-\mathbf{k}\downarrow}$, $\hat{a}_{-\mathbf{k}\downarrow} = u_{\mathbf{k}}\hat{b}_{-\mathbf{k}\downarrow} + v_{\mathbf{k}}\hat{b}^\dagger_{\mathbf{k}\uparrow}$, we recover the averages (3.16) and (3.17).

The excitations of the system are Bogoliubov quasiparticles, of energy E_k, which are coherent superpositions of a particle and a hole. Since the BCS state is a superposition of states with even particle numbers, a single quasiparticle corresponds to an unpaired fermion. Breaking a pair while conserving the total momentum creates two quasiparticles, at a minimal cost $2\min_k E_k$.

3.2.4 BCS equations

The quasiparticle spectrum depends on the parameters μ and Δ, which are determined self-consistently.

Gap equation. Inserting the expression (3.25) of $u_{\mathbf{k}}v_{\mathbf{k}}$ in the definition (3.20) of the gap, we obtain $\Delta = -(g_0/V)\sum_{\mathbf{k}} \Delta/2E_k$, i.e. for $\Delta \neq 0$

$$-\frac{1}{g_0} = \frac{1}{V}\sum_{k<k_c} \frac{1}{2E_k}. \tag{3.27}$$

The right-hand side diverges linearly with the cutoff k_c, as $1/g_0$ does. Using the renormalization relation (3.18) to eliminate g_0 in favor of the scattering length, we obtain the gap equation, in which the limit $k_c \to \infty$ can be safely taken:

$$-\frac{m}{4\pi\hbar^2 a} = \int \left(\frac{1}{2E_k} - \frac{1}{2\epsilon_k}\right)\frac{\mathrm{d}^3k}{(2\pi)^3}. \tag{3.28}$$

The same equation is obtained with the pseudo-potential formalism, by subtracting the vanishing term $\int \Lambda(k)/(2\epsilon_k)\,\mathrm{d}^3k$ (see the AQM notes).

Number equation. The total density is obtained from the momentum distribution (3.16), summed over the two spin states:

$$n = \frac{2}{V}\sum_{\mathbf{k}} v_{\mathbf{k}}^2 = \int \left(1 - \frac{\xi_k}{E_k}\right) \frac{\mathrm{d}^3 k}{(2\pi)^3}. \tag{3.29}$$

This integral is convergent, since $v_{\mathbf{k}}^2 \simeq \Delta^2/4\epsilon_k^2$ at large momentum, and it does not involve the interaction.

Thermodynamic potential. The ground-state energy (3.26) is the grand potential $\Omega = \langle \hat{H} \rangle$ at zero temperature. Eliminating g_0, we obtain a cutoff-independent expression

$$\frac{\Omega}{V} = -\frac{m\Delta^2}{4\pi\hbar^2 a} + \int \left(\xi_k - E_k + \frac{\Delta^2}{2\epsilon_k}\right) \frac{\mathrm{d}^3 k}{(2\pi)^3}. \tag{3.30}$$

One checks that the gap equation (3.28) is equivalent to the stationarity condition $\partial\Omega/\partial\Delta = 0$, as expected for a variational calculation, and that the number equation (3.29) is recovered from $n = -\partial(\Omega/V)/\partial\mu$.

Dimensionless form. For given n and a, the two equations (3.28) and (3.29) determine the chemical potential μ and the gap Δ. Measuring wave-vectors in units of k_{F} and energies in units of E_{F}, i.e. introducing $x = k/k_{\mathrm{F}}$, $\tilde{\mu} = \mu/E_{\mathrm{F}}$, $\tilde{\Delta} = \Delta/E_{\mathrm{F}}$ and $\tilde{E}(x) = \sqrt{(x^2 - \tilde{\mu})^2 + \tilde{\Delta}^2}$, the two equations become

$$-\frac{\pi}{2k_{\mathrm{F}}a} = \int_0^\infty \left(\frac{x^2}{\tilde{E}(x)} - 1\right) \mathrm{d}x, \tag{3.31}$$

$$\frac{2}{3} = \int_0^\infty x^2 \left(1 - \frac{x^2 - \tilde{\mu}}{\tilde{E}(x)}\right) \mathrm{d}x, \tag{3.32}$$

where we used $\hbar^2/m = 2E_{\mathrm{F}}/k_{\mathrm{F}}^2$ and $n = k_{\mathrm{F}}^3/3\pi^2$. The ratios μ/E_{F} and Δ/E_{F} thus only depend on the interaction parameter $1/k_{\mathrm{F}}a$, as expected from dimensional analysis. We first solve these equations analytically in the two limits $1/k_{\mathrm{F}}a \to \mp\infty$, before discussing the numerical solution for arbitrary interactions.

3.2.5 The BCS limit

The BCS limit corresponds to a weak attraction, $k_{\mathrm{F}}a \to 0^-$. The left-hand side of the gap equation (3.31) then tends to $+\infty$, which requires a vanishing gap $\tilde{\Delta} \to 0$, for which the integrand develops a logarithmic singularity at $x = \sqrt{\tilde{\mu}}$.

Chemical potential. For $\Delta \ll E_{\mathrm{F}}$, the factor $1 - \xi_k/E_k$ in the number equation is close to a step function $2\theta(\mu - \epsilon_k)$, so that the number equation gives $\mu \simeq E_{\mathrm{F}}$, up to small corrections of order Δ^2/E_{F}. The momentum distribution $v_{\mathbf{k}}^2$ is close to the one of the Fermi sea, smoothened over an energy range $\sim \Delta$ around the Fermi surface.

Gap. We now evaluate the gap equation for $\tilde{\mu} = 1$ and $\tilde{\Delta} \ll 1$. Introducing the variable $\tilde{\xi} = x^2 - 1$, we write the integral as

$$I(\tilde{\Delta}) = \int_0^\infty \left(\frac{x^2}{\tilde{E}} - 1 \right) \mathrm{d}x = \frac{1}{2} \int_{-1}^\infty \left(\frac{\sqrt{1+\tilde{\xi}}}{\sqrt{\tilde{\xi}^2 + \tilde{\Delta}^2}} - \frac{1}{\sqrt{1+\tilde{\xi}}} \right) \mathrm{d}\tilde{\xi}. \tag{3.33}$$

For $\tilde{\Delta} \to 0$, the only singular contribution comes from the vicinity of the Fermi surface $\tilde{\xi} = 0$, where $\sqrt{1+\tilde{\xi}} \simeq 1$. We isolate it as

$$\frac{1}{2} \int_{-1}^1 \frac{\mathrm{d}\tilde{\xi}}{\sqrt{\tilde{\xi}^2 + \tilde{\Delta}^2}} = \operatorname{arcsinh} \frac{1}{\tilde{\Delta}} \simeq \ln \frac{2}{\tilde{\Delta}}. \tag{3.34}$$

In the remaining part of the integral, we can set $\tilde{\Delta} = 0$, and elementary integrations give

$$\frac{1}{2} \int_{-1}^1 \frac{\sqrt{1+\tilde{\xi}} - 1}{|\tilde{\xi}|} \mathrm{d}\tilde{\xi} + \frac{1}{2} \int_1^\infty \frac{\mathrm{d}\tilde{\xi}}{\tilde{\xi}\sqrt{1+\tilde{\xi}}} - \frac{1}{2} \int_{-1}^1 \frac{\mathrm{d}\tilde{\xi}}{\sqrt{1+\tilde{\xi}}} = \ln 4 - 2. \tag{3.35}$$

We thus obtain $I(\tilde{\Delta}) \simeq \ln(8/\tilde{\Delta}) - 2$, which we checked numerically. The gap equation then gives

$$\mu \simeq E_\mathrm{F}, \qquad \Delta \simeq \frac{8}{\mathrm{e}^2} E_\mathrm{F} \, \mathrm{e}^{-\pi/(2k_\mathrm{F}|a|)}. \tag{3.36}$$

Discussion. The gap is exponentially small and non-analytic in the interaction strength, as anticipated from the Cooper problem. Compared with the Cooper binding energy (3.11), the exponent is divided by two, so that $|\epsilon| = (\mathrm{e}^2/8)\Delta^2/E_\mathrm{F} \ll \Delta$: the self-consistent many-body pairing is much stronger than the pairing of a single pair above a frozen Fermi sea.

The quasiparticle dispersion relation $E_k = \sqrt{(\epsilon_k - \mu)^2 + \Delta^2}$ is shown in Fig. 13a. It reaches its minimum Δ on the Fermi surface $k = \sqrt{2m\mu}/\hbar \simeq k_\mathrm{F}$, and it coincides away from the Fermi surface with the particle-hole excitation spectrum $|\epsilon_k - E_\mathrm{F}|$ of the ideal Fermi gas. The gap Δ is the minimal energy of a quasiparticle, so that breaking a Cooper pair costs at least 2Δ. The pair size, estimated from the width $\delta k \sim \Delta/\hbar v_\mathrm{F}$ of the momentum shell involved in pairing, is the coherence length $\hbar v_\mathrm{F}/\Delta \gg 1/k_\mathrm{F}$.

Beyond mean field. Two corrections to the mean-field result (3.36) are known in the weak-coupling limit. First, the chemical potential includes the Hartree shift, $\mu \simeq E_\mathrm{F} + gn/2 = E_\mathrm{F}[1 + 4k_\mathrm{F}a/(3\pi)]$, consistent with the expansion (3.1), which is missed by the mean-field theory, as explained above. Second, the induced interaction mediated by density fluctuations of the medium (screening) reduces the gap by a factor $(4\mathrm{e})^{1/3} \simeq 2.2$, as shown by Gor'kov and Melik-Barkhudarov [35]. Since this correction is of order 1, the mean-field theory only gives the correct exponent of the gap, not its prefactor.

3.2.6 The BEC limit

The BEC limit corresponds to a strong attraction, $k_\mathrm{F}a \to 0^+$, for which a two-body bound state exists, of binding energy $E_\mathrm{b} = \hbar^2/ma^2 \gg E_\mathrm{F}$. We look for a solution with a large negative chemical potential $|\mu| \gg \Delta, E_\mathrm{F}$.

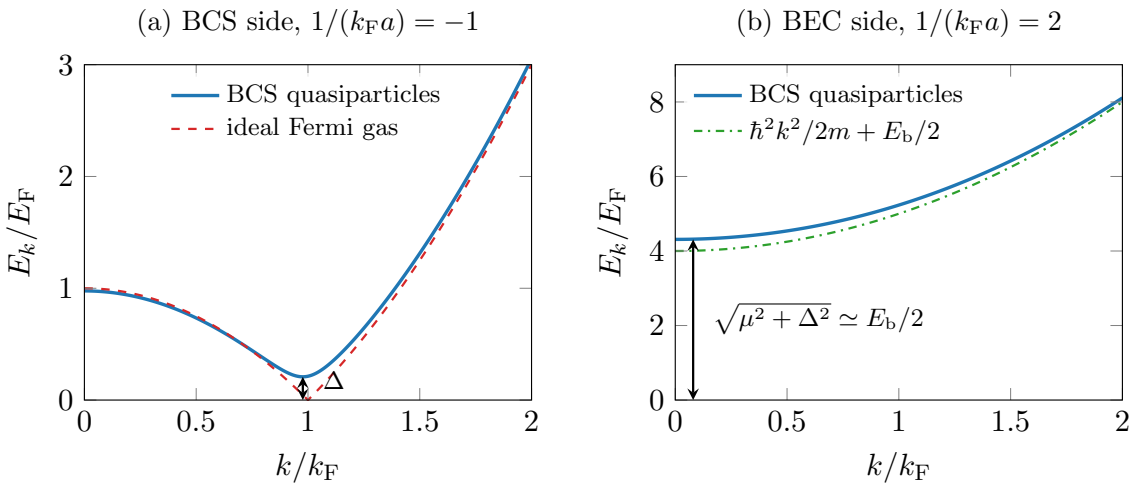


Figure 13: Quasiparticle dispersion relation E_k in the mean-field theory (blue lines), with μ and Δ obtained by solving the BCS equations. (a) BCS side, $1/k_\mathrm{F}a = -1$ ($\mu = 0.95\,E_\mathrm{F}$, $\Delta = 0.21\,E_\mathrm{F}$): the minimum Δ is reached close to the Fermi surface, and the dispersion relation is close to the particle-hole spectrum $|\epsilon_k - E_\mathrm{F}|$ of the ideal Fermi gas (dashed red line) away from it. (b) BEC side, $1/k_\mathrm{F}a = 2$ ($\mu = -3.89\,E_\mathrm{F}$, $\Delta = 1.85\,E_\mathrm{F}$): the minimum $\sqrt{\mu^2+\Delta^2} \simeq E_\mathrm{b}/2$ is reached for $k = 0$, and the dispersion relation is close to the energy $\epsilon_k + E_\mathrm{b}/2$ of a free atom released by the dissociation of a molecule (dash-dotted green line).

Chemical potential. To lowest order, we can neglect Δ in $E_k \simeq \epsilon_k + |\mu|$. The gap equation (3.28) then reads

$$-\frac{m}{4\pi\hbar^2 a} = -\frac{|\mu|}{2}\int \frac{1}{\epsilon_k(\epsilon_k+|\mu|)}\frac{\mathrm{d}^3k}{(2\pi)^3} = -\frac{|\mu|}{2}\,\frac{1}{2\pi^2}\left(\frac{2m}{\hbar^2}\right)^2 \int_0^\infty \frac{\mathrm{d}k}{k^2+q^2} = -\frac{mq}{4\pi\hbar^2}, \tag{3.37}$$

with $q^2 = 2m|\mu|/\hbar^2$. We obtain $q = 1/a$, i.e.

$$\mu \simeq -\frac{\hbar^2}{2ma^2} = -\frac{E_\mathrm{b}}{2}. \tag{3.38}$$

The gap equation thus reduces to the Schrödinger equation for the two-body bound state (see section 2): the chemical potential of an atom is half the energy of a molecule.

Gap. In the number equation, we use $v_\mathbf{k}^2 \simeq \Delta^2/4(\epsilon_k+|\mu|)^2 \ll 1$, which gives

$$n \simeq \frac{\Delta^2}{2}\int \frac{1}{(\epsilon_k+|\mu|)^2}\frac{\mathrm{d}^3k}{(2\pi)^3} = \frac{\Delta^2}{2}\,\frac{1}{2\pi^2}\left(\frac{2m}{\hbar^2}\right)^2 \int_0^\infty \frac{k^2\,\mathrm{d}k}{(k^2+q^2)^2} = \frac{m^2 a\,\Delta^2}{4\pi\hbar^4}, \tag{3.39}$$

where we used $\int_0^\infty k^2/(k^2+q^2)^2\,\mathrm{d}k = \pi/4q$. Using $n = k_\mathrm{F}^3/3\pi^2$, we obtain

$$\Delta \simeq \sqrt{\frac{16}{3\pi k_\mathrm{F}a}}\,E_\mathrm{F} = \frac{2}{\sqrt{3\pi}}(k_\mathrm{F}a)^{3/2}E_\mathrm{b}. \tag{3.40}$$

Interpretation. In this limit, the BCS state describes a Bose-Einstein condensate of molecules. Indeed, the pair wave-function in momentum space reads $\Gamma_{\mathbf{k}} = -v_{\mathbf{k}}/u_{\mathbf{k}} \propto 1/(k^2 + 1/a^2)$, which is the Fourier transform of the molecular wave-function $\mathrm{e}^{-r/a}/r$. All occupation numbers $v_{\mathbf{k}}^2 \sim (k_\mathrm{F} a)^3$ are small, so that the pair operator $\hat{C}^\dagger$ behaves as a bosonic operator, and the coherent state (3.13) is a condensate of molecules. The gap Δ has a very different meaning than in the BCS limit: it scales as the square root of the density, and it measures the amplitude of the molecular condensate, i.e. it plays the role of the condensate wave-function. It is *not* the energy required to break a pair. The quasiparticle dispersion relation (see Fig. 13b) has its minimum at $k = 0$, with $\min_k E_k = \sqrt{\mu^2 + \Delta^2} \simeq E_\mathrm{b}/2$, so that breaking a pair costs the molecular binding energy E_b, as expected.

Pushing the expansion to the next order, one finds $\mu \simeq -E_\mathrm{b}/2 + \pi\hbar^2 a n/m$ (we checked this result numerically). This correction corresponds to the mean-field interaction energy of a condensate of molecules of mass $2m$ and density $n/2$, with a molecule-molecule scattering length $a_\mathrm{dd} = 2a$. The exact four-body calculation gives instead $a_\mathrm{dd} \simeq 0.6\, a$ [29], which illustrates the limitations of mean-field theory, even in the BEC limit.

3.2.7 Solution for all interaction strengths

For arbitrary interactions, we solve numerically the two equations (3.31) and (3.32) for μ and Δ. The results are shown in Fig. 14. Both quantities evolve smoothly between the BCS and BEC asymptotic behaviors, without any singularity: the BEC-BCS evolution is a crossover, and not a phase transition. The chemical potential changes sign for $1/k_\mathrm{F} a \simeq 0.55$, which marks the point where the minimum of the quasiparticle dispersion relation moves from a finite wave-vector to $k = 0$. At unitarity ($1/k_\mathrm{F} a = 0$), we obtain

$$\mu \simeq 0.591\, E_\mathrm{F}, \qquad \Delta \simeq 0.686\, E_\mathrm{F}. \tag{3.41}$$

These values are not quantitatively correct. The most accurate measurements and numerical calculations give $\mu \simeq 0.37\, E_\mathrm{F}$ and $\Delta \simeq 0.44\, E_\mathrm{F}$ at unitarity (see section 4). The mean-field theory is not controlled in the strongly interacting regime, where no small parameter is available, but it provides a qualitatively correct and physically transparent picture of the crossover.

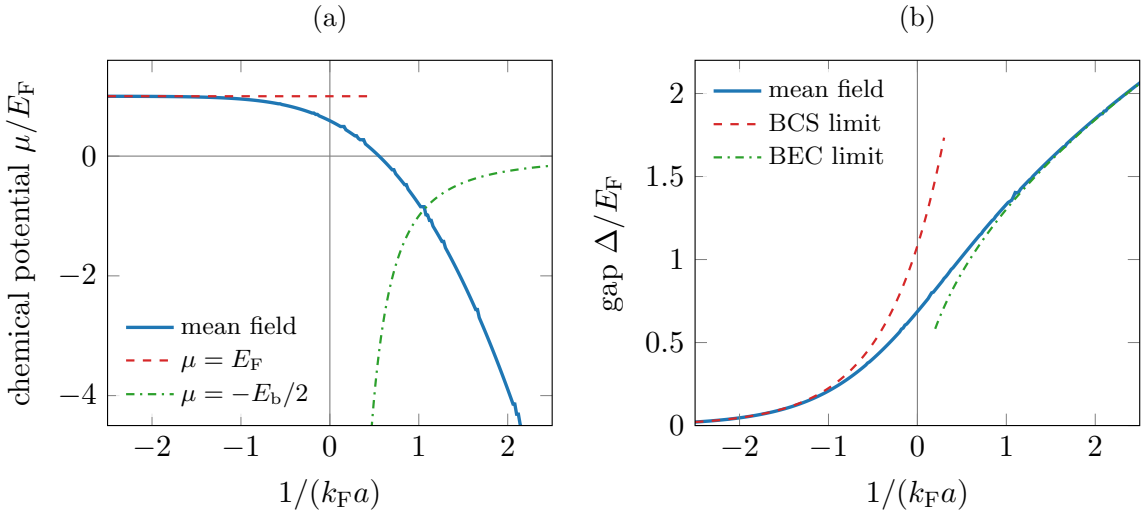


Figure 14: Chemical potential μ (a) and gap Δ (b) in the mean-field theory of the BEC-BCS crossover at zero temperature, as a function of the interaction parameter $1/k_\mathrm{F}a$ (blue lines, numerical solution of Eqs. (3.31) and (3.32)). The dashed red lines show the BCS asymptotic behaviors $\mu = E_\mathrm{F}$ and $\Delta = (8/\mathrm{e}^2)E_\mathrm{F}\mathrm{e}^{\pi/(2k_\mathrm{F}a)}$, and the dash-dotted green lines the BEC asymptotic behaviors $\mu = -E_\mathrm{b}/2$ and $\Delta = \sqrt{16/(3\pi k_\mathrm{F}a)}\,E_\mathrm{F}$.

3.3 Superfluid critical temperature

We now discuss the superfluid transition at finite temperature. We first extend the mean-field theory to finite temperature, which gives a critical temperature consistent with the standard BCS result in the weak-coupling limit. We then show that this approach fails on the BEC side, where it predicts the temperature of molecule formation instead of the condensation temperature.

3.3.1 Finite-temperature BCS theory

At finite temperature, we treat the Bogoliubov quasiparticles of the mean-field Hamiltonian (3.26) as an ideal gas of fermions, with occupation numbers $\langle \hat{b}^\dagger_{\mathbf{k}\sigma}\hat{b}_{\mathbf{k}\sigma}\rangle = f(E_k) = 1/(\mathrm{e}^{E_k/k_\mathrm{B}T}+1)$. Using the inverse Bogoliubov transformation, the anomalous average and the momentum distribution become

$$\langle \hat{a}_{-\mathbf{k}\downarrow}\hat{a}_{\mathbf{k}\uparrow}\rangle = -u_\mathbf{k}v_\mathbf{k}\left[1-2f(E_k)\right], \qquad \langle \hat{a}^\dagger_{\mathbf{k}\sigma}\hat{a}_{\mathbf{k}\sigma}\rangle = u^2_\mathbf{k}f(E_k) + v^2_\mathbf{k}\left[1-f(E_k)\right]. \tag{3.42}$$

Using $1-2f(E) = \tanh(E/2k_\mathrm{B}T)$, the gap and number equations read

$$-\frac{m}{4\pi\hbar^2 a} = \int\left(\frac{\tanh(E_k/2k_\mathrm{B}T)}{2E_k} - \frac{1}{2\epsilon_k}\right)\frac{\mathrm{d}^3k}{(2\pi)^3}, \tag{3.43}$$

$$n = \int\left(1 - \frac{\xi_k}{E_k}\tanh\frac{E_k}{2k_\mathrm{B}T}\right)\frac{\mathrm{d}^3k}{(2\pi)^3}. \tag{3.44}$$

They can be equivalently obtained by minimizing the grand potential

$$\frac{\Omega}{V} = -\frac{m\Delta^2}{4\pi\hbar^2 a} + \int\left(\xi_k - E_k + \frac{\Delta^2}{2\epsilon_k} - 2k_\mathrm{B}T\ln\left(1+\mathrm{e}^{-E_k/k_\mathrm{B}T}\right)\right)\frac{\mathrm{d}^3k}{(2\pi)^3} \tag{3.45}$$

with respect to Δ. These equations determine μ and Δ as functions of T/T_F and $1/k_\mathrm{F}a$. The gap decreases with temperature, and it vanishes at the critical temperature T_c, obtained by solving the two equations with $\Delta = 0$ (i.e. $E_k = |\xi_k|$).

3.3.2 The BCS limit

In the BCS limit, $\mu \simeq E_\mathrm{F}$ at all temperatures $T \leq T_\mathrm{c}$, and the critical temperature is obtained by comparing the gap equation at $\Delta = 0$, $T = T_\mathrm{c}$ with the one at $T = 0$. Both equations only differ in a shell around the Fermi surface, where the density of states can be taken as constant. Introducing an energy $\hbar\omega$ such that $\Delta, k_\mathrm{B}T_\mathrm{c} \ll \hbar\omega \ll E_\mathrm{F}$, the contributions of this shell read respectively

$$\int_0^{\hbar\omega} \frac{\tanh(\xi/2k_\mathrm{B}T_\mathrm{c})}{\xi}\mathrm{d}\xi \simeq \ln\frac{2\mathrm{e}^\gamma\hbar\omega}{\pi k_\mathrm{B}T_\mathrm{c}}, \qquad \int_0^{\hbar\omega} \frac{\mathrm{d}\xi}{\sqrt{\xi^2+\Delta^2}} \simeq \ln\frac{2\hbar\omega}{\Delta}, \tag{3.46}$$

where $\gamma \simeq 0.577$ is Euler's constant. Since the integrands coincide outside the shell, the two expressions must be equal, which gives the celebrated BCS ratio

$$k_\mathrm{B}T_\mathrm{c} = \frac{\mathrm{e}^\gamma}{\pi}\Delta(T=0) \simeq 0.567\,\Delta(T=0), \tag{3.47}$$

i.e. $T_\mathrm{c} \simeq 0.61\,T_\mathrm{F}\,\mathrm{e}^{-\pi/(2k_\mathrm{F}|a|)}$ using (3.36). Including the Gor'kov-Melik-Barkhudarov correction [35], which reduces both the gap and the critical temperature by the factor $(4\mathrm{e})^{1/3}$, the critical temperature in the weak-coupling limit reads

$$T_\mathrm{c} \simeq 0.28\,T_\mathrm{F}\,\mathrm{e}^{-\pi/(2k_\mathrm{F}|a|)}. \tag{3.48}$$

In the BCS limit, pair formation and pair condensation occur simultaneously at T_c: above the critical temperature, there are no preformed pairs and the gas is a normal Fermi liquid.

3.3.3 The BEC limit

In the BEC limit, the mean-field critical temperature becomes very large. At $T = T_\mathrm{c}$ we have $\Delta = 0$ and $\mu \simeq -E_\mathrm{b}/2$, as shown by the gap equation (3.43) with $|\mu| \gg k_\mathrm{B}T$, for which $\tanh(|\xi_k|/2k_\mathrm{B}T) \simeq 1$. The number equation (3.44) then describes a non-degenerate gas of free atoms, with $n = 2\mathrm{e}^{\mu/k_\mathrm{B}T}/\lambda^3$, where $\lambda = \sqrt{2\pi\hbar^2/mk_\mathrm{B}T}$ is the thermal de Broglie wavelength. We obtain

$$k_\mathrm{B}T_\mathrm{c}^\mathrm{MF} \simeq \frac{E_\mathrm{b}/2}{\ln\left[2/(n\lambda^3)\right]}, \tag{3.49}$$

which scales as E_b, up to a logarithm, and diverges for $k_\mathrm{F}a \to 0^+$. This temperature $T^* \equiv T_\mathrm{c}^\mathrm{MF}$ has a clear physical meaning: it is the temperature below which the chemical equilibrium between free atoms and molecules favors molecules, i.e. the dissociation temperature of molecules, given by a Saha-like law. It is not related to superfluidity.

The actual superfluid transition, in the BEC limit, is the Bose-Einstein condensation of an ideal gas of molecules of mass $2m$ and density $n/2$, which occurs at the temperature

$$k_\mathrm{B}T_\mathrm{c}^\mathrm{BEC} = \frac{2\pi\hbar^2}{2m}\left(\frac{n/2}{\zeta(3/2)}\right)^{2/3} = \frac{\pi\hbar^2}{m}\left(\frac{n}{2\zeta(3/2)}\right)^{2/3} = \frac{2\pi}{\left[6\pi^2\zeta(3/2)\right]^{2/3}}E_\mathrm{F} \simeq 0.218\,E_\mathrm{F}, \tag{3.50}$$

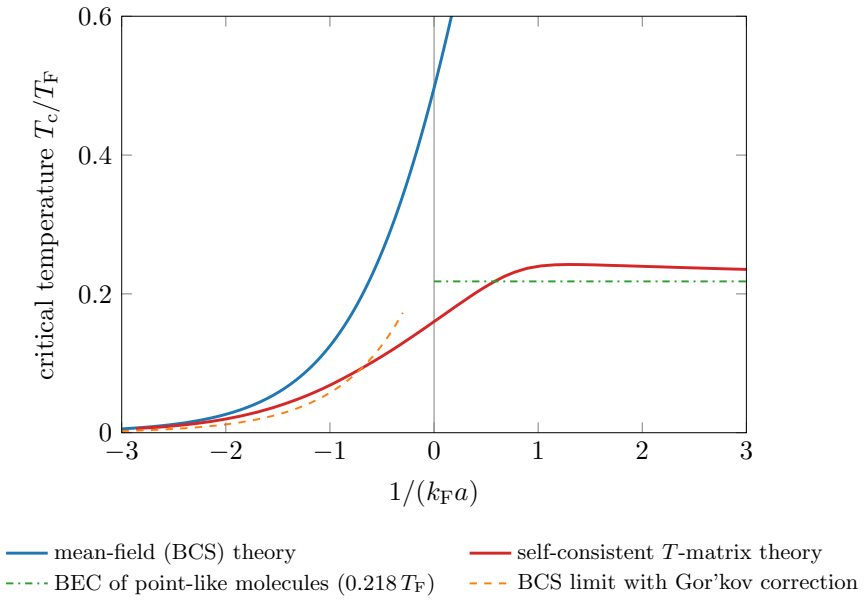


Figure 15: Superfluid critical temperature in the BEC-BCS crossover. Blue line: mean-field (BCS) theory, obtained by solving numerically the finite-temperature BCS equations with $\Delta = 0$, which diverges on the BEC side as the molecule dissociation temperature. Red line: self-consistent T-matrix theory of Ref. [39], including pair fluctuations. Dash-dotted green line: condensation temperature $0.218\,T_F$ of an ideal gas of point-like molecules. Dashed orange line: weak-coupling result $0.28\,T_F e^{\pi/(2k_F a)}$ including the Gor'kov-Melik-Barkhudarov correction.

with $\zeta(3/2) \simeq 2.612$. For $T^* > T > T_c^{\mathrm{BEC}}$, the gas is a normal gas of preformed pairs. The mean-field theory fails to capture this regime, because it only includes pairs of zero total momentum, while the thermal excitations of a gas of molecules consist of molecules of non-zero momentum. Describing the condensation of pairs requires to include pair fluctuations, as done by Nozières and Schmitt-Rink [6] and in subsequent works [36].

3.3.4 Critical temperature in the crossover

The mean-field critical temperature, obtained by solving numerically Eqs. (3.43) and (3.44) with $\Delta = 0$, is shown in Fig. 15. It is only correct in the BCS limit (up to the Gor'kov correction). At unitarity, it gives $T_c \simeq 0.50\,T_F$, about three times larger than the accurate values $T_c \simeq 0.15$–$0.17\,T_F$ obtained from quantum Monte Carlo simulations [37] and measurements [38]. We also show the result of a self-consistent T-matrix theory including pair fluctuations [39], which interpolates smoothly between the BCS and BEC limits, with a weak maximum on the BEC side due to the interactions between molecules. The determination of the critical temperature across the crossover is a notoriously difficult problem, since no small parameter is available in the strongly interacting regime and numerical simulations are challenging. To date, no theory provides a controlled description of the critical temperature over the whole crossover.

3.4 Short-range correlations: Tan's contact

The zero-range character of the interaction has striking consequences on the short-distance structure of the many-body wave-function. In this subsection, we show that all short-distance (or large-momentum) properties of the gas are controlled by a single quantity, the contact, introduced by S. Tan [40, 41, 42]. The contact is related to several observables by exact 'Tan relations', and it can be computed in the mean-field theory.

3.4.1 Short-range correlations

For a zero-range interaction, the many-body wave-function $\psi(\mathbf{r}_1, \dots, \mathbf{r}_N)$ satisfies the free Schrödinger equation whenever all particles are at different positions, supplemented by the Bethe-Peierls boundary condition when two particles of opposite spins approach each other (see section 2). Considering particles 1 ($\uparrow$) and 2 ($\downarrow$), we have

$$\psi(\mathbf{r}_1, \dots, \mathbf{r}_N) \underset{\mathbf{r}_1 \to \mathbf{r}_2}{\simeq} A_{12}\left(\frac{\mathbf{r}_1 + \mathbf{r}_2}{2}, \mathbf{r}_3, \dots, \mathbf{r}_N\right)\left(\frac{1}{|\mathbf{r}_1 - \mathbf{r}_2|} - \frac{1}{a}\right), \tag{3.51}$$

where the regular function A_{12} depends on the center of mass of the pair and on the positions of the other particles. This short-distance behavior has a direct consequence on the pair correlation function between opposite spins. Squaring the wave-function and summing over all pairs of opposite spins, we obtain, for $r \to 0$,

$$\left\langle \hat{n}_\uparrow\left(\mathbf{R} - \frac{\mathbf{r}}{2}\right)\hat{n}_\downarrow\left(\mathbf{R} + \frac{\mathbf{r}}{2}\right)\right\rangle \simeq \frac{C(\mathbf{R})}{16\pi^2}\left(\frac{1}{r^2} - \frac{2}{ar}\right) + O(1), \tag{3.52}$$

where we introduced the contact density

$$C(\mathbf{R}) = 16\pi^2\, N_\uparrow N_\downarrow \int |A_{12}(\mathbf{R}, \mathbf{r}_3, \dots, \mathbf{r}_N)|^2\, \mathrm{d}^3 r_3 \dots \mathrm{d}^3 r_N, \tag{3.53}$$

for a normalized wave-function. The total contact is $C = \int C(\mathbf{R})\, \mathrm{d}^3 R$. It has the dimension of an inverse length, and it measures the number of pairs of opposite spins at short distance: the probability to find such a pair within a small sphere of radius s scales as $\int_0^s 4\pi r^2 \mathrm{d}r\, C/(16\pi^2 r^2) = Cs/4\pi$. The $1/r^2$ divergence of the pair correlation function is a direct consequence of the zero-range interaction, and it does not occur in a gas with finite-range interactions at distances smaller than the range.

3.4.2 Tan relations

The contact is related to several other physical quantities by exact relations, valid for any state (ground state or thermal equilibrium, homogeneous or trapped, superfluid or normal) [40, 41, 42, 43, 44].

Tail of the momentum distribution. The singular part $1/r$ of the wave-function (3.51) has the Fourier transform $4\pi/k^2$, which dominates the large-momentum behavior of the relative wave-function. Squaring it, the momentum distribution of each spin component, normalized such that $\int n_\sigma(\mathbf{k})\, \mathrm{d}^3 k/(2\pi)^3 = N_\sigma$, decays as

$$n_\sigma(\mathbf{k}) \underset{k \to \infty}{\simeq} \frac{C}{k^4}, \qquad \text{i.e.} \qquad C = \lim_{k \to \infty} k^4 n_\sigma(\mathbf{k}), \tag{3.54}$$

where the limit is taken for k much larger than the typical momenta $k_{\rm F}$, $1/|a|$ and $\sqrt{mk_{\rm B}T}/\hbar$. The kinetic energy $\int \epsilon_k n_\sigma(\mathbf{k})\,\mathrm{d}^3k$ is thus UV divergent for a zero-range interaction, this divergence being compensated by the interaction energy.

Adiabatic relation. The contact also gives the variation of the energy with the scattering length,

$$\frac{\mathrm{d}E}{\mathrm{d}(1/a)} = -\frac{\hbar^2 C}{4\pi m}. \tag{3.55}$$

This relation can be derived by considering two eigenstates ψ_1, ψ_2 of energies E_1, E_2, corresponding to scattering lengths a_1, a_2. Since both satisfy the free Schrödinger equation away from the contact points, the quantity $(E_1 - E_2)\langle\psi_2|\psi_1\rangle$ reduces, using Green's theorem, to surface terms around the singularities $r_{ij} \to 0$. Close to a contact point, the wave-functions behave as $A^{(i)}(1/r - 1/a_i)$, and the relative motion has the kinetic energy $-(\hbar^2/m)\Delta_{\mathbf{r}}$ (reduced mass $m/2$). The surface term on a small sphere of radius r involves

$$\psi_2^* \partial_r \psi_1 - \psi_1 \partial_r \psi_2^* \simeq A^{(2)*} A^{(1)} \left(\frac{1}{a_2} - \frac{1}{a_1}\right) \frac{1}{r^2}, \tag{3.56}$$

which, multiplied by the area $4\pi r^2$, gives a finite contribution. Taking the limit $a_2 \to a_1$ and using the definition of the contact, one obtains the relation (3.55). At finite temperature, it holds for the free energy at fixed entropy, and for the grand potential at fixed μ and T.

Example: a single molecule. We check these relations for a single molecule (one $\uparrow$ and one $\downarrow$ particle, $a > 0$) of zero momentum in a volume V. Its relative wave-function is $\phi(\mathbf{r}) = \mathrm{e}^{-r/a}/(r\sqrt{2\pi a})$, normalized to unity, and the pair correlation function is $|\phi(\mathbf{r})|^2/V \simeq (1/2\pi a V)(1/r^2 - 2/ar)$, giving $C = 8\pi/a$. The Fourier transform $\tilde\phi(\mathbf{k}) = 4\pi/[\sqrt{2\pi a}(k^2 + 1/a^2)]$ gives $k^4|\tilde\phi(\mathbf{k})|^2 \to 8\pi/a$, in agreement with (3.54). Finally, the energy $E = -\hbar^2/ma^2$ gives $\mathrm{d}E/\mathrm{d}(1/a) = -2\hbar^2/ma = -\hbar^2 C/(4\pi m)$, in agreement with (3.55).

Other relations. The contact also determines the tail of radio-frequency spectra (which decay as $\omega^{-3/2}$), the large-momentum part of the static structure factor, and it enters the expression of the total energy as a sum of kinetic, interaction and trapping contributions [40, 43, 44]. These relations provide several independent methods to measure the contact (see section 4).

3.4.3 Contact in the BEC-BCS crossover

Limiting cases. In the BEC limit, the gas consists of $N/2$ molecules, each contributing $8\pi/a$ to the contact, so that $C \simeq 4\pi N/a$. In the BCS limit, the energy is given by the expansion (3.1), whose first-order term $E \simeq \pi\hbar^2 a n^2 V/m$ gives, using the adiabatic relation (3.55) with $\mathrm{d}a/\mathrm{d}(1/a) = -a^2$,

$$C \simeq 4\pi^2 a^2 n^2 V. \tag{3.57}$$

In this limit, the short-range correlations between opposite spins are of second order in $k_{\rm F}a$, and they are not related to pairing.

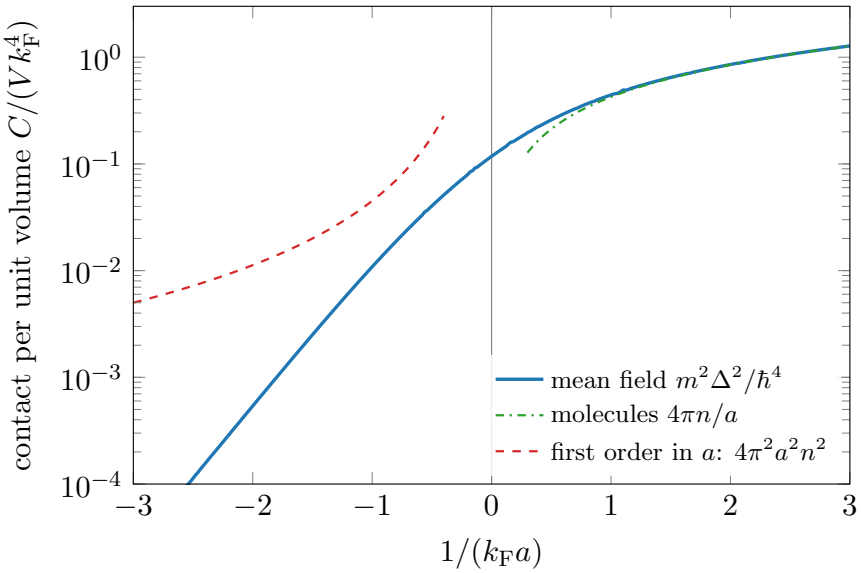


Figure 16: Contact per unit volume in the BEC-BCS crossover at zero temperature. Blue line: mean-field theory, $C/V = m^2\Delta^2/\hbar^4$. Dash-dotted green line: BEC limit $C/V = 4\pi n/a$, i.e. $C/(Vk_F^4) = 4/(3\pi k_F a)$. Dashed red line: BCS limit, at first order in the interaction, $C/V = 4\pi^2a^2n^2$, i.e. $C/(Vk_F^4) = 4(k_Fa)^2/9\pi^2$, which is not captured by the mean-field theory.

Mean-field contact. In the mean-field theory, the momentum distribution (3.16) decays at large momentum as $v_{\mathbf{k}}^2 \simeq \Delta^2/4\epsilon_k^2 = m^2\Delta^2/\hbar^4k^4$, giving

$$\frac{C}{V} = \frac{m^2\Delta^2}{\hbar^4}. \tag{3.58}$$

The same result is obtained from the adiabatic relation applied to the grand potential (3.30): since Ω is stationary with respect to Δ, only the explicit dependence on $1/a$ contributes, $\partial(\Omega/V)/\partial(1/a) = -m\Delta^2/4\pi\hbar^2$. In the BEC limit, the expression (3.40) of the gap gives $C = 4\pi N/a$, in agreement with the exact result. On the contrary, in the BCS limit, the mean-field contact is exponentially small, much smaller than the exact result $4\pi^2a^2n^2V$: the mean-field theory misses the short-range correlations of the normal Fermi liquid, which are related to the Hartree term that we neglected. At unitarity, the mean-field theory gives $C \simeq 0.118\, k_F^4V$, i.e. $C \simeq 3.5\, Nk_F$, of the same order as the values obtained with more accurate methods. The variation of the contact across the crossover is shown in Fig. 16.

3.5 The unitary Fermi gas

The center of the crossover, $1/k_Fa = 0$, corresponds to a diverging scattering length. In this unitary limit, the interaction does not introduce any length scale, and the gas acquires universal properties, which we discuss in this subsection. These properties are shared by any system of fermions with resonant short-range interactions, such as dilute neutron matter.

3.5.1 Scale invariance

We recall the s-wave scattering amplitude for a zero-range interaction, $f_k = -a/(1+\mathrm{i}ka)$. At unitarity ($a = \infty$), it becomes

$$f_k = -\frac{1}{\mathrm{i}k} = \frac{\mathrm{i}}{k}, \tag{3.59}$$

which saturates the bound $|f_k| \leq 1/k$ imposed by the unitarity of the S-matrix, hence the name 'unitary gas'. The scattering amplitude no longer involves any length scale other than the de Broglie wavelength.

Let us consider a spatial dilation by a factor λ, $\mathbf{r} \to \lambda\mathbf{r}$. It changes the physical quantities as follows:

- wave-vectors $\mathbf{k} \to \mathbf{k}/\lambda$ and kinetic energies $E_{\mathrm{kin}} \to E_{\mathrm{kin}}/\lambda^2$;
- densities $n \to n/\lambda^3$;
- the scattering amplitude at unitarity, $f_k \to f_{k/\lambda} = \lambda f_k$, which scales as a length, as any length of the problem;
- the interaction energy, which scales as $\hbar^2 f/m$ times a density, $E_{\mathrm{int}} \to E_{\mathrm{int}}/\lambda^2$.

Kinetic and interaction energies thus have the same scaling. More rigorously, the unitary gas is described by the free Hamiltonian, supplemented by the Bethe-Peierls boundary condition $\psi \propto 1/r_{ij} + O(r_{ij})$ (without constant term since $1/a = 0$) when two particles of opposite spins approach each other. This boundary condition is invariant under dilations. If $\psi(\mathbf{r}_1, \ldots, \mathbf{r}_N)$ is an eigenstate of energy E, then

$$\psi_\lambda(\mathbf{r}_1, \ldots, \mathbf{r}_N) = \frac{1}{\lambda^{3N/2}} \psi\left(\frac{\mathbf{r}_1}{\lambda}, \ldots, \frac{\mathbf{r}_N}{\lambda}\right) \tag{3.60}$$

is also a normalized eigenstate, of energy E/λ^2. The spectrum of the unitary gas in a box thus scales as $1/L^2$ with the box size L, as for an ideal gas. We note that this scale invariance would be broken by a finite scattering length, or by a finite range of the interaction potential. It also requires that no three-body bound states (Efimov states) appear, which is the case for two-component fermions.

3.5.2 Universal thermodynamics

We write the free energy of a homogeneous unitary gas as $F = N\, f(n, T)$, where the free energy per particle f only depends on the density n and temperature T (and on $\hbar$, m, k_{B}). Scale invariance implies the relation

$$f\left(\frac{n}{\lambda^3}, \frac{T}{\lambda^2}\right) = \frac{f(n,T)}{\lambda^2}. \tag{3.61}$$

Choosing $\lambda = (n/n_0)^{1/3}$ for an arbitrary reference density n_0, we deduce that the free energy is a universal function

$$f(n,T) = E_{\mathrm{F}}\, \varphi\left(\frac{k_{\mathrm{B}}T}{E_{\mathrm{F}}}\right), \tag{3.62}$$

of a single variable. The thermodynamics of the unitary gas is thus fully determined by a universal function of T/T_{F}, as for the ideal Fermi gas [45]. We discuss three consequences of this result.

Zero temperature. At $T = 0$, the energy per particle is proportional to the Fermi energy, i.e. scales as $n^{2/3}$ as for an ideal Fermi gas. We write it as

$$E = \xi \frac{3}{5} N E_{\mathrm{F}}, \tag{3.63}$$

where ξ is a universal number, called the Bertsch parameter. The equation of state is that of an ideal Fermi gas with a renormalized Fermi energy. In particular, the chemical potential reads $\mu = \partial E/\partial N = \xi E_{\mathrm{F}}$ and the pressure $P = (2/5)\xi n E_{\mathrm{F}}$. The determination of ξ was proposed by G. Bertsch as a challenge for many-body theories in 1999. The mean-field theory gives $\xi = \mu/E_{\mathrm{F}} \simeq 0.59$, while the best experimental and numerical determinations give $\xi \simeq 0.37$ (see section 4).

Finite temperature. All thermodynamic quantities are universal functions of T/T_{F}. For instance, the critical temperature for superfluidity is a universal fraction $T_{\mathrm{c}}/T_{\mathrm{F}}$ of the Fermi temperature, and the entropy per particle S/Nk_{B} is a universal function of T/T_{F}. Equivalently, in the grand-canonical ensemble, the density can be written as $n\lambda^3 = h(\mu/k_{\mathrm{B}}T)$, where h is a universal function and λ the thermal de Broglie wavelength.

Virial theorem. At fixed entropy S and particle number N, a dilation of the box by a factor λ maps each eigenstate to an eigenstate of energy divided by λ^2, without changing the occupation probabilities. The energy thus satisfies $E(\lambda^3 V, S, N) = E(V, S, N)/\lambda^2$. Differentiating with respect to λ at $\lambda = 1$, we obtain $3V\partial E/\partial V = -2E$, i.e., using $P = -(\partial E/\partial V)_{S,N}$,

$$PV = \frac{2}{3} E. \tag{3.64}$$

This relation, which holds for the ideal gas, remains true at unitarity in spite of the strong interactions. It does not hold for a finite scattering length, for which the correction can be expressed in terms of the contact, $PV = 2E/3 + \hbar^2 C/(12\pi m a)$ [42].

4 Experimental characterization of the BEC-BCS crossover

In this section, we describe a selection of experiments that characterized the properties of strongly interacting Fermi gases across the BEC-BCS crossover. Since the mean-field theory of section 3 is only qualitatively correct, these measurements provide benchmarks for many-body theories. We first discuss the thermodynamics of the unitary Fermi gas, whose universality allows for precise tests. We then describe measurements of the ground-state properties across the crossover, of Tan's contact, of the superfluid gap, and of superfluidity itself. We then consider spin-imbalanced gases, which have no equivalent in conventional superconductors. We end with a discussion of some open questions in the field.

In all experiments discussed below, the gas is held in a smooth trapping potential $U(\mathbf{r})$, usually harmonic, and the interactions are tuned with a magnetic Feshbach resonance (see section 2). Most experiments use ^{6}Li atoms, the others using ^{40}K atoms.

4.1 Thermodynamics of the unitary Fermi gas

At unitarity, the thermodynamics of the gas is described by universal functions of $T/T_{\rm F}$ (see section 3). We describe how this universality was tested, how the equation of state was measured, and what was learned on the normal and superfluid phases.

4.1.1 Testing the scale invariance

The scale invariance of the unitary gas implies the virial theorem (3.64), $PV = 2E/3$, which can be tested in a harmonic trap. We describe the trapped gas in the local density approximation (LDA), in which the gas behaves locally as a homogeneous system, with a local pressure $P(\mathbf{r})$ and energy density $\varepsilon(\mathbf{r})$ (kinetic and interaction energy) related by $P = 2\varepsilon/3$. The mechanical equilibrium of a fluid element reads

$$\nabla P(\mathbf{r}) + n(\mathbf{r})\nabla U(\mathbf{r}) = \mathbf{0}. \tag{4.1}$$

We multiply this relation by $\mathbf{r}$ and integrate over space. For a harmonic potential $U(\mathbf{r}) = \frac{1}{2}m(\omega_x^2 x^2 + \omega_y^2 y^2 + \omega_z^2 z^2)$, we have $\mathbf{r}\cdot\nabla U = 2U$, so that the second term gives $2N\langle U\rangle$. Integrating the first term by parts, we obtain $\int \mathbf{r}\cdot\nabla P\,\mathrm{d}^3r = -3\int P\,\mathrm{d}^3r = -2E_{\rm int}$, where $E_{\rm int} = \int \varepsilon\,\mathrm{d}^3r$ is the internal (kinetic and interaction) energy. We thus obtain $E_{\rm int} = N\langle U\rangle$, i.e. the total energy $E = E_{\rm int} + N\langle U\rangle$ satisfies

$$N\langle U\rangle = \frac{E}{2}, \tag{4.2}$$

exactly as for an ideal gas. The total energy of the gas can thus be measured from its mean-square size, $E = 2N\langle U\rangle = 3Nm\omega_z^2\langle z^2\rangle$, where the last equality uses the equipartition of $\langle U\rangle$ between the three axes which holds within LDA.

This prediction was tested by the group of J. Thomas at Duke University [46]. A unitary gas of ^{6}Li was prepared with a variable energy E, by applying a controlled energy input from the ground state of energy E_0, and its mean-square size $\langle x^2\rangle$ was measured. The results, shown in Fig. 17, exhibit a linear relation between $\langle x^2\rangle$ and E, with a unit slope in normalized variables, confirming the virial theorem, and hence the scale invariance of the unitary gas, over the whole explored temperature range, including the superfluid regime.

4.1.2 Ground-state energy at unitarity: history

The Bertsch parameter ξ, which gives the ground-state energy $E = \xi\,\frac{3}{5}NE_{\rm F}$ of the unitary gas, has been the subject of an intense theoretical and experimental activity. Its history is summarized in Fig. 18. Analytical approaches (such as the mean-field theory, which gives $\xi \simeq 0.59$, or various resummations of diagrammatic expansions) gave widely scattered values. The first quantum Monte Carlo simulations gave $\xi \simeq 0.44$ [47]. Since these calculations are variational (the fixed-node approximation gives an upper bound to the energy), they progressively decreased with improved trial wave-functions, and various lattice Monte Carlo methods were developed. The first experimental values, deduced from the size of trapped clouds, had large uncertainties, mostly due to the uncertainty on the position of the Feshbach resonance and on the temperature of the gas. The determination of ξ eventually converged around $\xi \simeq 0.37$. The most precise measurement, based on the thermodynamic method described below, gives $\xi = 0.376(4)$ [38], in agreement with the most recent numerical results [48].

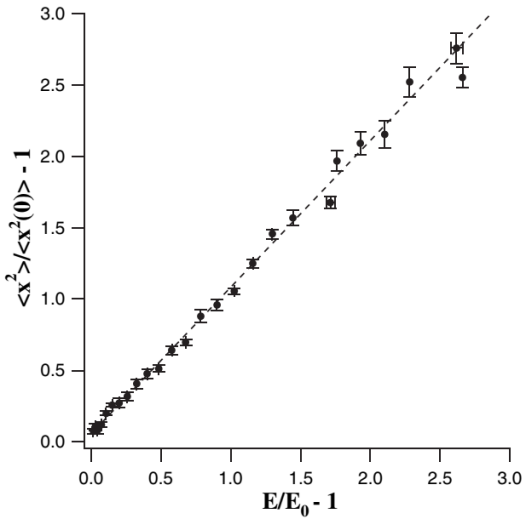


Figure 17: Test of the virial theorem for a unitary gas of ^{6}Li atoms in a harmonic trap. The mean-square cloud size $\langle x^2 \rangle$, normalized to its value in the ground state, is plotted as a function of the energy E normalized to the ground-state energy E_0. The dashed line of unit slope corresponds to the prediction $E \propto \langle x^2 \rangle$. From Ref. [46].

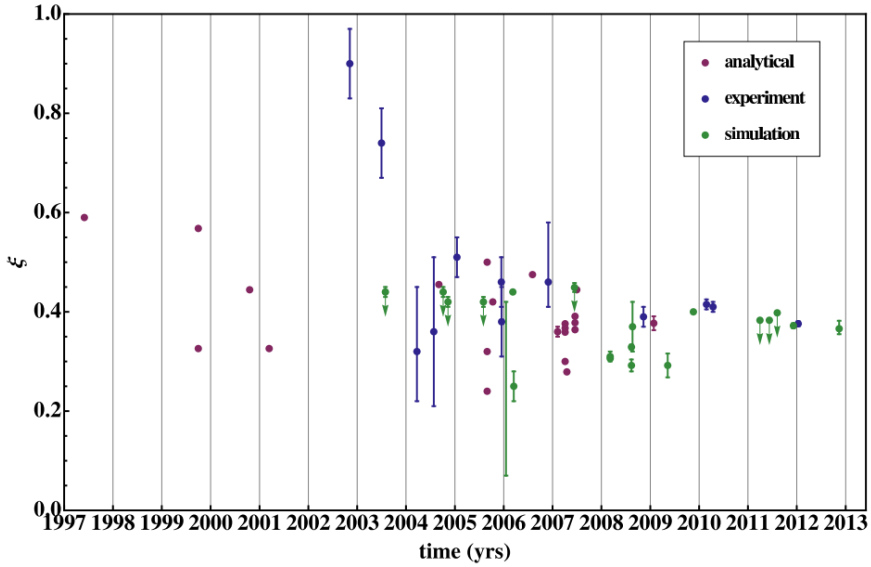


Figure 18: History of the determination of the Bertsch parameter ξ, giving the ground-state energy of the unitary Fermi gas, from analytical calculations (purple), experiments (blue) and numerical simulations (green; arrows indicate upper bounds). From Ref. [48].

4.1.3 Equation of state measurement

The trapping potential $U(\mathbf{r})$ varies slowly at the scale of the inter-particle distance, so that the gas can be described within LDA, i.e. as a collection of homogeneous systems in local equilibrium. The thermodynamic equilibrium conditions read

$$\nabla T = \mathbf{0}, \qquad \nabla P = n\nabla\mu = -n\nabla U, \tag{4.3}$$

where we used the Gibbs-Duhem relation $\mathrm{d}P = n\,\mathrm{d}\mu + s\,\mathrm{d}T$ (with s the entropy density) at uniform temperature, and the mechanical equilibrium (4.1). The temperature is thus uniform, and the local chemical potential reads

$$\mu(\mathbf{r}) = \mu_0 - U(\mathbf{r}). \tag{4.4}$$

A single trapped cloud thus samples the equation of state $n(\mu, T)$ of the homogeneous gas for all chemical potentials below μ_0, at a fixed temperature: the density profile along the potential U directly maps the density as a function of μ. In practice, the local density can be reconstructed from absorption images by an inverse Abel transform, exploiting the symmetry of the trap.

The pressure is obtained by integrating the density over the chemical potential, $P(\mu_0, T) = \int_{-\infty}^{\mu_0} n(\mu, T)\,\mathrm{d}\mu$. Remarkably, it can be measured directly from absorption images [49]. For a harmonic trapping potential in the transverse plane, the doubly integrated density profile reads

$$\bar{n}(z) = \iint n(x, y, z)\,\mathrm{d}x\,\mathrm{d}y = \frac{2\pi}{m\omega_x\omega_y}\int_0^\infty n(\mu_z - u)\,\mathrm{d}u = \frac{2\pi}{m\omega_x\omega_y}P(\mu_z, T), \tag{4.5}$$

where $\mu_z = \mu_0 - U(0, 0, z)$, and where we used the change of variable $u = m(\omega_x^2 x^2 + \omega_y^2 y^2)/2$, with $\mathrm{d}x\,\mathrm{d}y = 2\pi\mathrm{d}u/(m\omega_x\omega_y)$. The doubly integrated profile, obtained from an absorption image integrated along one more axis, thus directly gives the pressure along the z axis.

An example of measurement is shown in Fig. 19 [50]. The density of a unitary gas, measured as a function of the trapping potential, gives the equation of state $n\lambda^3$ as a function of $\mu/k_\mathrm{B}T$, where $\lambda = \sqrt{2\pi\hbar^2/mk_\mathrm{B}T}$ is the thermal de Broglie wavelength. Thanks to scale invariance, all measurements, at different temperatures and densities, collapse on a single universal curve. The measurement was compared with a numerical calculation based on bold diagrammatic Monte Carlo, which sums the diagrammatic expansion of the many-body problem to high orders. The excellent agreement in the normal phase validated this new numerical approach.

4.1.4 Equation of state in the normal phase

The equation of state can be expressed in terms of the pressure normalized to the one of an ideal two-component Fermi gas at the same chemical potential and temperature, P/P_ideal, as a function of the inverse fugacity $\zeta = \exp(-\mu/k_\mathrm{B}T)$. This universal function was measured using the pressure method described above, at temperatures down to the superfluid transition [51] (see Fig. 20). This measurement had two main outcomes.

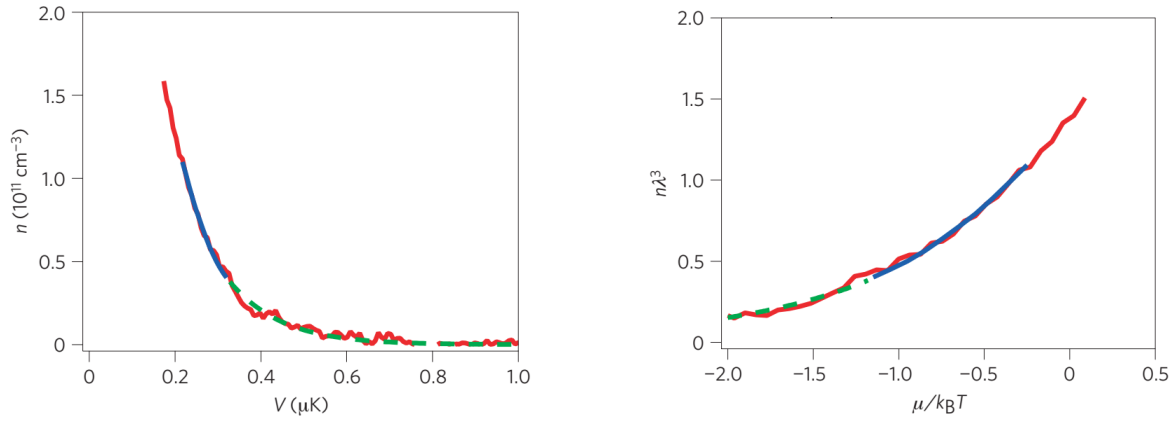


Figure 19: Measurement of the equation of state of the unitary Fermi gas in the normal phase. Left: density n of a trapped gas as a function of the trapping potential U (denoted V in the figure), deduced from absorption images (red line). Right: the same data expressed as the universal equation of state $n\lambda^3$ as a function of $\mu/k_{\rm B}T$. The blue line is the bold diagrammatic Monte Carlo calculation, and the green dashed line the virial expansion valid at high temperature. From Ref. [50].

Discriminating between theories. At the time of the measurement, the theoretical predictions for the unitary gas in the normal phase were scattered, and the measured equation of state allowed one to discriminate between them (see Fig. 20). At low temperature, the normal phase was found to be well described by a Fermi liquid, in spite of the strong interactions.

Virial coefficients. At high temperature ($\zeta \gg 1$), the pressure can be expanded in powers of the fugacity $z = {\rm e}^{\mu/k_{\rm B}T} = 1/\zeta$, as

$$P = \frac{2k_{\rm B}T}{\lambda^3}\left(z + b_2 z^2 + b_3 z^3 + b_4 z^4 + \dots\right). \tag{4.6}$$

The virial coefficient b_n is determined by the solution of the n-body problem. At unitarity, the second-order coefficient is known exactly, $b_2 = 3\sqrt{2}/8$, and the third-order coefficient was computed from the solution of the three-body problem, $b_3 \simeq -0.29$ [52]. The measurement of the equation of state allowed one to check the value of b_3, and to obtain the first determination of the fourth-order coefficient b_4 [51], which is related to the four-body problem. The measurement of a macroscopic quantity thus gives access to the solution of few-body problems.

4.1.5 Superfluid λ transition

The thermodynamics of the unitary gas across the superfluid transition was measured at MIT, by combining measurements of the density and of the compressibility, both obtained from the density profiles [38]. These quantities give access to the pressure, the energy, the entropy and the specific heat, as functions of $T/T_{\rm F}$, without any calibration of the temperature. The specific heat at constant volume, shown in Fig. 21, exhibits a sharp peak at the superfluid transition, at the critical temperature

$$T_{\rm c} = 0.167(13)\, T_{\rm F}. \tag{4.7}$$

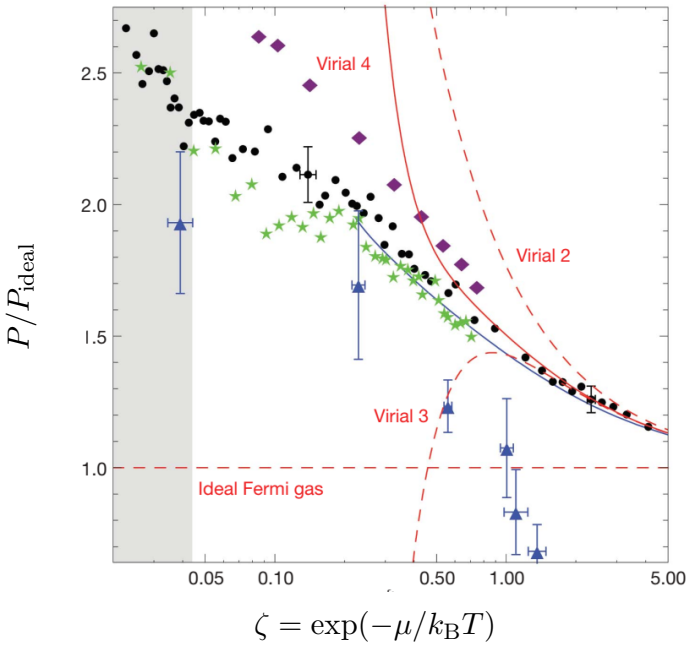


Figure 20: Equation of state of the unitary Fermi gas in the normal phase, expressed as the pressure P normalized to the pressure $P_{\rm ideal}$ of an ideal Fermi gas at the same μ and T, as a function of the inverse fugacity $\zeta = \exp(-\mu/k_{\rm B}T)$. Black dots: measurement of Ref. [51]. The other symbols correspond to other theoretical and experimental determinations, and the red lines are the virial expansions up to orders 2, 3 and 4. The gray area corresponds to the superfluid phase. From Ref. [51].

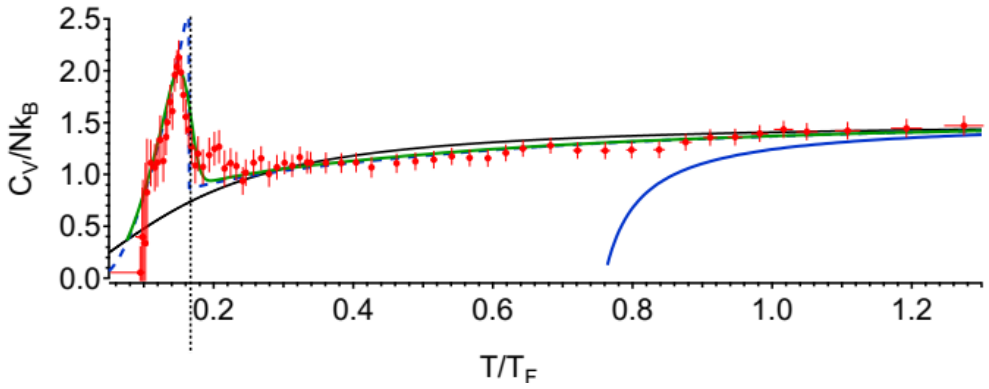


Figure 21: Specific heat per particle C_V/Nk_B of a homogeneous unitary Fermi gas as a function of T/T_F (red points), deduced from the measured equation of state. The sharp peak signals the superfluid transition at $T_\mathrm{c} = 0.167(13)\,T_\mathrm{F}$ (vertical dotted line). The black line is the specific heat of an ideal Fermi gas, which tends to the classical value 3/2 at high temperature; the other lines are theoretical models. From Ref. [38].

This λ-shaped anomaly is reminiscent of the superfluid transition of liquid ^{4}He. Below the transition, the specific heat drops rapidly, as expected for a gapped superfluid whose low-energy excitations are phonons. The same measurement gave the Bertsch parameter $\xi = 0.376(4)$, from the low-temperature limit of the equation of state. At the time of the measurement, no theory was able to quantitatively reproduce the full behavior of the specific heat across the transition.

4.2 Ground state in the BEC-BCS crossover

Away from unitarity, the equation of state also depends on the interaction parameter $1/k_\mathrm{F}a$. We first discuss the ground-state energy across the crossover, which was computed with quantum Monte Carlo methods, and then explain how the collective modes of a trapped gas probe this equation of state.

4.2.1 Ground-state energy in the BEC-BCS crossover

By dimensional analysis, the ground-state energy of a homogeneous gas can be written as

$$E = \frac{3}{5} N E_\mathrm{F}\, \xi\!\left(\frac{1}{k_\mathrm{F}a}\right), \tag{4.8}$$

where $\xi(1/k_\mathrm{F}a)$ is a universal function of the interaction parameter, with $\xi(0)$ the Bertsch parameter and $\xi \to 1$ in the BCS limit. On the BEC side, the energy is dominated by the molecular binding energy $-NE_\mathrm{b}/2$. Fig. 22 shows the energy per particle, from which the molecular binding energy has been subtracted, calculated with the fixed-node diffusion Monte Carlo method [53]. This method is variational in nature: it gives the lowest energy compatible with the nodal structure of a trial wave-function, which was taken of the BCS form. In the BCS regime, the results are close to the perturbative expansion (3.1), while in the BEC regime they are well described by a weakly interacting gas of bosonic molecules with the molecule-molecule scattering length $a_\mathrm{dd} \simeq 0.6\,a$.

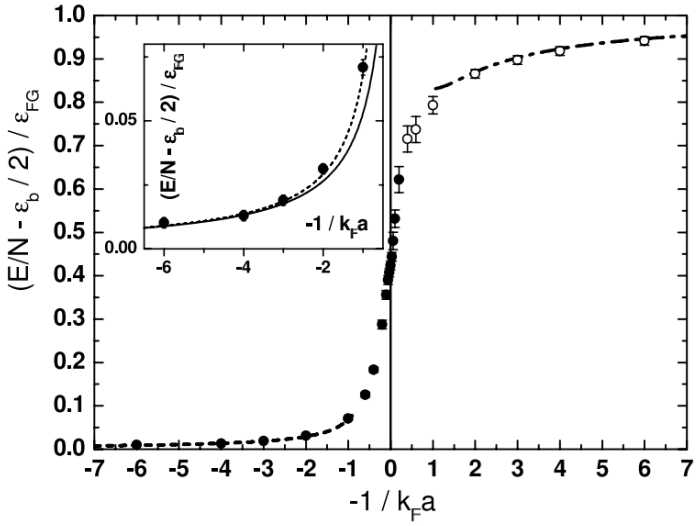


Figure 22: Ground-state energy per particle in the BEC-BCS crossover, calculated with fixed-node diffusion Monte Carlo, as a function of the interaction parameter $-1/k_{\rm F}a$ (BEC side on the left, BCS side on the right). The molecular binding energy contribution $\epsilon_{\rm b}/2$ per particle is subtracted ($\epsilon_{\rm b} = -E_{\rm b}$ on the BEC side, $\epsilon_{\rm b} = 0$ on the BCS side), and the energy is normalized to the energy $\epsilon_{\rm FG} = 3E_{\rm F}/5$ per particle of the ideal Fermi gas. The dashed lines are the asymptotic expansions of a weakly interacting Bose gas of molecules (left) and of the perturbative expansion of a Fermi gas (right). The inset is a zoom on the BEC side. From Ref. [53].

The mean-field theory of section 3 is only qualitatively correct: it gives the correct asymptotic behaviors (except for the Hartree term on the BCS side and the molecular interactions on the BEC side), but it overestimates the energy in the strongly interacting regime ($\xi \simeq 0.59$ instead of 0.37 at unitarity). On the contrary, the Monte Carlo results are quantitatively accurate, as confirmed by the measurement of the equation of state across the crossover [54].

4.2.2 Collective mode measurements

The frequencies of the collective modes of a trapped gas are sensitive to its equation of state, and they can be measured with high precision. We consider a superfluid gas at zero temperature, described by the equations of superfluid hydrodynamics,

$$\partial_t n + \nabla \cdot (n\mathbf{v}) = 0, \qquad m\partial_t \mathbf{v} + \nabla\left(\frac{1}{2}mv^2 + \mu_{\rm loc}(n) + U(\mathbf{r})\right) = \mathbf{0}, \tag{4.9}$$

where $\mu_{\rm loc}(n)$ is the chemical potential of a homogeneous gas of density n. We assume a polytropic equation of state $\mu_{\rm loc} \propto n^\gamma$, which describes the BEC limit ($\gamma = 1$, mean-field interactions between molecules), the unitary gas and the BCS limit ($\gamma = 2/3$, as for an ideal Fermi gas).

We consider a very elongated trap, $U = \frac{1}{2}m\omega_\perp^2\rho^2$ in the transverse plane, and the radial breathing mode. We look for a solution of the hydrodynamic equations in the form of a scaling of the equilibrium density profile n_0 in the transverse direction, $n(\boldsymbol{\rho}, z, t) = n_0(\boldsymbol{\rho}/b(t), z)/b(t)^2$, with the velocity field $\mathbf{v} = (\dot{b}/b)\boldsymbol{\rho}$, which satisfies the

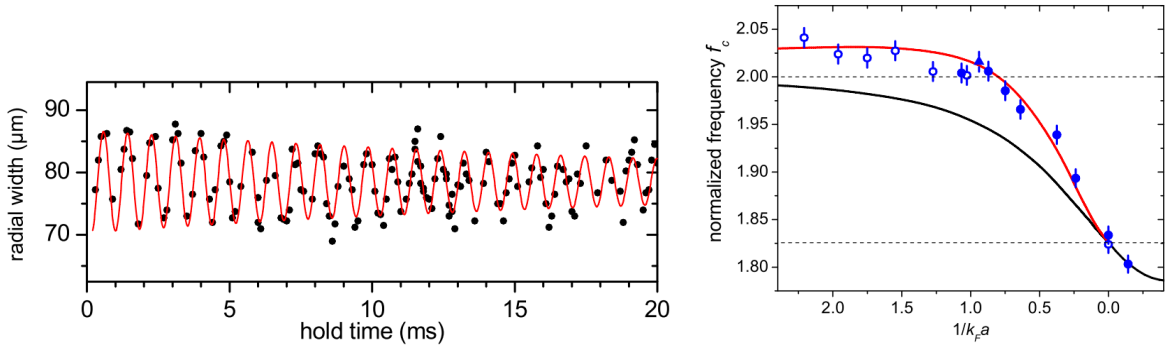


Figure 23: (a) Oscillation of the radial width of an elongated ^{6}Li cloud after the excitation of the radial breathing mode, with a fit by a damped sinusoid (red line). (b) Frequency of the radial breathing mode, normalized to the transverse trap frequency, as a function of $1/k_F a$. The dashed lines indicate the hydrodynamic values 2 (BEC limit) and $\sqrt{10/3} \simeq 1.826$ (unitarity). The red and black lines are the predictions obtained from the Monte Carlo and mean-field equations of state, respectively. From Ref. [55].

continuity equation. The equilibrium profile satisfies $\mu_{\rm loc}(n_0(\boldsymbol{\rho})) = \mu_0 - \frac{1}{2}m\omega_\perp^2\rho^2$, so that, for a polytropic equation of state,

$$\mu_{\rm loc}(n) = \frac{1}{b^{2\gamma}}\left(\mu_0 - \frac{m\omega_\perp^2\rho^2}{2b^2}\right). \tag{4.10}$$

Inserting this expression in the Euler equation, and using $\partial_t \mathbf{v} + \nabla(v^2/2) = (\ddot{b}/b)\boldsymbol{\rho}$, we obtain the scaling equation

$$\ddot{b} = -\omega_\perp^2 b + \frac{\omega_\perp^2}{b^{2\gamma+1}}. \tag{4.11}$$

Linearizing around $b = 1$, we obtain the frequency of the radial breathing mode

$$\omega_{\rm c} = \sqrt{2(\gamma+1)}\,\omega_\perp, \tag{4.12}$$

which equals $2\,\omega_\perp$ in the BEC limit and $\sqrt{10/3}\,\omega_\perp \simeq 1.826\,\omega_\perp$ at unitarity and in the BCS limit (for a superfluid in the hydrodynamic regime).

The radial breathing mode was studied in Innsbruck with a gas of ^{6}Li atoms [55]. The mode was excited by a rapid change of the transverse confinement, and the radial width of the cloud was measured as a function of time (see Fig. 23a). The measured frequency is shown as a function of the interaction parameter in Fig. 23b. It reaches the value $1.826\,\omega_\perp$ at unitarity, confirming the hydrodynamic behavior. On the BEC side, it exceeds the mean-field value $2\,\omega_\perp$: this upward shift is due to the beyond-mean-field (Lee-Huang-Yang) correction to the equation of state of the molecular condensate, which increases the effective polytropic index. The measurement is in excellent agreement with the frequency calculated with the Monte Carlo equation of state (red line), while the mean-field BCS theory (black line) predicts a downward shift, which is ruled out.

4.3 Measurement of the contact

Tan's relations (see section 3) provide several independent methods to measure the contact. The first measurements were performed at JILA with a ^{40}K Fermi gas [56].

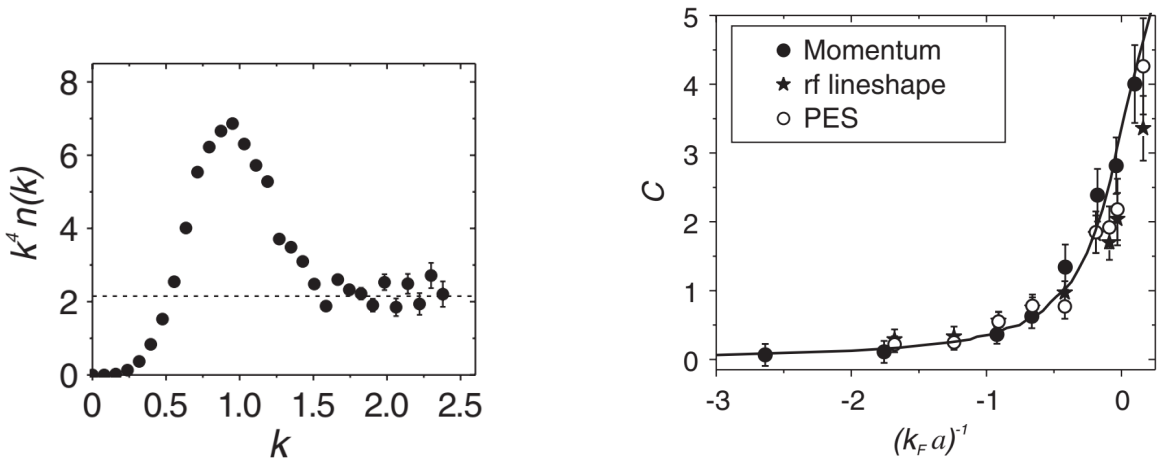


Figure 24: (a) Momentum distribution of a strongly interacting ^{40}K gas multiplied by k^4, as a function of k in units of k_F; the plateau at large momentum gives the contact (dashed line). (b) Contact (in units of Nk_F) measured as a function of the interaction parameter $1/k_\mathrm{F}a$, from the momentum distribution (filled circles), from the tail of radio-frequency spectra (stars) and from photoemission spectroscopy (open circles). The line is a theoretical prediction for the trapped gas at zero temperature. From Ref. [56].

Momentum distribution. The momentum distribution of the gas was measured by ballistic expansion, after a fast magnetic field ramp to the zero of the scattering length, which suppresses the interaction energy release during expansion. As shown in Fig. 24a, the quantity $k^4 n(k)$ reaches a plateau at large momentum, as expected from the relation (3.54), whose height gives the contact.

Other observables. The contact was also measured from the large-frequency tails of radio-frequency spectra, from momentum-resolved radio-frequency spectroscopy (photoemission spectroscopy) [56], from the variation of the equation of state with the scattering length using the adiabatic relation (3.55) [54], and from the pair correlations measured by Bragg spectroscopy at large momentum [57].

Results. The values of the contact obtained with the different methods, shown in Fig. 24b, agree with each other, which confirms the universal relations. They also agree with the theoretical prediction for the trapped gas at low temperature. At finite temperature, the evolution of the contact, in particular across the superfluid transition, remained less well understood theoretically at the time of these measurements.

4.4 Excitations and superfluid gap

The superfluid gap Δ can be measured by radio-frequency spectroscopy, which consists in transferring atoms from one of the two spin states to an initially empty third internal state, weakly interacting with the other two. The energy required to remove an atom from the gas depends on its environment: removing an atom from a pair requires to break it, which shifts the resonance frequency with respect to the bare atomic transition. The spectrum of a superfluid thus provides information on the pairing energy, but

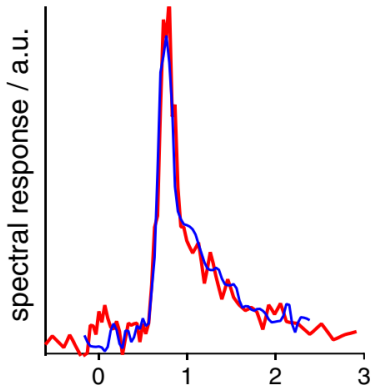


Figure 25: Radio-frequency spectrum of the unpaired majority atoms in a spin-imbalanced unitary superfluid, as a function of the excitation energy (horizontal axis). The spectral peak corresponds to the transfer of quasiparticles close to the minimum of the dispersion relation. From Ref. [58].

its interpretation is complicated by final-state interactions and by the pair-breaking continuum.

A cleaner determination of the gap was obtained at MIT with a slightly spin-imbalanced unitary gas [58]. The excess atoms of the majority component cannot be paired, and they occupy quasiparticle states of the superfluid, at the minimum of the dispersion relation. The radio-frequency spectrum of these unpaired atoms (see Fig. 25) differs from the spectrum of paired atoms, and the comparison of the two spectra gives the quasiparticle dispersion relation close to its minimum. At unitarity, this measurement gives

$$\Delta = 0.44(3)\, E_{\mathrm{F}}, \tag{4.13}$$

significantly smaller than the mean-field prediction $0.69\, E_{\mathrm{F}}$, consistent with the reduction of the gap by the induced interactions already discussed in the BCS limit (see section 3).

4.5 Superfluidity

The pair condensate is expected to be superfluid across the whole crossover. Superfluidity, i.e. the ability to flow without friction, was demonstrated in two ways: by the existence of a critical velocity below which a moving obstacle does not create excitations, and by the observation of quantized vortices in a rotating gas.

4.5.1 Critical velocity

According to Landau's criterion, an obstacle moving at a velocity v can only create excitations of momentum $\hbar\mathbf{k}$ and energy $\epsilon(\mathbf{k})$ if $v \geq \epsilon(\mathbf{k})/\hbar k$. The superfluid flow is thus dissipationless below the critical velocity

$$v_{\mathrm{c}} = \min_{\mathbf{k}} \frac{\epsilon(\mathbf{k})}{\hbar k}. \tag{4.14}$$

In the BEC-BCS crossover, two types of excitations compete:

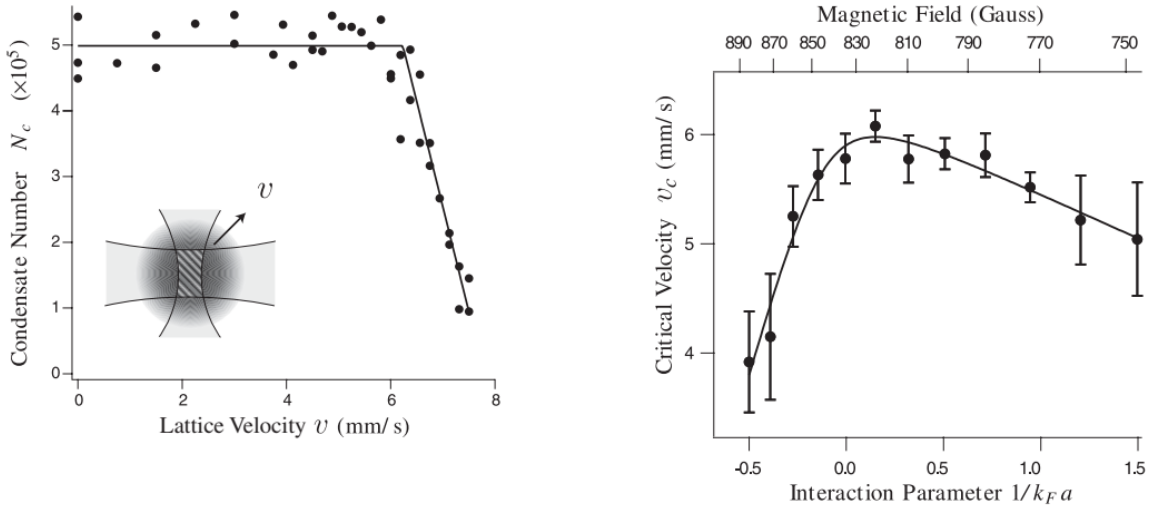


Figure 26: Critical velocity of a fermionic superfluid. Left: number of condensed pairs after the passage of a moving optical lattice (inset), as a function of the lattice velocity. Right: critical velocity as a function of the interaction parameter $1/k_{\rm F}a$ (bottom axis) and of the magnetic field (top axis). From Ref. [59].

- The phonons (Bogoliubov-Anderson mode), which propagate at the sound velocity $c = \sqrt{(n/m)\,\partial\mu/\partial n}$. In the BEC limit, the sound velocity is the Bogoliubov sound velocity of the molecular condensate, which vanishes when the molecular interactions vanish ($k_{\rm F}a \to 0^+$). At unitarity, using $\mu = \xi E_{\rm F} \propto n^{2/3}$, we obtain $c = \sqrt{\xi/3}\, v_{\rm F} \simeq 0.35\, v_{\rm F}$.
- The pair-breaking excitations, which create two quasiparticles. The corresponding critical velocity is $v_{\rm pb} = \min_k E_k/\hbar k = \sqrt{(\sqrt{\mu^2+\Delta^2}-\mu)/m}$, as shown in the AQM notes. In the BCS limit, it reads $v_{\rm pb} \simeq \Delta/\hbar k_{\rm F}$, which is exponentially small. At unitarity, using $\mu \simeq 0.37\, E_{\rm F}$ and $\Delta \simeq 0.44\, E_{\rm F}$, we obtain $v_{\rm pb} \simeq 0.32\, v_{\rm F}$.

The critical velocity is thus limited by phonon emission on the BEC side and by pair breaking on the BCS side, and it reaches a maximum in the strongly interacting regime, where both mechanisms have similar critical velocities.

This behavior was observed at MIT [59]. A one-dimensional optical lattice, formed by two laser beams of slightly different frequencies, was moved through the center of the superfluid at an adjustable velocity v. After the perturbation, the number of condensed pairs was measured. As shown in Fig. 26, the condensate is unaffected below a critical velocity $v_{\rm c}$, and it rapidly decays above $v_{\rm c}$. The critical velocity, measured across the crossover, reaches a maximum close to unitarity, as expected. The measured values are smaller than the predictions for a homogeneous gas, since the critical velocity is reduced in the low-density regions of the trapped cloud.

4.5.2 Quantized vortices

The pair condensate is described by a complex order parameter, proportional to the gap $\Delta(\mathbf{r}) = |\Delta(\mathbf{r})|e^{i\theta(\mathbf{r})}$, which plays the role of a macroscopic wave-function for the

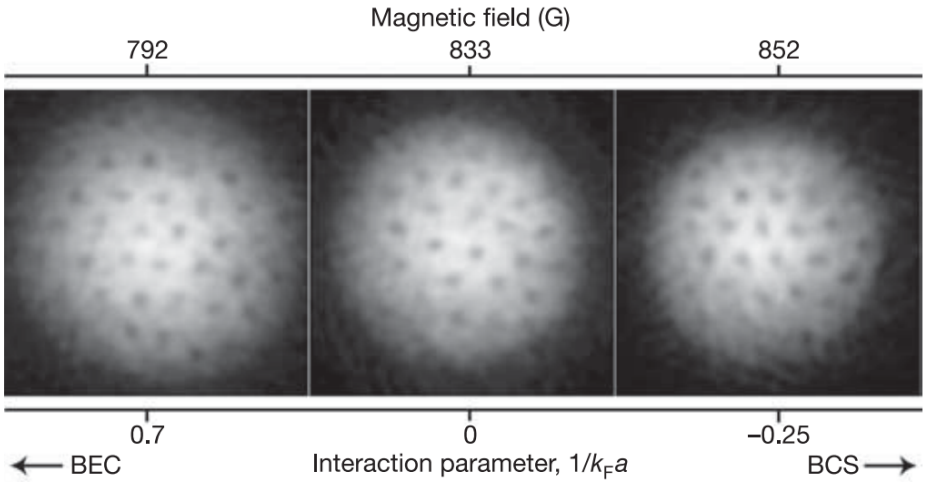


Figure 27: Vortex lattices in a rotating strongly interacting Fermi gas of ^{6}Li, observed across the BEC-BCS crossover, for interaction parameters $1/k_\mathrm{F}a = 0.7$ (BEC side), 0 (unitarity) and -0.25 (BCS side). From Ref. [13].

center-of-mass motion of the pairs. As for a Bose-Einstein condensate of particles of mass M described by a classical field $\psi = \sqrt{n}\mathrm{e}^{\mathrm{i}\theta}$, the superfluid velocity is given by the gradient of the phase,

$$\mathbf{v} = \frac{\hbar}{M}\nabla\theta, \qquad M = 2m, \tag{4.15}$$

where the relevant mass is the mass $2m$ of a pair. The flow is thus irrotational, $\nabla \times \mathbf{v} = \mathbf{0}$, wherever the order parameter does not vanish. Since the order parameter is single-valued, its phase can only change by a multiple of 2π along a closed contour $\mathcal{C}$, so that the circulation of the velocity is quantized:

$$\oint_\mathcal{C} \mathbf{v}\cdot\mathrm{d}\boldsymbol{l} = \frac{\hbar}{2m}\oint_\mathcal{C}\nabla\theta\cdot\mathrm{d}\boldsymbol{l} = p\,\frac{h}{2m}, \qquad p\in\mathbb{Z}. \tag{4.16}$$

A superfluid can thus only rotate through the nucleation of vortex lines, around which the phase winds by 2π and on which the order parameter vanishes. The vorticity is concentrated on these singular lines. For a superfluid rotating at an angular frequency Ω, the vortices arrange in a regular (Abrikosov) lattice, whose density $2\Omega/(h/2m) = 4m\Omega/h$ is such that the superfluid mimics on average a solid-body rotation (Feynman's relation).

Vortex lattices were observed at MIT across the whole BEC-BCS crossover [13], providing an unambiguous proof of superfluidity (see Fig. 27). The superfluid was set in rotation by a rotating laser beam, and imaged after time-of-flight expansion. In order to make the vortex cores visible, the magnetic field was rapidly ramped to the BEC side at the beginning of the expansion, converting the pairs into tightly bound molecules, whose condensate has smaller vortex cores and a larger density contrast.

4.6 Spin-imbalanced Fermi gases

Since the numbers of atoms in the two spin states are separately conserved (in the absence of spin-changing collisions), one can prepare gases with unequal populations $N_\uparrow \neq N_\downarrow$. The spin imbalance frustrates pairing, and it gives rise to a rich phase diagram.

Zeeman field and Chandrasekhar-Clogston limit. In the grand-canonical ensemble, a spin imbalance corresponds to different chemical potentials $\mu_\uparrow \neq \mu_\downarrow$. We write $\mu_{\uparrow,\downarrow} = \mu \pm h$, where $h = (\mu_\uparrow - \mu_\downarrow)/2$ plays the role of a Zeeman field acting on the spin. In the BCS limit, the BCS state is unaffected by a small field $h < \Delta$, since all quasiparticle states are gapped and remain empty: the superfluid remains unpolarized. For large fields, the normal state gains a Zeeman energy by polarizing, i.e. $-\nu(E_\mathrm{F})h^2$ per unit volume, where $\nu(E_\mathrm{F})$ is the density of states per spin state and per unit volume at the Fermi surface. The superfluid has a lower energy than the normal state by the condensation energy $\nu(E_\mathrm{F})\Delta^2/2$ per unit volume. Equating these two energies, we obtain the critical field for the first-order transition to the polarized normal state, called the Chandrasekhar-Clogston limit [60, 61]:

$$h_c = \frac{\Delta}{\sqrt{2}}. \tag{4.17}$$

In superconductors, this pair-breaking mechanism is usually not accessible, since a magnetic field is expelled from the superconductor by the Meissner effect, and its orbital effect destroys superconductivity before the Zeeman effect becomes relevant. With neutral atoms, the population imbalance can be controlled independently of any orbital effect.

Phase diagram at unitarity. At unitarity and zero temperature, the phase of the homogeneous gas only depends on the ratio $\mu_\downarrow/\mu_\uparrow$ (for $\mu_\uparrow > \mu_\downarrow$), as a consequence of scale invariance. The phase diagram, shown in Fig. 28, contains three phases:

- For $\mu_\downarrow/\mu_\uparrow < -0.615$, the minority atoms are absent and the gas is a fully polarized ideal Fermi gas of $\uparrow$ atoms. The critical value corresponds to the energy $-0.615\,\mu_\uparrow$ of a single $\downarrow$ atom immersed in the Fermi sea of $\uparrow$ atoms, dressed by the interactions (Fermi polaron).
- For $-0.615 < \mu_\downarrow/\mu_\uparrow < 0.02$, the gas is a partially polarized normal mixture, well described by a Fermi liquid of polarons.
- For $\mu_\downarrow/\mu_\uparrow > 0.02$, the gas is an unpolarized superfluid, with $n_\uparrow = n_\downarrow$. The transition between the normal and superfluid phases is of first order, with a jump of the polarization.

Trapped gas: phase separation. In a harmonic trap, the local chemical potentials $\mu_\sigma(\mathbf{r}) = \mu_\sigma^0 - U(\mathbf{r})$ decrease from the center to the edges of the cloud, so that the ratio $\mu_\downarrow(\mathbf{r})/\mu_\uparrow(\mathbf{r})$ decreases outwards. Within LDA, the cloud thus exhibits a shell structure, with an unpolarized superfluid core, surrounded by a partially polarized normal shell, and an outer shell of fully polarized majority atoms. This phase separation was observed by directly imaging the in-situ density profiles of both spin components, first at Rice and MIT [62, 63]. Fig. 29a shows the reconstructed three-dimensional density profiles: the densities of the two components are equal in the superfluid core, up to a radius R_c at which the minority density jumps, signaling the first-order phase transition. By varying the polarization and the temperature, the phase diagram of the imbalanced gas at unitarity was mapped out [64] (see Fig. 29b). The first-order transition between the superfluid and the normal phase at low temperature turns into a second-order transition at high temperature, the two lines meeting at a tricritical point.

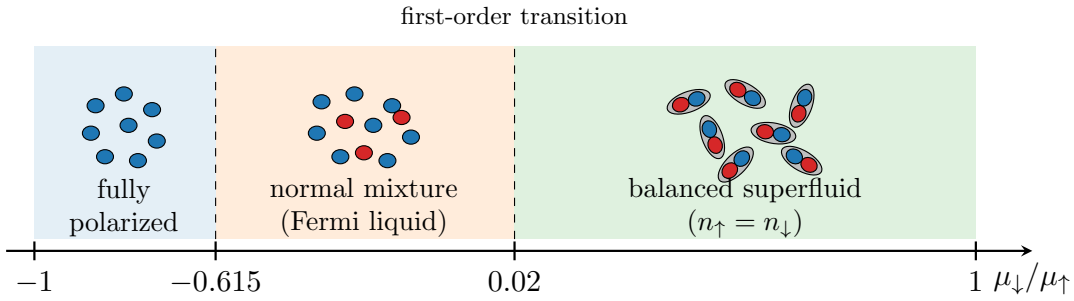


Figure 28: Zero-temperature phase diagram of a homogeneous spin-imbalanced unitary Fermi gas as a function of the ratio $\mu_\downarrow/\mu_\uparrow$ of the chemical potentials of the minority and majority components (blue: $\uparrow$ atoms, red: $\downarrow$ atoms).

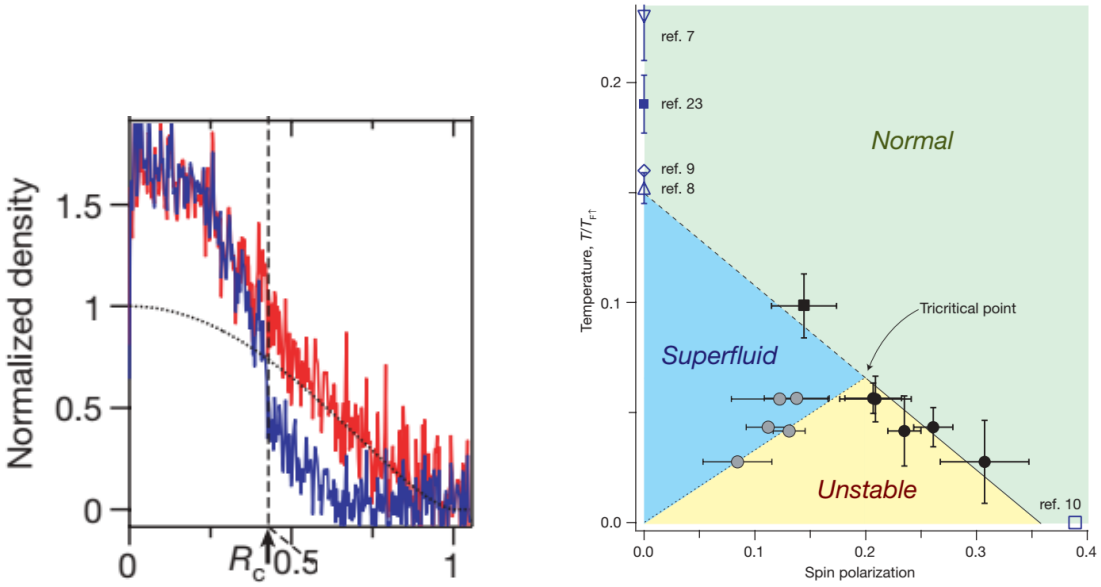


Figure 29: (a) Normalized in-situ density profiles of the majority (red) and minority (blue) components of a spin-imbalanced unitary gas, as a function of the radius normalized to the cloud size. The densities are equal in the superfluid core, up to the radius R_c of the first-order transition. (b) Phase diagram of the imbalanced unitary gas as a function of the spin polarization and of the temperature normalized to the Fermi temperature of the majority component, showing the superfluid phase, the normal phase and the region of phase separation (unstable for a homogeneous system), separated by first-order (solid) and second-order (dashed) transition lines meeting at a tricritical point. From Ref. [64].

4.7 Open questions

We conclude this section with a few research directions that were open at the time of these lectures, and in which ultracold Fermi gases offer unique possibilities.

Exotic superfluidity in weakly imbalanced gases. For a spin imbalance just above the Chandrasekhar-Clogston limit, Fulde and Ferrell [65], and Larkin and Ovchinnikov [66], proposed that pairing can occur at a finite center-of-mass momentum $\hbar\mathbf{q}$. When the two Fermi spheres have different radii $k_{\mathrm{F}\uparrow} > k_{\mathrm{F}\downarrow}$, pairing between $\mathbf{k} + \mathbf{q}/2$ and $-\mathbf{k} + \mathbf{q}/2$ with $q \simeq k_{\mathrm{F}\uparrow} - k_{\mathrm{F}\downarrow}$ allows one to match the two Fermi surfaces in a region of momentum space (see Fig. 30). The resulting FFLO superfluid has an order parameter modulated in space, $\Delta(\mathbf{r}) \propto \mathrm{e}^{\mathrm{i}\mathbf{q}\cdot\mathbf{r}}$ or $\cos(\mathbf{q}\cdot\mathbf{r})$, which spontaneously breaks translation symmetry. In three dimensions, this phase is expected in a narrow region of the phase diagram, and it has not been observed with ultracold atoms. It is expected to be more robust in one dimension, where indirect evidence was reported [67].

Mixtures of different species. Mixtures of fermionic atoms of different elements (such as ^{6}Li-^{40}K or ^{161}Dy-^{40}K) give rise to Fermi superfluids with mass imbalance, whose pairing properties differ from the equal-mass case. For a large mass ratio, three-body bound states (Efimov trimers) can form, made of two heavy fermions and one light atom. For identical fermions, the Efimov effect only occurs for a mass ratio larger than 13.6; at smaller mass ratios, non-Efimovian trimers can exist. The occurrence of three-body bound states breaks the universality of the two-component problem, and it could lead to new many-body phases. Efimov trimers, predicted in 1970 [68], were first observed with bosonic caesium atoms [27].

Low dimensions. In two dimensions, thermal fluctuations destroy long-range order at any finite temperature, but a superfluid transition still occurs, of Berezinskii-Kosterlitz-Thouless (BKT) type, driven by the unbinding of vortex-antivortex pairs. The BKT transition and the condensation of fermion pairs in the two-dimensional BEC-BCS crossover were observed with ^{6}Li [69, 70]. In one dimension, interacting fermions form a Luttinger liquid, whose low-energy excitations are collective density and spin waves, propagating at different velocities (spin-charge separation).

Artificial gauge fields. Neutral atoms do not experience the Lorentz force, but they can be subjected to artificial gauge fields, created by rotation or by laser-induced couplings between internal states [71]. This would allow the realization of the quantum Hall effect, the hallmark of which is the quantization of the Hall resistance of a two-dimensional electron gas in a strong magnetic field [72], as well as topological insulators and topological superfluids with ultracold atoms.

References

[1] B. DeMarco and D. S. Jin. Onset of Fermi degeneracy in a trapped atomic gas. *Science*, 285:1703, 1999.

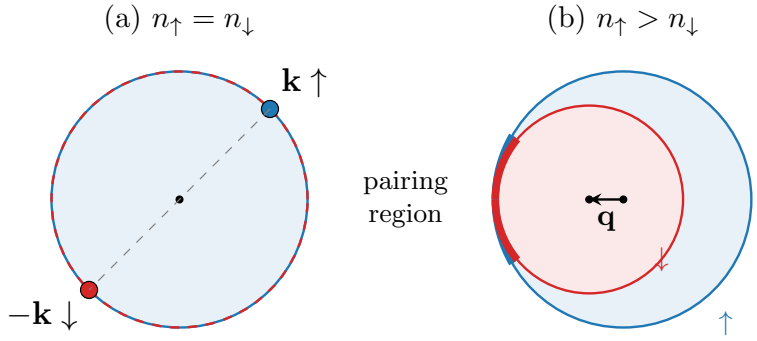


Figure 30: (a) In a balanced gas, the Fermi spheres of the two spin states coincide, and Cooper pairs ($\mathbf{k}\uparrow, -\mathbf{k}\downarrow$) have a zero center-of-mass momentum. (b) In an imbalanced gas, the Fermi spheres have different radii. Pairing with a finite center-of-mass momentum $\hbar\mathbf{q}$, as in the FFLO state, amounts to shifting the minority Fermi sphere (red) by $\mathbf{q}$, such that the two Fermi surfaces match in a region of momentum space (thick lines).

[2] L. N. Cooper. Bound electron pairs in a degenerate Fermi gas. *Phys. Rev.*, 104:1189, 1956.

[3] J. Bardeen, L. N. Cooper, and J. R. Schrieffer. Theory of superconductivity. *Phys. Rev.*, 108:1175, 1957.

[4] D. M. Eagles. Possible pairing without superconductivity at low carrier concentrations in bulk and thin-film superconducting semiconductors. *Phys. Rev.*, 186:456, 1969.

[5] A. J. Leggett. Cooper pairing in spin-polarized Fermi systems. *J. Phys. Colloques*, 41:C7–19, 1980.

[6] P. Nozières and S. Schmitt-Rink. Bose condensation in an attractive fermion gas: from weak to strong coupling superconductivity. *J. Low Temp. Phys.*, 59:195, 1985.

[7] K. M. O'Hara, S. L. Hemmer, M. E. Gehm, S. R. Granade, and J. E. Thomas. Observation of a strongly interacting degenerate Fermi gas of atoms. *Science*, 298:2179, 2002.

[8] M. Greiner, C. A. Regal, and D. S. Jin. Emergence of a molecular Bose-Einstein condensate from a Fermi gas. *Nature*, 426:537, 2003.

[9] S. Jochim, M. Bartenstein, A. Altmeyer, G. Hendl, S. Riedl, C. Chin, J. Hecker Denschlag, and R. Grimm. Bose-Einstein condensation of molecules. *Science*, 302:2101, 2003.

[10] M. W. Zwierlein, C. A. Stan, C. H. Schunck, S. M. F. Raupach, S. Gupta, Z. Hadzibabic, and W. Ketterle. Observation of Bose-Einstein condensation of molecules. *Phys. Rev. Lett.*, 91:250401, 2003.

[11] C. A. Regal, M. Greiner, and D. S. Jin. Observation of resonance condensation of fermionic atom pairs. *Phys. Rev. Lett.*, 92:040403, 2004.

[12] M. W. Zwierlein, C. A. Stan, C. H. Schunck, S. M. F. Raupach, A. J. Kerman, and W. Ketterle. Condensation of pairs of fermionic atoms near a Feshbach resonance. *Phys. Rev. Lett.*, 92:120403, 2004.

[13] M. W. Zwierlein, J. R. Abo-Shaeer, A. Schirotzek, C. H. Schunck, and W. Ketterle. Vortices and superfluidity in a strongly interacting Fermi gas. *Nature*, 435:1047, 2005.

[14] S. Giorgini, L. P. Pitaevskii, and S. Stringari. Theory of ultracold atomic Fermi gases. *Rev. Mod. Phys.*, 80:1215, 2008.

[15] W. Ketterle and M. W. Zwierlein. Making, probing and understanding ultracold Fermi gases. *Riv. Nuovo Cimento*, 31:247, 2008.

[16] W. Zwerger, editor. *The BCS-BEC Crossover and the Unitary Fermi Gas*, volume 836 of *Lecture Notes in Physics*. Springer, Berlin, 2012.

[17] B. DeMarco, J. L. Bohn, J. P. Burke, Jr., M. Holland, and D. S. Jin. Measurement of p-wave threshold law using evaporatively cooled fermionic atoms. *Phys. Rev. Lett.*, 82:4208, 1999.

[18] G. F. Gribakin and V. V. Flambaum. Calculation of the scattering length in atomic collisions using the semiclassical approximation. *Phys. Rev. A*, 48:546, 1993.

[19] K. Huang and C. N. Yang. Quantum-mechanical many-body problem with hard-sphere interaction. *Phys. Rev.*, 105:767, 1957.

[20] S. Inouye, M. R. Andrews, J. Stenger, H.-J. Miesner, D. M. Stamper-Kurn, and W. Ketterle. Observation of Feshbach resonances in a Bose-Einstein condensate. *Nature*, 392:151, 1998.

[21] C. Chin, R. Grimm, P. Julienne, and E. Tiesinga. Feshbach resonances in ultracold gases. *Rev. Mod. Phys.*, 82:1225, 2010.

[22] C. A. Regal and D. S. Jin. Measurement of positive and negative scattering lengths in a Fermi gas of atoms. *Phys. Rev. Lett.*, 90:230404, 2003.

[23] M. Bartenstein, A. Altmeyer, S. Riedl, R. Geursen, S. Jochim, C. Chin, J. Hecker Denschlag, R. Grimm, A. Simoni, E. Tiesinga, C. J. Williams, and P. S. Julienne. Precise determination of ^{6}Li cold collision parameters by radio-frequency spectroscopy on weakly bound molecules. *Phys. Rev. Lett.*, 94:103201, 2005.

[24] T. D. Lee, K. Huang, and C. N. Yang. Eigenvalues and eigenfunctions of a Bose system of hard spheres and its low-temperature properties. *Phys. Rev.*, 106:1135, 1957.

[25] N. Navon, S. Piatecki, K. Günter, B. Rem, T. C. Nguyen, F. Chevy, W. Krauth, and C. Salomon. Dynamics and thermodynamics of the low-temperature strongly interacting Bose gas. *Phys. Rev. Lett.*, 107:135301, 2011.

[26] R. Lopes, C. Eigen, N. Navon, D. Clément, R. P. Smith, and Z. Hadzibabic. Quantum depletion of a homogeneous Bose-Einstein condensate. *Phys. Rev. Lett.*, 119:190404, 2017.

[27] T. Kraemer, M. Mark, P. Waldburger, J. G. Danzl, C. Chin, B. Engeser, A. D. Lange, K. Pilch, A. Jaakkola, H.-C. Nägerl, and R. Grimm. Evidence for Efimov quantum states in an ultracold gas of caesium atoms. *Nature*, 440:315, 2006.

[28] T. Weber, J. Herbig, M. Mark, H.-C. Nägerl, and R. Grimm. Three-body recombination at large scattering lengths in an ultracold atomic gas. *Phys. Rev. Lett.*, 91:123201, 2003.

[29] D. S. Petrov, C. Salomon, and G. V. Shlyapnikov. Weakly bound dimers of fermionic atoms. *Phys. Rev. Lett.*, 93:090404, 2004.

[30] J. Cubizolles, T. Bourdel, S. J. J. M. F. Kokkelmans, G. V. Shlyapnikov, and C. Salomon. Production of long-lived ultracold Li_2 molecules from a Fermi gas. *Phys. Rev. Lett.*, 91:240401, 2003.

[31] K. E. Strecker, G. B. Partridge, and R. G. Hulet. Conversion of an atomic Fermi gas to a long-lived molecular Bose gas. *Phys. Rev. Lett.*, 91:080406, 2003.

[32] C. A. Regal, M. Greiner, and D. S. Jin. Lifetime of molecule-atom mixtures near a Feshbach resonance in ^{40}K. *Phys. Rev. Lett.*, 92:083201, 2004.

[33] C. A. Regal, C. Ticknor, J. L. Bohn, and D. S. Jin. Creation of ultracold molecules from a Fermi gas of atoms. *Nature*, 424:47, 2003.

[34] T. D. Lee and C. N. Yang. Many-body problem in quantum mechanics and quantum statistical mechanics. *Phys. Rev.*, 105:1119, 1957.

[35] L. P. Gor'kov and T. K. Melik-Barkhudarov. Contribution to the theory of superfluidity in an imperfect Fermi gas. *Sov. Phys. JETP*, 13:1018, 1961.

[36] C. A. R. Sá de Melo, M. Randeria, and J. R. Engelbrecht. Crossover from BCS to Bose superconductivity: transition temperature and time-dependent Ginzburg-Landau theory. *Phys. Rev. Lett.*, 71:3202, 1993.

[37] E. Burovski, N. Prokof'ev, B. Svistunov, and M. Troyer. Critical temperature and thermodynamics of attractive fermions at unitarity. *Phys. Rev. Lett.*, 96:160402, 2006.

[38] M. J. H. Ku, A. T. Sommer, L. W. Cheuk, and M. W. Zwierlein. Revealing the superfluid lambda transition in the universal thermodynamics of a unitary Fermi gas. *Science*, 335:563, 2012.

[39] R. Haussmann, W. Rantner, S. Cerrito, and W. Zwerger. Thermodynamics of the BCS-BEC crossover. *Phys. Rev. A*, 75:023610, 2007.

[40] S. Tan. Energetics of a strongly correlated Fermi gas. *Ann. Phys.*, 323:2952, 2008.

[41] S. Tan. Large momentum part of a strongly correlated Fermi gas. *Ann. Phys.*, 323:2971, 2008.

[42] S. Tan. Generalized virial theorem and pressure relation for a strongly correlated Fermi gas. *Ann. Phys.*, 323:2987, 2008.

[43] E. Braaten and L. Platter. Exact relations for a strongly interacting Fermi gas from the operator product expansion. *Phys. Rev. Lett.*, 100:205301, 2008.

[44] F. Werner and Y. Castin. General relations for quantum gases in two and three dimensions: two-component fermions. *Phys. Rev. A*, 86:013626, 2012.

[45] T.-L. Ho. Universal thermodynamics of degenerate quantum gases in the unitarity limit. *Phys. Rev. Lett.*, 92:090402, 2004.

[46] J. E. Thomas, J. Kinast, and A. Turlapov. Virial theorem and universality in a unitary Fermi gas. *Phys. Rev. Lett.*, 95:120402, 2005.

[47] J. Carlson, S.-Y. Chang, V. R. Pandharipande, and K. E. Schmidt. Superfluid Fermi gases with large scattering length. *Phys. Rev. Lett.*, 91:050401, 2003.

[48] M. G. Endres, D. B. Kaplan, J.-W. Lee, and A. N. Nicholson. Lattice Monte Carlo calculations for unitary fermions in a finite box. *Phys. Rev. A*, 87:023615, 2013.

[49] T.-L. Ho and Q. Zhou. Obtaining the phase diagram and thermodynamic quantities of bulk systems from the densities of trapped gases. *Nature Phys.*, 6:131, 2010.

[50] K. Van Houcke, F. Werner, E. Kozik, N. Prokof'ev, B. Svistunov, M. J. H. Ku, A. T. Sommer, L. W. Cheuk, A. Schirotzek, and M. W. Zwierlein. Feynman diagrams versus Fermi-gas Feynman emulator. *Nature Phys.*, 8:366, 2012.

[51] S. Nascimbène, N. Navon, K. J. Jiang, F. Chevy, and C. Salomon. Exploring the thermodynamics of a universal Fermi gas. *Nature*, 463:1057, 2010.

[52] X.-J. Liu, H. Hu, and P. D. Drummond. Virial expansion for a strongly correlated Fermi gas. *Phys. Rev. Lett.*, 102:160401, 2009.

[53] G. E. Astrakharchik, J. Boronat, J. Casulleras, and S. Giorgini. Equation of state of a Fermi gas in the BEC-BCS crossover: a quantum Monte Carlo study. *Phys. Rev. Lett.*, 93:200404, 2004.

[54] N. Navon, S. Nascimbène, F. Chevy, and C. Salomon. The equation of state of a low-temperature Fermi gas with tunable interactions. *Science*, 328:729, 2010.

[55] A. Altmeyer, S. Riedl, C. Kohstall, M. J. Wright, R. Geursen, M. Bartenstein, C. Chin, J. Hecker Denschlag, and R. Grimm. Precision measurements of collective oscillations in the BEC-BCS crossover. *Phys. Rev. Lett.*, 98:040401, 2007.

[56] J. T. Stewart, J. P. Gaebler, T. E. Drake, and D. S. Jin. Verification of universal relations in a strongly interacting Fermi gas. *Phys. Rev. Lett.*, 104:235301, 2010.

[57] E. D. Kuhnle, H. Hu, X.-J. Liu, P. Dyke, M. Mark, P. D. Drummond, P. Hannaford, and C. J. Vale. Universal behavior of pair correlations in a strongly interacting Fermi gas. *Phys. Rev. Lett.*, 105:070402, 2010.

[58] A. Schirotzek, Y. Shin, C. H. Schunck, and W. Ketterle. Determination of the superfluid gap in atomic Fermi gases by quasiparticle spectroscopy. *Phys. Rev. Lett.*, 101:140403, 2008.

[59] D. E. Miller, J. K. Chin, C. A. Stan, Y. Liu, W. Setiawan, C. Sanner, and W. Ketterle. Critical velocity for superfluid flow across the BEC-BCS crossover. *Phys. Rev. Lett.*, 99:070402, 2007.

[60] B. S. Chandrasekhar. A note on the maximum critical field of high-field superconductors. *Appl. Phys. Lett.*, 1:7, 1962.

[61] A. M. Clogston. Upper limit for the critical field in hard superconductors. *Phys. Rev. Lett.*, 9:266, 1962.

[62] G. B. Partridge, W. Li, R. I. Kamar, Y. Liao, and R. G. Hulet. Pairing and phase separation in a polarized Fermi gas. *Science*, 311:503, 2006.

[63] M. W. Zwierlein, A. Schirotzek, C. H. Schunck, and W. Ketterle. Fermionic superfluidity with imbalanced spin populations. *Science*, 311:492, 2006.

[64] Y. Shin, C. H. Schunck, A. Schirotzek, and W. Ketterle. Phase diagram of a two-component Fermi gas with resonant interactions. *Nature*, 451:689, 2008.

[65] P. Fulde and R. A. Ferrell. Superconductivity in a strong spin-exchange field. *Phys. Rev.*, 135:A550, 1964.

[66] A. I. Larkin and Y. N. Ovchinnikov. Nonuniform state of superconductors. *Sov. Phys. JETP*, 20:762, 1965.

[67] Y. Liao, A. S. C. Rittner, T. Paprotta, W. Li, G. B. Partridge, R. G. Hulet, S. K. Baur, and E. J. Mueller. Spin-imbalance in a one-dimensional Fermi gas. *Nature*, 467:567, 2010.

[68] V. Efimov. Energy levels arising from resonant two-body forces in a three-body system. *Phys. Lett. B*, 33:563, 1970.

[69] M. G. Ries, A. N. Wenz, G. Zürn, L. Bayha, I. Boettcher, D. Kedar, P. A. Murthy, M. Neidig, T. Lompe, and S. Jochim. Observation of pair condensation in the quasi-2D BEC-BCS crossover. *Phys. Rev. Lett.*, 114:230401, 2015.

[70] P. A. Murthy, I. Boettcher, L. Bayha, M. Holzmann, D. Kedar, M. Neidig, M. G. Ries, A. N. Wenz, G. Zürn, and S. Jochim. Observation of the Berezinskii-Kosterlitz-Thouless phase transition in an ultracold Fermi gas. *Phys. Rev. Lett.*, 115:010401, 2015.

[71] J. Dalibard, F. Gerbier, G. Juzeliūnas, and P. Öhberg. Colloquium: Artificial gauge potentials for neutral atoms. *Rev. Mod. Phys.*, 83:1523, 2011.

[72] K. von Klitzing, G. Dorda, and M. Pepper. New method for high-accuracy determination of the fine-structure constant based on quantized Hall resistance. *Phys. Rev. Lett.*, 45:494, 1980.